AD-770 852

AERODYNAMICS OF GUIDED AND UNGUIDED WEAPONS. PART 1. THEORY AND APPLICATION

Frank G. Moore

Naval Weapons Laboratory
Dahlgren, Virginia

December 1973

UNCLASSIFIED
Security Classification

AD-770852

DOCUMENT CONTROL DATA - R & D

Security classification of title, body of abstract and indexing annotation must be entered when the overall report is classified

1 ORIGINATING ACTIVITY (Corporate author)

Naval Weapons Laboratory
Dahlgren, Virginia 22448

2a. REPORT SECURITY CLASSIFICATION
UNCLASSIFIED

2b GROUP

3 REPORT TITLE

AERODYNAMICS OF GUIDED AND UNGUIDED WEAPONS, PART 1 - THEORY AND APPLICATION

4 DESCRIPTIVE NOTES (Type of report and, inclusive dates)

5 AUTHOR(S) (First name, middle initial, last name)

Frank G. Moore

6 REPORT DATE
December 1973

7a. TOTAL NO OF PAGES
105

7b. NO OF REFS

8a CONTRACT OR GRANT NO

b PROJECT NO

c

d

9a. ORIGINATOR'S REPORT NUMBER(S)
NWL TR-3018

9b. OTHER REPORT NO(S) (Any other numbers that may be assigned this report)

10 DISTRIBUTION STATEMENT

Approved for public release; distribution unlimited.

11 SUPPLEMENTARY NOTES

12 SPONSORING MILITARY ACTIVITY

13 ABSTRACT

Several theoretical and empirical procedures are combined into a single computer program to predict lift, drag, and center of pressure on quite general wing-body geometries. The method is applicable for Mach number zero to three and angle-of-attack zero to about fifteen degrees. Computed results for several configurations compare well with experimental and other analytical results. It costs about five dollars per Mach number to compute the static aerodynamics of a typical wing-body shape on the CDC 6700 computer.

DD FORM 1 NOV 68 1473 (PAGE 1)
S/N 0102-014-6700

UNCLASSIFIED
Security Classification

NWL Technical Report No. TR-3018
December 1973

AERODYNAMICS OF GUIDED AND UNGUIDED WEAPONS

PART I – THEORY AND APPLICATION

by

Frank G. Moore
Surface Warfare Department

Approved for public release; distribution unlimited.

17

FOREWORD

This work was performed to provide a design tool for use in estimating the aerodynamics of guided and unguided projectiles. Support for the work was provided by the Naval Ordnance Systems Command under ORDTASK 35A-501 [illegible]-1/UF 32-323-505.

The current report was reviewed and approved by Mr. D. A. Jones, III, Head of the Aeroballistics Group and by Mr. C. A. Cooper, Head of the Guided Projectile Division.

Released by:

R. L. Topping

R. L. TOPPING, CDR, USN
Assistant Head, Surface
Warfare Department

ABSTRACT

Several theoretical and empirical procedures are combined into a single computer program to predict lift, drag, and center of pressure on quite general wing-body geometries. The method is applicable for Mach number zero to three and angle-of-attack zero to about fifteen degrees. Computed results for several configurations compare well with experimental and other analytical results. It costs about five dollars per Mach number to compute the static aerodynamics of a typical wing-body shape on the CDC 6700 computer.

CONTENTS

LIST OF FIGURES

LIST OF FIGURES (Continued)

I. INTRODUCTION

The goal of the present research is to develop the capability to compute static aerodynamics on configurations such as guided and unguided projectiles for the Mach number range zero to three and angle-of-attack range zero to about twenty degrees. The Mach number and angle-of-attack range cover a majority of present and probable future design requirements for gun launched weapons. This work, therefore, is a natural extension to the body alone aerodynamic prediction methodology developed in Reference 1. Included herein is an outline of the theoretical and empirical methods used to compute lift, drag, and pitching moment on wings and tails. Also included are procedures to determine the various interference effects which occur between the wing-tail or body-tail. A description and listing of the entire wing-body computer program will appear as part II of this report.

The overall guiding principle of the current work is to use analytical methods which yield reasonable accuracies and require reasonable computational time. For areas where the state-of-the-art is such that analytical procedures do not meet the above requirements on accuracy and cost, empirical procedures are employed. This problem occurs mainly in transonic flow.

There have been several works which pertain to the present problem. The first of these is that of Saffell, et al[2] who developed a computer program to compute static aerodynamics on low aspect ratio missile configurations. The method could be applied for large angles-of-attack and for subsonic through supersonic Mach numbers. However, the drag was computed using handbook techniques and the lift of the wing alone was found from an empirical formula for low aspect ratio wings. Thus, drag results are quite inaccurate (at small angles-of-attack), as well as lift for high aspect ratio configurations.

Another method which is available for spin-stabilized (or body alone) projectiles is the GE 'Spinner' program.[3] This program, which is completely empirical, gives good results for most standard shaped projectiles but is too limited in scope to meet the present needs.

The most detailed method of those previously available is that of Woodward.[4] Woodward uses perturbation theory to compute the pressure distribution on wing-body combinations in subsonic and supersonic flow. However, the bodies must be pointed and the wing leading edge sharp. Also, he does not calculate the base and skin-friction drag or the non-linear angle-of-attack effects.

As is apparent from the above discussion, none of the previous works can in itself accurately compute total lift, drag, and pitching moment on wing-body

combinations for Mach numbers 0 to 3, and angles-of-attack 0° to 20°. Moreover, no attempt is made to handle the complicated body and wing geometries (see Figure 1) which arise from gun launched guided weapons.

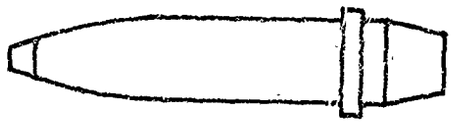

a. SPIN STABILIZED PROJECTILE

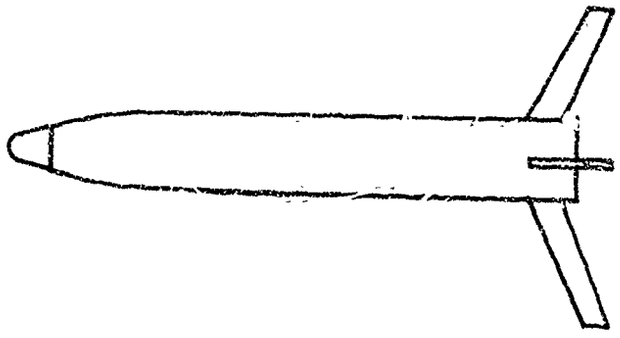

b. UNGUIDED FIN-STABILIZED PROJECTILE

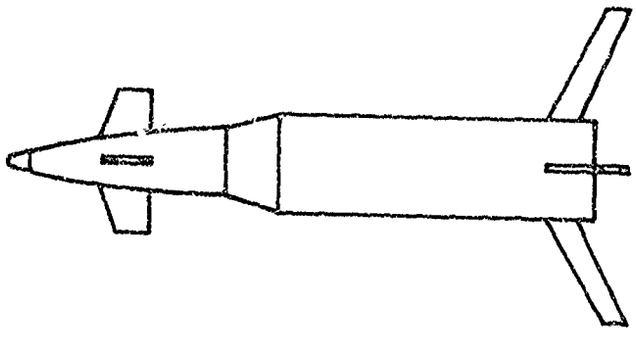

c. GUIDED FIN-STABILIZED PROJECTILE

FIGURE I. BASIC CONFIGURATIONS (ILLUSTRATION ONLY)

II. ANALYSIS

The approach of the present work is to break the missile configuration down into its individual components composed of body alone, wings, and canards and then to account separately for the various interference effects. This is opposed to mathematically modelling the entire configuration simultaneously as was done in the work of Woodward[4] Woodward considered the wing-body simultaneously through an appropriate source and sink distribution, where the sources from the body were allowed to influence the wing solution and vice versa. This is fairly straightforward for pointed nosed bodies and wings with sharp leading edges, but for blunt nosed bodies and blunt leading edge wings, as is the case in the present work, the problem is complicated considerably. Moreover, assuming perturbation theories are used to calculate the inviscid aerodynamics, the approach of considering the individual components separately should yield total forces and moments which are as good as those that would be obtained by considering the configuration as a whole.

A. Body Alone Aerodynamics

The body alone aerodynamic analysis appears in Reference 1 and will not be repeated here. However, a summary of the various methods for computing body alone aerodynamics appears in Figure 2. All the methods are standard in the literature (References 5 through 10) with the exception of the empirical schemes derived for transonic lift and wave drag and the combined Newtonian-perturbation theory for calculating nose wave drag in supersonic flow The combined Newtonian-perturbation theory was developed so reasonable results for static aerodynamics could be obtained at low supersonic Mach numbers for blunt nosed configurations. Previously, the available theories were either too inaccurate[11] or too complicated[12] for use at the lower end of the supersonic Mach range ($1.2 \leq M_\infty \leq 2.0$).

B. Tail or Canard Drag

As in the case of an axisymmetric body, the three-dimensional wing drag is composed of wave, skin-friction, and a trailing edge separation drag if the trailing edge is blunt or the rear section of the airfoil has a large slope This trailing edge separation drag is analogous to base pressure drag on a body of revolution. In addition to these drag components the wings can cause an additional drag from body base pressure changes due to the presence of fins. Each of these wing drag components will be treated separately below

COMPONENT \ MACH NUMBER REGION	SUBSONIC	TRANSONIC	SUPERSONIC
NOSE WAVE DRAG	——	Wu and AOYOMA PLUS EMPIRICAL	2nd ORDER VAN DYKE PLUS MODIFIED NEWTONIAN
BOATTAIL WAVE DRAG	——	Wu and AOYOMA	2nd ORDER VAN DYKE
SKIN FRICTION DRAG	VAN DRIEST II		
BASE DRAG	EMPIRICAL		
INVISCID LIFT and PITCHING MOMENT	EMPIRICAL	Wu and AOYOMA PLUS EMPIRICAL	TSIEN 1st ORDER CROSSFLOW
VISCOUS LIFT and PITCHING MOMENT	ALLEN and PERKINS CROSSFLOW		

FIGURE 2 METHODS USED TO COMPUTE BODY ALONE AERODYNAMICS

1. Wave Drag

It will be assumed *apriori* that the wing is symmetric about the x-y plane so that no camber is present. Furthermore, the wing will be assumed to be thin with either a modified double wedge (Figure 3A) or biconvex airfoil section (Figure 3B). However, by assuming a modified double wedge only requires that straight lines exist between points A and B, B and D, and D and E (see Figure 3A). These straight lines could then be any percentage of the entire chord. For example, if BD were zero the airfoil would be a double wedge design or if both BD and DE were zero, the airfoil would be a wedge. Also, either the biconvex or modified double wedge design may have blunt leading and trailing edges and the thickness to chord ratio may vary along the span. The wing generators GK, HL, IM, and JN are assumed straight.

Since the wing is thin, the linearized three-dimensional equation of motion governing the steady flow field is:[13]

$$\beta^2 \phi_{xx} - \phi_{yy} - \phi_{zz} = 0 \tag{1}$$

where subscripts indicate partial differentiation. Here, the velocity potential ϕ is related to the perturbation velocities by:

$$\phi_x = u \tag{2a}$$

$$\phi_y = v \tag{2b}$$

$$\phi_z = w \tag{2c}$$

The boundary conditions required for the solution of the linear partial differential Equation (1) are that the flow must be tangent to the surface:

$$w(x,y) = \phi_z(x,y,0^-) = \phi_z(x,y,0^+) = \frac{\partial F}{\partial x}(x,y) \tag{3}$$

and that the perturbation velocities must vanish upstream of the most forward point of the wing. Referring to Figure 3A, this most forward point is at $x = 0^-$ so that the second boundary condition is:

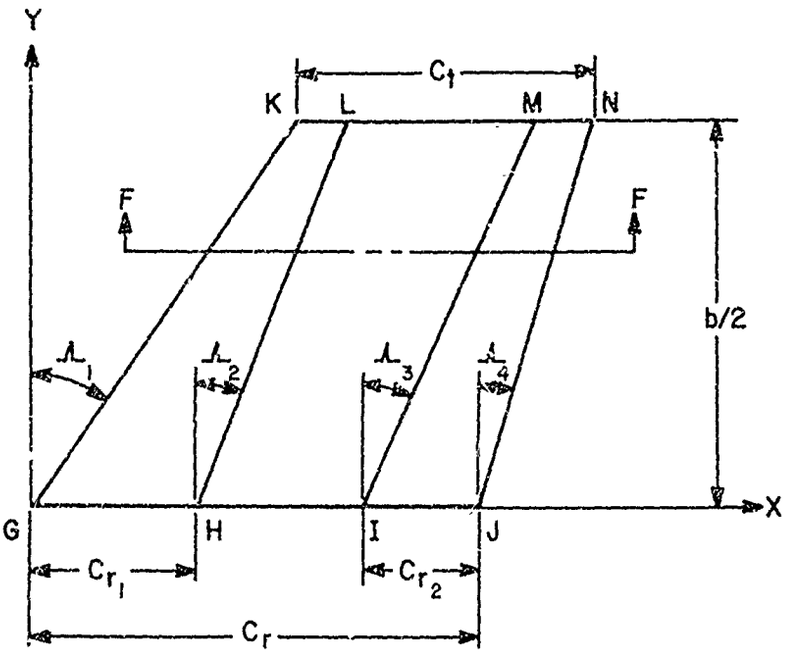

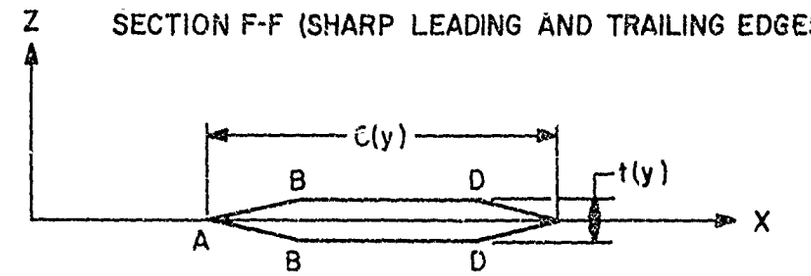

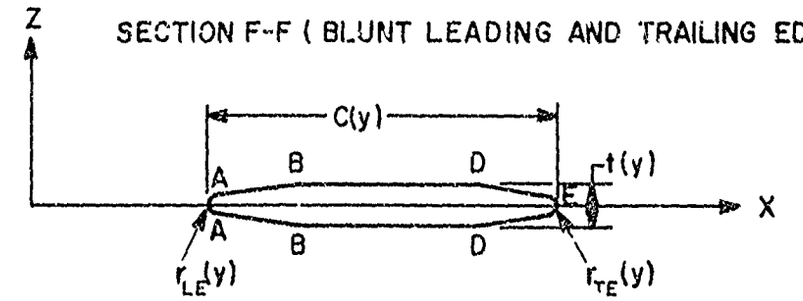

FIGURE 3A. WING WITH MODIFIED DOUBLE WEDGE AIRFOIL SECTION

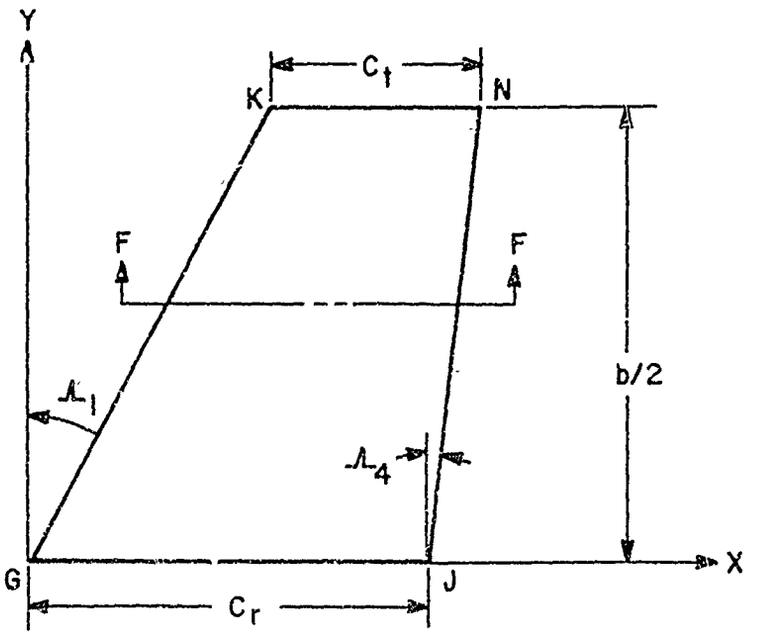

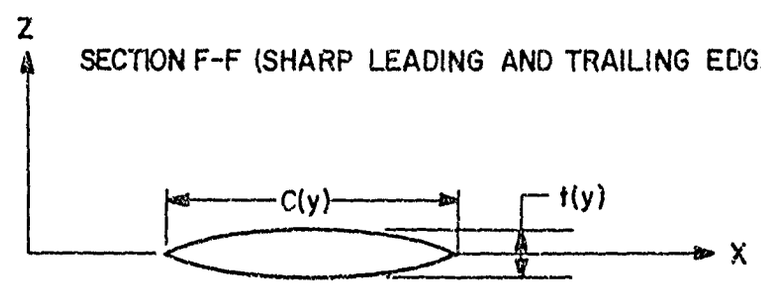

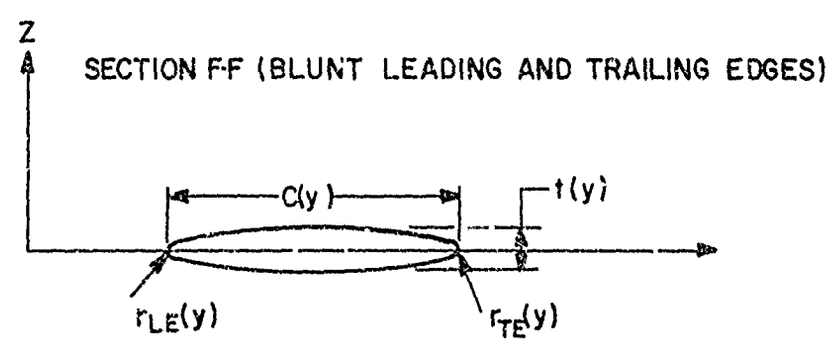

FIGURE 3B. WING WITH BICONVEX AIRFOIL SECTION

$$\phi_x(0^-,y,z) = \phi_x(0^+,y,z) = \phi(0^-,y,z) = 0 \qquad (4)$$

The plus or minus superscript means the particular axis is approached from the positive or negative side, respectively. Due to the symmetry of the airfoil, Equation (3) indicates that it makes no difference from which side one approaches the axis $z = 0$.

Equation (1) is valid only where the perturbation velocities are small. This means that in the neighborhood of a blunt leading or trailing edge, some other method must be applied. Consider first a general three-dimensional wing with sharp leading and trailing edges.

The general solution to Equation (1) along the airfoil surface ($z \cong 0$) is[14]

$$\phi(x,y,0) = -\frac{1}{\pi}\iint_{\Sigma}\frac{w(x_1,y_1)dx_1dy_1}{\sqrt{(x-x_1)^2-\beta^2(y-y_1)^2}} \qquad (5)$$

where Σ indicates the region of integration. The source strength $w(x_1, y_1)$ is related to the local slope of the airfoil surface through the boundary condition Equation (3).

In previous works, $w(x_1,y_1)$ was assumed constant or a function of x only (the slope of the airfoil surface was the same all along the span), so the integration of the above integral could be carried out in closed form for simple wing planforms.[13] In the present analysis, the slope of the wing is allowed to vary in the spanwise as well as the chordwise direction so the integration of Equation (5) cannot, in general, be carried out in closed form. The most straightforward method of solution, is then to define the slope of the given surface and carry out the double integration by numerical quadrature. However, one must be aware of the singular nature of the double integral where $(x-x_1)^2 = \beta^2(y-y_1)^2$ during the integration process. Another alternative is to assume that on a small element of the wing surface, $w(x_1,y_1)$ is constant. Then, if the region of integration of Equation (5), Σ is assumed to be over a small element of the wing, one may write.

$$\phi(x,y,0) = \frac{w(x,y)}{\pi}\iint_{\Sigma}\frac{dx_1dy_1}{\sqrt{(x-x_1)^2-\beta^2(y-y_1)^2}} \qquad (6)$$

Equation (6) is now in the form given in Reference 13 for simple planform geometries and the integration can be carried out directly. Again it should be emphasized that w(x,y) is the slope of the airfoil surface at a given point and varies for each element on the wing.

The closed form solution of Equation (6) depends on whether the wing generators are subsonic or supersonic. Referring to Figure 3A, a subsonic wing generator would exist if the Mach number normal to line GK were less than one and a supersonic wing generator would exist if $M_n > 1$. The same applies to each of the other wing generators HL, IM, and IN. For the biconvex airfoil, Figure 3B, a continuous distribution of wing generators is placed between the lines GK and JN. Each wing generator is analogous to a line of sources and sinks with strengths sufficient to keep the flow tangent to the surface.

a. Subsonic Source or Sink Line (SOSL)

If the wing generator is subsonic, the induced velocity at a given point P, due to the SOSL, is dependent on the location of P relative to the SOSL. Referring to Figure 4A, if $P = P_1$ the induced velocity is:[13]

$$\phi_1 = \frac{2w(x_{p1}, y_{p1})}{\pi\beta\sqrt{\eta^2 - 1}} \cosh^{-1}\sqrt{\frac{\eta^2 - 1}{\sigma^2 - 1}} \tag{7}$$

where w is determined from the boundary condition and is (for the airfoil section at $y = y_{p1}$):

$$w(x_{p1}, y_{p1}) = \left.\frac{dz}{dx}\right|_{x = x_{p1}}$$

In Equation (7), the definitions

$$\eta = k/\beta$$

$$k = \tan\Lambda \tag{7a}$$

$$\sigma = k y_p / x_p$$

have been used. If $P = P_2$, the induced velocity at P_2 due to a given SOSL is:

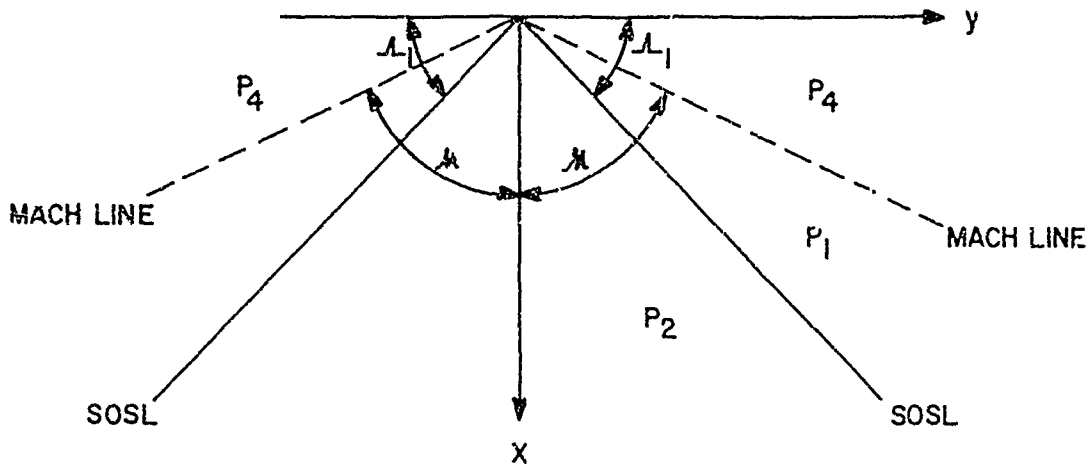

FIGURE 4A. TRIANGULAR SURFACE SYMMETRIC ABOUT X AXIS

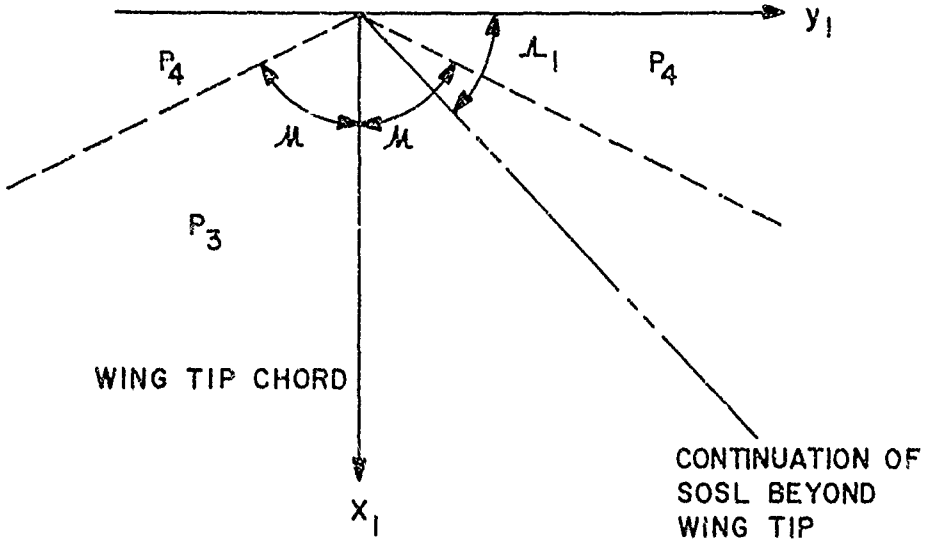

FIGURE 4B. WING TIP EFFECTS

FIGURE 4. SUBSONIC SOURCE OR SINK LINE

$$\phi_{\backslash} = - \frac{2w(x_{p_2}, y_{p_2})}{\pi\beta\sqrt{\eta^2 - 1}} \cosh^{-1} \sqrt{\frac{\eta^2 - \sigma^2}{1 - \sigma^2}} \tag{8}$$

At the wing tip, there is an additional disturbance within the Mach line emanating from the tip leading edge (Figure 4B). The induced velocity in this region, $P = P_3$, is

$$\phi_{\backslash} = - \frac{w(x_{p_3}, y_{p_3})}{\pi\beta\sqrt{\eta^2 - 1}} \cosh^{-1} \left[\frac{\eta^2 + |\sigma|}{\eta(|\sigma| + 1)}\right] \tag{9}$$

The absolute value of σ is taken because σ is actually negative for the point P_3. The induced velocity at any point, say $P = P_4$, outside of the Mach lines emanating from the beginning of the SOSL is zero since this point is out of the zone of influence.

b. Supersonic SOSL

If the wing generator is supersonic, the Mach lines from point 0 in Figure 5A lie behind the SOSL. If in Figure 5, $P = P_1$, then the induced velocity at P_1 due to the disturbance caused by the SOSL is.[13]

$$\phi_{\backslash} = - \frac{w(x_{p_1}, y_{p_1})}{\beta\sqrt{1 - \eta^2}} \tag{10}$$

If $P = P_2$, the induced velocity is

$$\phi_{\backslash} = - \frac{w(x_{p_2}, y_{p_2})}{\pi\beta\sqrt{1 - \sigma^2}} \left[\pi - 2 \sin^{-1} \sqrt{\frac{\eta^2 - \sigma^2}{1 - \sigma^2}}\right] \tag{11}$$

Referring to Figure 5B, the additional induced velocity inside the area bounded by the tip and the Mach line emanating from the tip ($P = P_3$) is:

$$\phi_{\backslash} = - \frac{w(x_{p_3}, y_{p_3})}{\pi\beta\sqrt{1 - \eta^2}} \cos^{-1} \left[\frac{|\sigma| + \eta^2}{\eta(1 + |\sigma|)}\right] \tag{12}$$

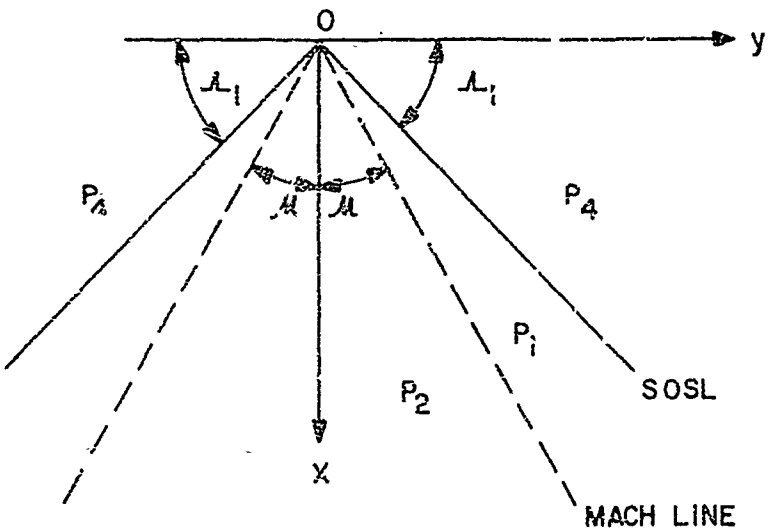

FIGURE 5A. TRIANGULAR SURFACE SYMMETRIC ABOUT X-AXIS

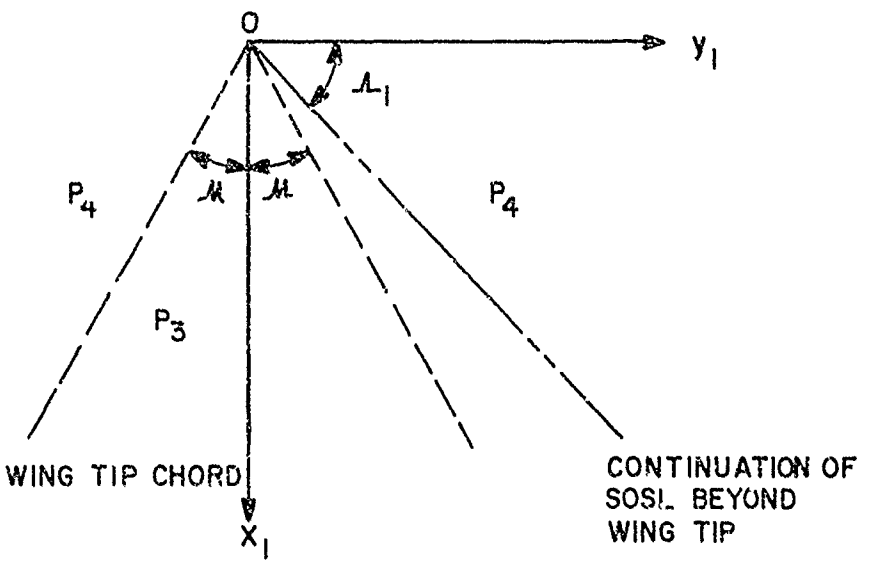

FIGURE 5B. WING TIP EFFECTS

FIGURE 5. SUPERSONIC SOURCE OR SINK LINE

Again if $P = P_4$, the point is out of the zone of influence of the SOSL and thus the induced velocity is zero.

The induced velocity at a given point on any wing geometry can now be computed by the proper superposition of the triangular SOSL shown in Figures 4 and 5. This is because of the linear nature of the governing flow-field Equation (1). As an example of how the above superposition principle works, consider the wing shown in Figure 6. For simplicity, the slopes χ_1 and χ_2 are constant. The wing AHJD can be represented by the superposition of five SOSL. The first has the planform AEH and source intensity:

$$w(x_p, y_p) = V_\infty \chi_1$$

where χ_1 is the slope of the segment AB. The second has the planform BIF and intensity

$$w(x_p, y_p) = (\chi_2 - \chi_1) V_\infty$$

and the third the planform DJG and intensity

$$w(x_p, y_p) = -\chi_2 V_\infty$$

The other two SOSL represent the tip effects. They are the planforms HJL and IJK and have source intensities of opposite signs than those representing the wing.

The above procedure can be applied to a wing of general planform. The only difference is that for each point in question, the slope is not constant as was the case in the simplified example. Then for some general point located on the wing surface, the total induced velocity due to all sources and sinks is found by applying one of the Equations (7) through (12) for each SOSL. The particular equation applied depends upon the location of the point relative to the SOSL and the Mach line as discussed earlier. These individual contributions are then summed to get the total induced velocity. Knowing the total induced velocity at a point allows one to calculate the pressure coefficient at the given point by:

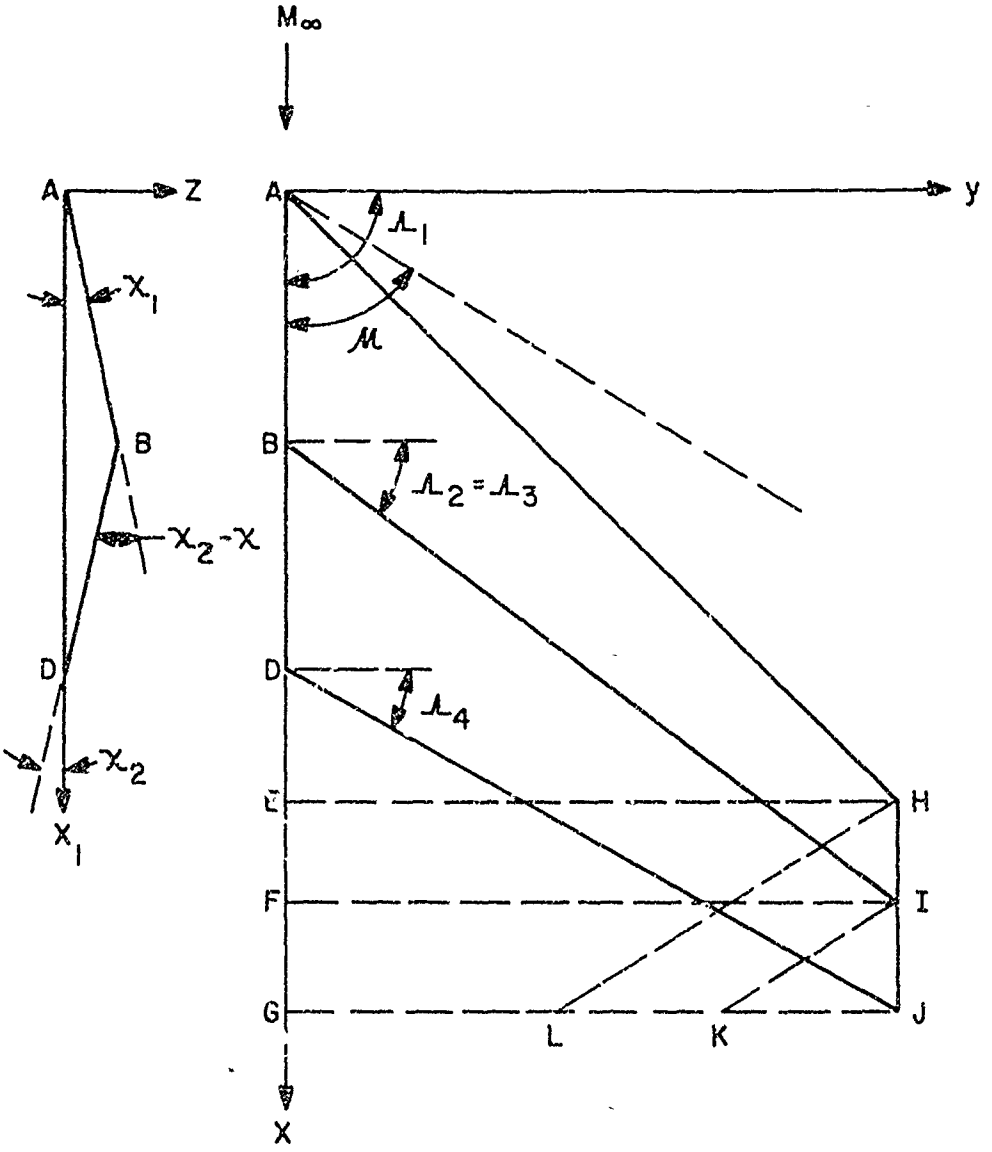

FIGURE 6. LINEAR SUPERPOSITION OF TRIANGULAR SOURCE AND SINK DISTRIBUTIONS.

$$C_p(x,y) = -2\phi_x(x,y,0) \tag{13}$$

The pressure coefficient can be calculated at a given number of spanwise and chordwise locations. The drag of a given airfoil section at the spanwise station $y = y_A$ is then

$$C_d = \frac{2}{c(y_A)} \int_0^{c(y_A)} C_p(x,y_A)w(x,y_A)dx \tag{14}$$

The total drag for one fin of semispan b/2 is then:

$$C_D = \frac{1}{S_w} \int_0^{b/2} C_d c(y)dy \tag{15}$$

where $S_w = b/2(c_r + c_t)$. For cruciform fins, the total drag coefficient is:

$$C_D = \frac{4}{S_w} \int_0^{b/2} C_d c(y)dy \tag{16}$$

If it is desired to base the drag coefficient on the body cross-sectional area, the equation (16) must be multiplied by the factor S_w/S_{ref}

Equations (14) and (16) can be integrated by numerical quadrature if the generators of the wing surface are supersonic. If the generators are subsonic, linear theory indicates the pressure coefficients go to infinity at the wing generators. Physically, this cannot be true which means that for subsonic SOSL, linear theory is not valid at the SOSL. The reason is that the velocity perturbations in the vicinity of the discontinuities are no longer small, violating one of the assumptions in linear theory. However, the velocity perturbations are small a slight distance from the SOSL so that linear theory can be applied. Numerical experiments indicated a distance of five thousandths of the chord length from the SOSL was sufficient and the value of pressure calculated at this point was assumed to exist up to the SOSL.

The previous analysis applies to airfoils with sharp leading and trailing edges. If the airfoil leading or trailing edge is blunt, some other method must be applied in the vicinity of the blunted portion because the assumptions of

perturbation theory are violated there. In analogy to the work of Reference 1, modified Newtonian Theory will be applied to the blunt leading edges and an empirical afterbody separation pressure correction applied at the blunt trailing edges as will be discussed later.

The modified Newtonian pressure coefficient is

$$C_P = C_{P_0} \sin^2 \theta \tag{17}$$

where θ is the angle between a tangent to the local body surface and the freestream direction and where the stagnation pressure coefficient behind a normal shock is:

$$C_{P_0} = \frac{2}{\gamma M_\infty^2} \left\{ \left[\frac{(\gamma+1)M_\infty^2}{2} \right]^{\frac{\gamma}{\gamma-1}} \left[\frac{\gamma+1}{2\gamma M_\infty^2 - (\gamma-1)} \right]^{\frac{\gamma}{\gamma-1}} - 1 \right\} \tag{18}$$

If the blunt leading edge of the wing is cylindrical in a direction perpendicular to the leading edge, then this circular shape appears as an ellipse in the streamwise direction for sweptback wings. Thus, for a given point on the airfoil leading edge with coordinates (x,y,z), it can be shown that (see Appendix A):

$$\theta(x,y,z) = \tan^{-1} \left\{ \frac{\cos \Lambda_l}{3} \left[r_{LI}(y) - x \cos \Lambda_l \right] \right\} \tag{19}$$

Note that Equation (19) assumes the leading edge radius may vary along the span, that is $r_{LE} = r_{LE}(y)$. The pressure coefficient over the elliptical leading edge can now be calculated at each airfoil section by combining Equations (17), (18), and (19).

The question that remains is where does one start the perturbation theory aft of the blunt leading edge and where does one end the modified Newtonian Theory. Before proceeding to answer this question, it is helpful to review the work of Reference 1, which combined the second order perturbation theory of Van Dyke with the modified Newtonian Theory to calculate wave drag on blunt bodies of revolution. In that work, the perturbation theory was started as far upstream on the spherical cap as possible while still getting reasonably accurate perturbation pressure coefficients. It was found that slopes of 25-30 degrees were

optimum. Although the results were unpublished, it was found in that work that if first-order perturbation theory were used, this angle must be reduced to about 15 degrees. Also, it was found that second-order theory accounted very well for the over-expansion region around the spherical cap whereas the first-order theory did not. The important analogy to be drawn from this discussion is that for three dimensional wings, a first-order (rather than a second-order) theory is combined with modified Newtonian Theory to calculate wave drag when the leading edge is blunt. Thus, in analogy to bodies of revolution, one would intuitively expect the angle where perturbation theory begins to be around 15°. A discontinuity in pressure coefficients of Newtonian and perturbation theory is expected at the match point due to the failure of the first-order theory to account for the over-expansion region.

Figure 7 compares, qualitatively, the first and second-order theories when combined with modified Newtonian Theory. The second-order theory is started at say $\theta_2 = 30°$ and the flow allowed to overexpand around the shoulder and recompress downstream. The pressure coefficient will usually intersect that of Newtonian Theory and this is the match point, x_2, indicated on the figure. This combined theory usually follows the experimental data reasonably well. The first-order theory starts at $\theta_1 = 15°$ and the pressure coefficient does not usually decrease enough to intersect the Newtonian theory. Hence, a discontinuity in the pressure coefficient curve for the entire configuration exists at the match point, x_1. For drag calculations, the Newtonian Theory is used up to the point x_1 (which usually will be at the juncture of the cylindrical leading edge and the airfoil after-body) and perturbation theory past x_1. The drag coefficient of the blunt leading edge is (see Appendix B):

$$C_{A_{LE}} = \frac{4 R_{avg} b C_{p_0} \cos^2 \Lambda_1}{S_{ref}} \left(\sin \theta_1 - \frac{\sin^3 \theta_1}{3} \right) \tag{20}$$

where

$$R_{avg} = \frac{(r_{LE})_r + (r_{LE})_t}{2}$$

The drag of the section aft of the cylindrical leading edge can be found by numerical quadrature of Equations (14) and (16).

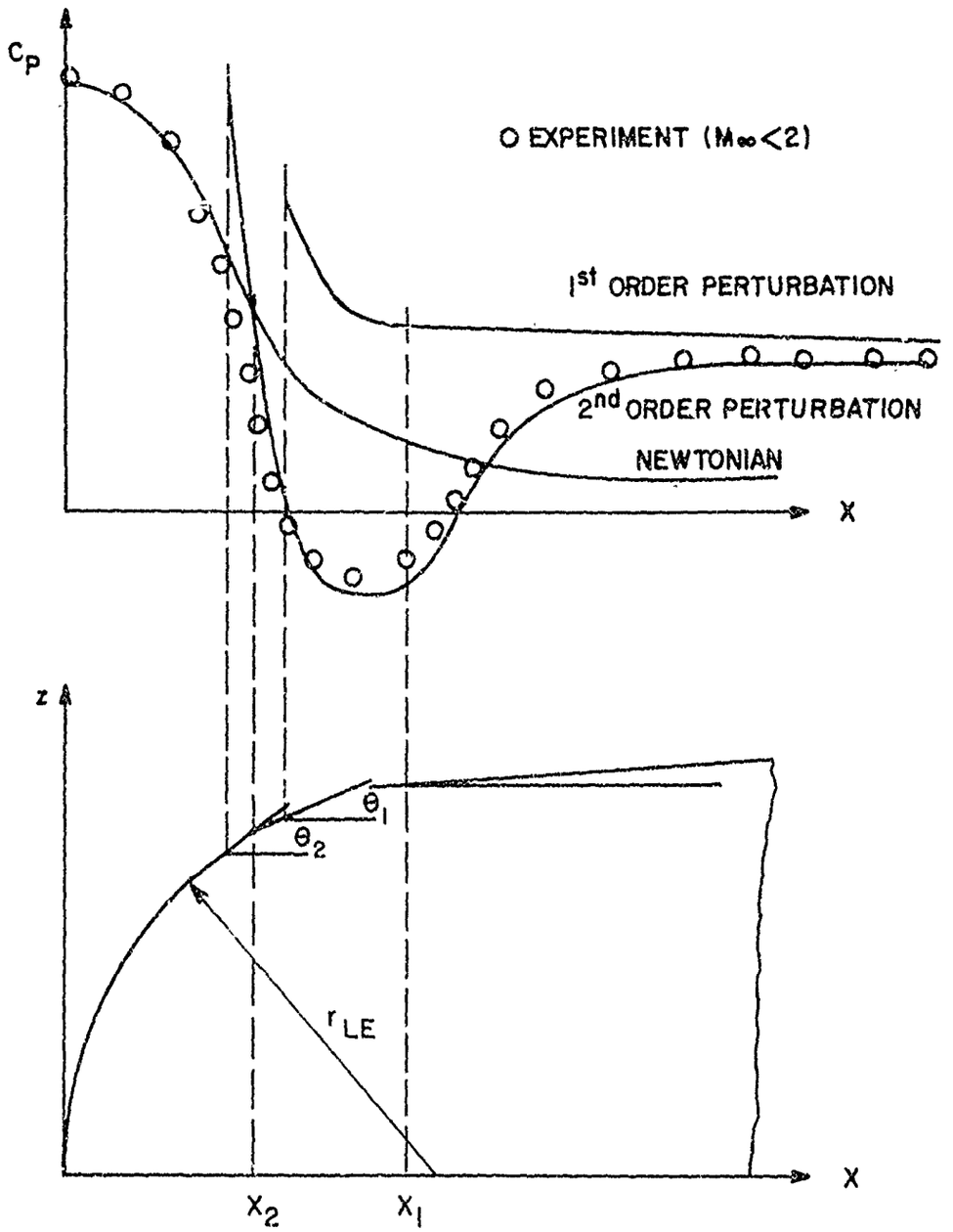

FIGURE 7. COMBINED NEWTONIAN AND PERTURBATION THEORY FOR A BLUNT LEADING EDGE.

2. Skin-Friction Drag

In general, the boundary layer consists of a laminar, transitional, and turbulent region; however, no appreciable errors in total drag will be realized by assuming a laminar and turbulent region with transition taking place instanteously. Moreover, transition from laminar to turbulent flow is assumed to occur at a Reynolds number of 500,000 based on the wing mean aerodynamic chord.

According to Van Driest, the skin-friction drag coefficient for a single wing is then:

$$C_{A_f} = \left\{ (C_{f_T})_{\bar{c}} + \left[(C_{f_\ell})_{\bar{x}} - (C_{f_T})_{\bar{x}} \right] \left(\frac{\bar{x}}{\bar{c}} \right) \right\} \frac{S_{wetted}}{S_{ref}} \tag{21}$$

Here $(C_{f_T})_{\bar{c}}$ and $(C_{f_T})_{\bar{x}}$ are the mean skin-friction coefficients of turbulent flow based on the mean chord and transitional location on the mean chord, respectively. They are computed by solving:

$$\frac{0.242}{A(C_{f_T})^{1/2}(T_w/T_\infty)^{1/2}} (\sin^{-1} B_1 + \sin^{-1} B_2) = \log_{10}(R_N C_{f_T}) - \left(\frac{1+2\eta}{2} \right) \log_{10} \left(\frac{T_w}{T_\infty} \right) \tag{22}$$

implicitly for C_{f_T} where η for air is 0.76. The constants A, B_1, and B_2 of Equation (22) are defined by:

$$B_1 = \frac{2A^2 - F}{(F^2 + 4A^2)^{1/2}} \quad ; \quad B_2 = \frac{F}{(F^2 + 4A^2)^{1/2}}$$

$$A = \left[\frac{(\gamma - 1)M_\infty^2}{2\, T_w/T_\infty} \right]^{1/2} \quad ; \quad F = \frac{1 + (\gamma - 1)/2M_\infty^2}{T_w/T_\infty} - 1$$

The Reynolds Number of Equation (22) is

$$R_N = \frac{V_\infty}{\nu_\infty} \ell \tag{23}$$

where ℓ is either $\bar{c}$ or $\bar{x}$. The wall temperature can be related to the freestream temperature by[1]:

$$T_w/T_\infty = 1 + 0.9\frac{\gamma - 1}{2} M_\infty^2 \tag{24}$$

Finally, the laminar skin-friction coefficient C_{f_ℓ} is[9]

$$(C_{f_\ell})_{\bar{x}} = \frac{1.328}{\sqrt{R_N}} \tag{25}$$

where the Reynolds number is based on $\bar{x}$.

3. Trailing Edge Separation Drag

If the trailing edge is blunt or if its slope is large, the boundary layer will separate somewhere on the rear of the wing. This results in a high drag region similar to that on the base of a projectile, except here the separation is a two-dimensional as opposed to a three-dimensional phenomenon. The pressure on the rear of the wing will then be that of a two-dimensional rearward facing step. Chapman[15] presents experimental results for a blunt wing with no slope at the trailing edge. These results are presented in Figure 8 as a function of Mach number. Note that the data for $M_\infty < 1.1$ has been extrapolated based on the general shape of the three-dimensional base pressure curve presented in Reference 1. If $(r_{TE})_r$ and $(r_{TE})_t$ are the radius of the trailing edge bluntness at the root and tip, respectively, the trailing edge separation drag for one fin is (see Appendix C):

$$C_{A_B} = \frac{bC_{P_B}}{S_{ref}} \left[\frac{(r_{TE})_r + (r_{TE})_t}{2}\right] \tag{26}$$

For cruciform fins this becomes:

$$C_{A_B} = \frac{2bC_{P_B}}{S_{ref}} \left[(r_{TE})_r + (r_{TE})_t\right] \tag{27}$$

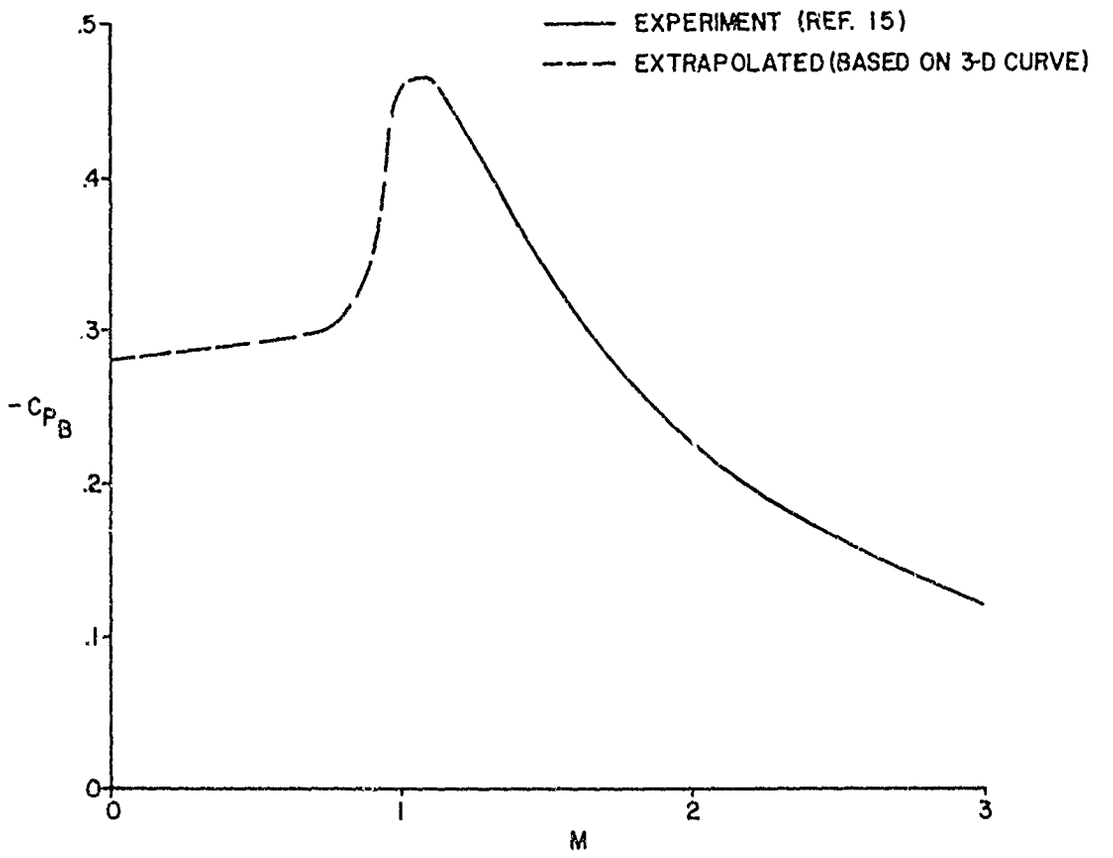

FIGURE 8. 2-D BASE PRESSURE COEFFICIENT

4. Base Pressure Drag Increase Due to Presence of Fins

There are several primary factors which determine the effect of fins on base pressure. These factors are fin location, thickness ratio, aspect ratio, profile, sweepback angle, and number of fins. Based on the small amount of experimental data available, it is not possible to accurately account for any of the above factors for a general configuration. However, order of magnitude effects of two of the variables, fin location and thickness ratio, can be estimated using References 16 through 19.

To estimate the effect of fin thickness to chord ratio on base pressure, it will be assumed the fins are flush with the base. The effect of the fins not being flush with the base will be accounted for shortly. Figure 9 is a plot of $\Delta C_{P_B}/(t/c)$ versus Mach number. Here

$$\Delta C_{P_B} = (C_{P_B})_{\text{with fins}} - (C_{P_B})_{\text{no fins}}$$

The points above $M_\infty = 1.5$ were taken from the data of References 16 and 17 whereas those points below $M_\infty = 1.5$ were taken from Reference 19. Again it should be emphasized that there are too few data points to put a great deal of confidence in this curve. For a given Mach number, M_1, the increment in base pressure due to the presence of fins is then:

$$(\Delta C_{P_B})_f = \left[\frac{\Delta C_{P_B}}{(t/c)}\right]_{M = M_1} \left(\frac{t}{c}\right) \tag{27}$$

The values of t/c which (27) was derived for were ten percent or less.

The work of Spahr and Dickey[17] has shown that if the fins were placed upstream a given distance rather than flush with the base, the effect on base pressure is not as great. Furthermore, if the fins were moved far enough from the base, they would have no effect on base pressure, the amount of this movement being dependent mainly on fin thickness to chord ratio and profile. As seen in Figure 10, this distance varies linearly with t/c up to values of 0.10. The curve in the figure is then extrapolated from t/c = 0.1 to t/c = 0.2.

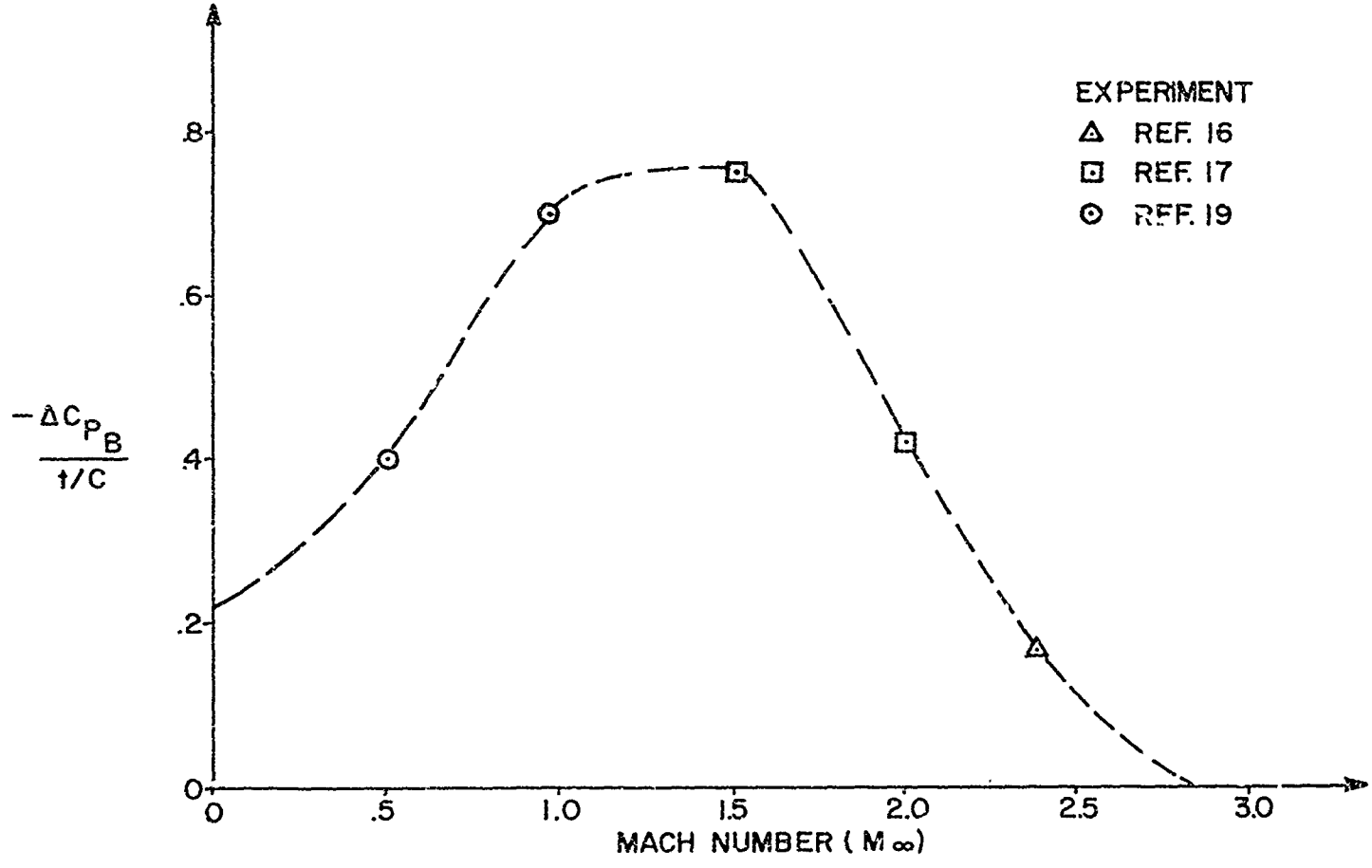

FIGURE 9. BASE PRESSURE COEFFICIENT CHANGE WITH FINS LOCATED FLUSH WITH BASE

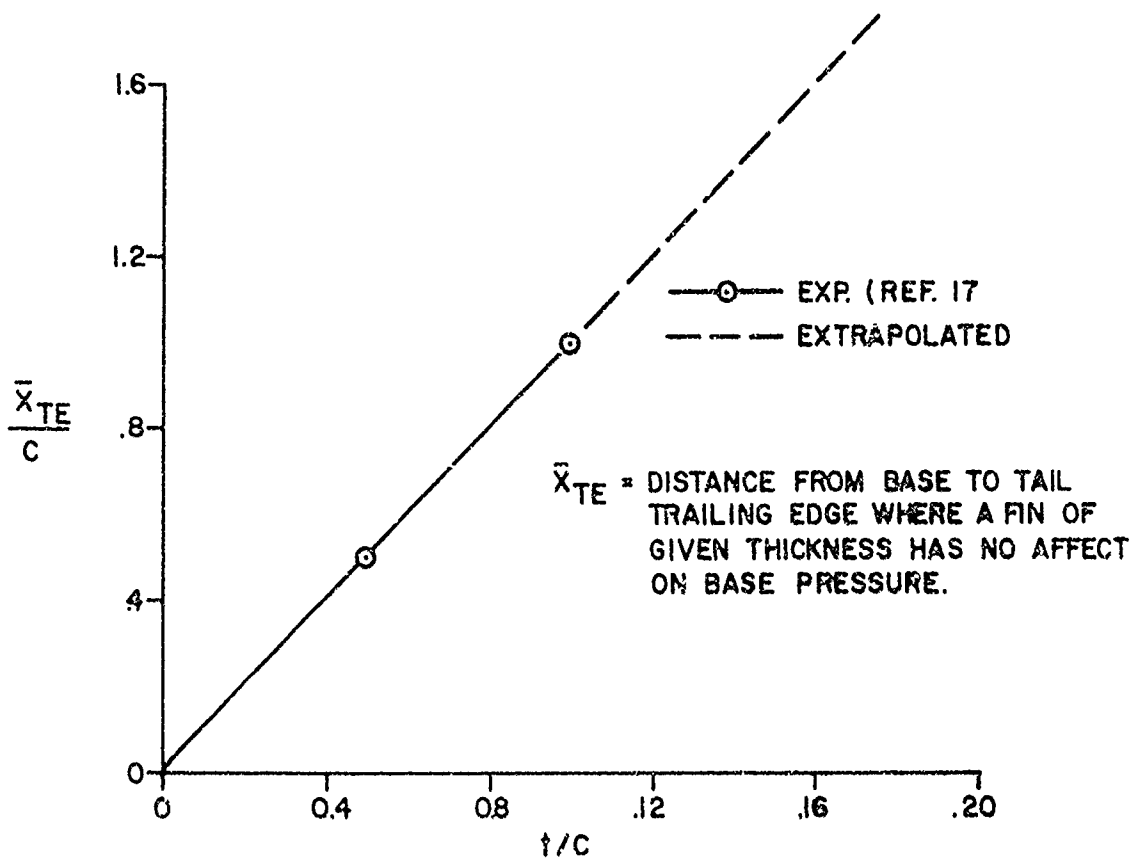

FIGURE 10. DISTANCE FROM BASE WHERE FINS DO NOT AFFECT BASE PRESSURE.

Now if a linear variation of $(\Delta C_{P_B})_f$ is assumed between its maximum when the fins are flush with the base and zero when the fins are far enough away from the base, then Equation (27) may be modified in the form:

$$(\Delta C_{P_B})_f = -\left[\frac{\Delta C_{P_B}}{(t/c)}\right]_{M=M_1}\left(\frac{t}{c} - 0.1\,\frac{x}{c}\right) \quad ; \; \frac{t}{c} \geq 0.1\,\frac{x}{c} \tag{28}$$

$$(\Delta C_{P_B})_f = 0 \quad ; \quad \frac{t}{c} < 0.1\,\frac{x}{c}$$

x/c in Equation (28) is the distance (in chord lengths) upstream of the base. This empirical relation was derived only for cruciform fins.

C Tail or Canard Alone Lift

To calculate the normal force, the wing is assumed to be represented by a flat plate of given planform with zero thickness and camber. This assumption is justified because thickness has only a second-order effect on lift (except for thick wings in transonic flow) and most missile configurations have wings with zero chamber. The methods used to compute the canard or tail alone lift are different for subsonic, supersonic, and transonic flow and will be discussed separately below.

1. Subsonic Flow

The basic equation of motion is Equation (1) with boundary conditions (3) and (4). The boundary condition (3), under the assumption of zero thickness and chamber, may be simplified to:

$$w(x,y) = \phi_z = -\alpha \tag{29}$$

In addition to these boundary conditions, the Kutta condition (which requires the velocity on the upper and lower surfaces at the trailing edge to be equal) is also imposed for subsonic flow. Equation (1) may be simplified somewhat by using Gothert's rule[20] to relate the compressible subsonic normal force or pitching moment to the incompressible case. That is:

$$(C_N)_{M_\infty, t/c, AR, \alpha} = \frac{(C_N)_{0, \beta t/c, \beta AR, \beta\alpha}}{1 - M_\infty^2} \tag{30}$$

$$(C_M)_{M_\infty, t/c, AR, \alpha} = \frac{(C_N)_{0, \beta t/c, \beta AR, \beta\alpha}}{1 - M_\infty^2} \tag{31}$$

However, it was assumed *apriori* that the only contribution to lift was due to angle-of-attack, so Equations (30) and (31) may be simplified to:

$$(C_N)_{M_\infty, AR, \alpha} = \frac{(C_N)_{0, \beta AR, \beta\alpha}}{1 - M_\infty^2} \tag{32}$$

$$(C_M)_{M_\infty, AR, \alpha} = \frac{(C_M)_{0, \beta AR, \beta\alpha}}{1 - M_\infty^2} \tag{33}$$

The way this rule is applied is as follows: given a wing of aspect ratio, AR, freestream Mach number, M_∞, and angle-of-attack, α, the normal force and pitching moment can be obtained by calculating the normal force and pitching moment on another wing of aspect ratio βAR, Mach number zero, and angle-of-attack $\beta\alpha$. Using the above relations, the normal force and pitching moment on a given wing at any subsonic Mach number may be found by calculating the aerodynamics of an affinely related wing at zero Mach number.

For $M_\infty = 0$, Equation (1) reduces to La Places Equation:

$$\phi_{xx} + \phi_{yy} + \phi_{zz} = 0 \tag{34}$$

The solution to Equation (34) can be shown to be:[21]

$$\phi(x,y,z) = -\frac{1}{8\pi} \iint_S \frac{\Delta C_p(x_1, y_1)}{(y - y_1)^2 + z^2} z \left[1 + \frac{x - x_1}{\sqrt{(x - x_1)^2 + (y - y_1)^2 + z^2}}\right] dx_1 dy_1 \tag{35}$$

where $\Delta C_p = C_{p_l} - C_{p_u}$. It is required to determine the pressure loading ΔC_p over the entire surface. Following Chadwick[22], Equation (35) is first differented with respect to and the limit as $\epsilon \to 0$ taken. The result is then equated to the boundary condition, Equation (29), to obtain:

$$\alpha = \frac{1}{8\pi} \iint \frac{\Delta C_p(x_1, y_1)}{(y - y_1)^2} \left[1 + \frac{x - x_1}{\sqrt{(x - x_1)^2 + (y - y_1)^2}} \right] dx_1 dy_1 \qquad (36)$$

The cross on the y_1 integral indicates a singularity at $y = y_1$, in which case Manglers principal-value technique[21] can be applied. The details of the solution of the integral Equation (36) for $\Delta C_p(x,y)$ will not be repeated here as they are given in detail in many references (see for example, Reference 22). Worthy of note, however, is the fact that Equation (36) is an integral equation for which the wing loading ΔC_p is to be found as a linear function of angle of attack.

Once the span loading $\Delta C_p(x,y)$ is known over the entire wing surface, the normal force at a given spanwise location is:

$$C_n = \frac{1}{c} \int_{x_{LE}}^{x_{TE}} \Delta C_p dx \qquad (37)$$

The total normal force for the entire wing is:

$$C_N = \frac{2}{S_{ref}} \int_0^{b/2} c C_n dy \qquad (38)$$

The pitching moment of a given airfoil section, about the point where the wing leading edge intersects the body, is then (positive leading edge up):

$$C_m = -\frac{1}{c\ell_{ref}} \int_{x_{LE}}^{x_{TE}} x \Delta C_p dx \qquad (39)$$

The total pitching moment becomes.

$$C_M = \frac{2}{S_{ref}} \int_0^{b/2} cC_m \, dy \tag{40}$$

If it is desired to calculate the pitching moment about some other reference point, then

$$C_{M_o} = C_M + C_N \frac{x_0}{\ell_{ref}} \tag{41}$$

where x_0 is the distance from the reference point to the juncture of the wing leading edge with the body. The center of pressure of an airfoil section is:

$$x_{CP} = -\frac{C_m}{C_n} \tag{42}$$

or of the entire wing

$$x_{CP} = -\frac{C_M}{C_N} \tag{43}$$

Finally, the spanwise center of pressure of a wing semispan is:

$$y_{CP} = \frac{\int_0^{b/2} cC_n y \, dy}{\int_0^{b/2} cC_n \, dy} \tag{44}$$

Equations (37), (38), (39), (40), and (44) can be solved by numerical quadrature, such as Simpson's rule, with special attention given to the leading edge singularity

2 Supersonic Flow

Here again Equation (1) is valid along with the boundary conditions (4) and (29). However, it will be assumed in the present work that the wing trailing edge is supersonic (Mach number normal to wing trailing edge is greater than one) so that the Kutta condition need not be applied. Two cases will be considered: supersonic leading edges and subsonic leading edges. For both cases the flow is conical in nature from the vertex point which is the intersection of the wing leading edge with the body.

a. Supersonic Leading Edge

Since the flow is conical, the flow properties are constant along rays emanating from the vertex point and lying behind the Mach line. Referring to Figure 11A, where the leading edge Mach line intersects the wing trailing edge, this means that if the flow properties at one point on the ray are known they are known all along the ray. It is then a matter of computing the induced velocities and hence lifting pressures on several rays from point 0. The lifting pressure on any one of these rays in region 2 is:[13]

$$\Delta C_p = \Delta C_{p_2} = \frac{4\alpha}{\beta\sqrt{1-\eta^2}}\left(1 - \frac{2}{\pi}\sin^{-1}\sqrt{\frac{\eta^2-\sigma^2}{1-\sigma^2}}\right) \tag{45}$$

where η and σ were defined by 7A. Ahead of the Mach line, in region 1, the flow is two-dimensional so the lifting pressure is constant at:

$$\Delta C_p = \Delta C_{p_1} = \frac{4\alpha}{\beta\sqrt{1-\eta^2}} \tag{46}$$

If the wing were tapered to a point, the above two relationships would allow complete determination of the lifting pressures over the wing. For most practical cases, the wing tip is not pointed so tip effects must be accounted for. The tip affects the pressure within the Mach line from the tip leading edge (region 3). Within this region, the flow is again conical along rays from point D so the lifting pressure caused by the tip is:[23]

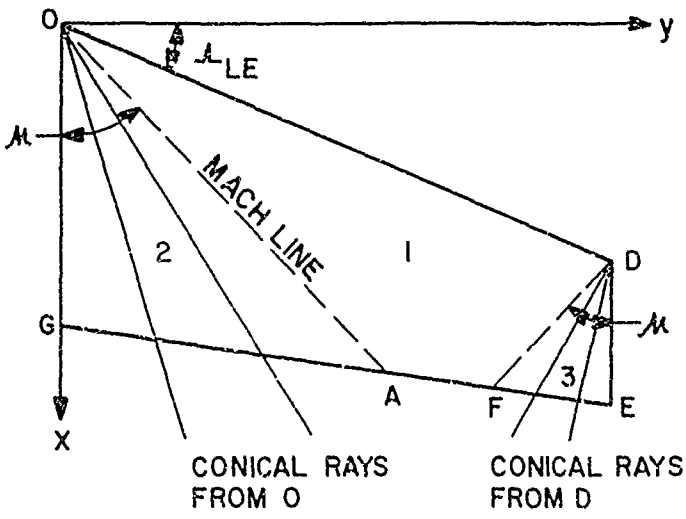

REGION	AREA
1	OAFD
2	OAG
3	DEF

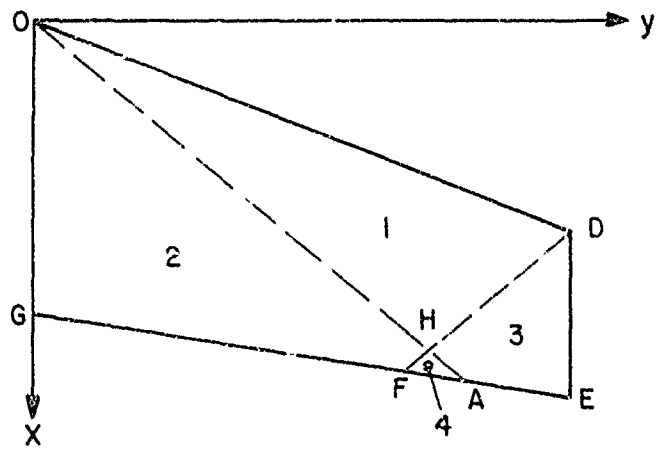

REGION	AREA
1	OHD
2	OHFG
3	DEAH
4	AHF

FIGURE IIA. FLAT PLATE WING PLANFORM WITH SUPERSONIC LEADING AND TRAILING EDGES; MACH LINE INTERSECTS WING TRAILING EDGE.

$$\Delta C_{P_3} = \frac{-8\alpha}{\pi\beta\sqrt{1-\eta^2}} \tan^{-1}\sqrt{\frac{\eta+\sigma_D}{-\sigma_D(1+\eta)}} \qquad (47)$$

The original equation of motion, Equation (1), is linear so that superposition of solutions is allowed. Thus, the total lifting pressure in region 3 is:

$$\Delta C_P = \Delta C_{P_1} + \Delta C_{P_3}$$

If the situation arises such that the Mach lines intersect, as shown at the bottom of Figure 11A, then an additional pressure of ΔC_{P_3} is created in region 4. Hence, the total lifting pressure in region 4 is

$$\Delta C_P = \Delta C_{P_2} + \Delta C_{P_3}$$

The second case to consider when the leading edge is supersonic is when the leading edge Mach line intersects the tip as illustrated in Figure 11B. The lifting pressures in regions 1, 2, 3, and 4 are calculated in the same manner as when the Mach line intersects the trailing edge. However, in region 5 the lift to be cancelled along the tip is variable (see Equation 45) as opposed to the constant value cancelled in regions 3 and 4 (see Equation 46). This complicates the problem somewhat in that a summation (or integration) must now be performed to calculate the cancellation lift in region 5. Referring to Figure 11B, the region 5 is broken down into a finite number of intervals, in the following manner. Conical rays from the vertex at 0 are projected behind the Mach line 0A and intersect the wing tip at equal intervals along the tip (for example, rays OJ and OK). Lines are then drawn from the points of intersection on the wing tip parallel to the Mach line AI until the point P(x,y) is enclosed. The difference in ΔC_P across one of these intervals is what must be cancelled throughout the region 5. For any given interval then, say JK, this difference in pressure is found by applying Equation (45) to each of the rays from 0 passing through J and K. That is:

$$\Delta C_{P_{JK}}(x,b/2) = \Delta C_{P_J}(x,b/2) - \Delta C_{P_K}(x,b/2)$$

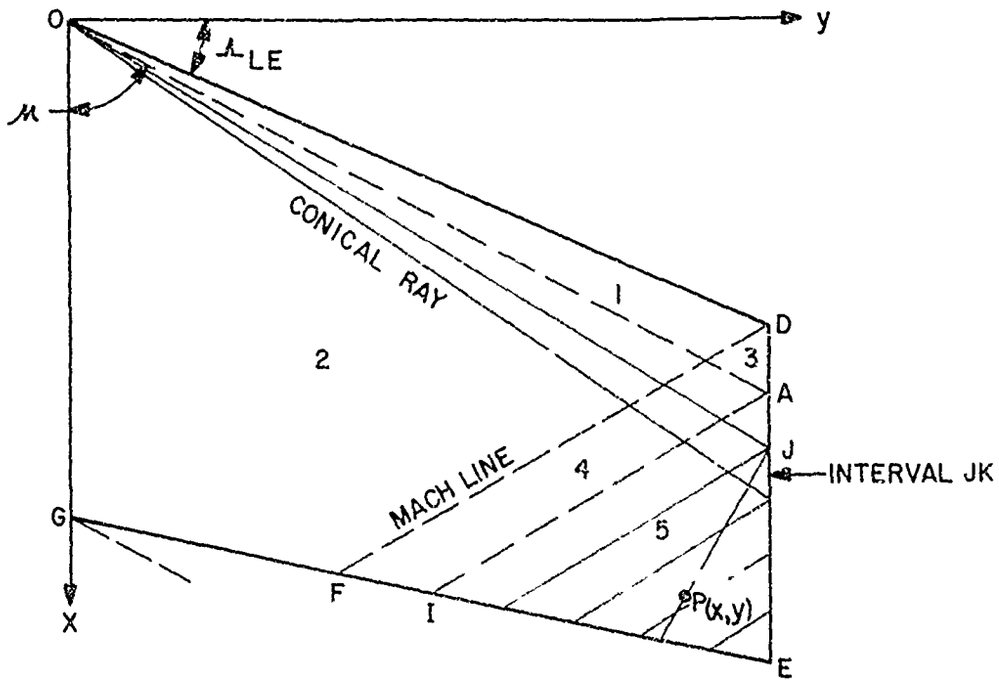

REGION	AREA
1	ODH
2	OHFG
3	AHD
4	FHAI
5	AEI

$$\sigma_{JP} = \tan \Lambda_{LE} \frac{y - b/2}{X - X_J}$$

FIGURE IIB. FLAT PLATE WING PLANFORM WITH SUPERSONIC LEADING AND TRAILING EDGES; MACH LINE INTERSECTS WING TIP.

$$\Delta C_{P_{JK}}(x,b/2) = \frac{8\alpha}{\pi\beta\sqrt{1-\eta^2}}\left[\sin^{-1}\sqrt{\frac{\eta^2-\sigma_{0K}^2}{1-\sigma_{0K}^2}} - \sin^{-1}\sqrt{\frac{\eta^2-\sigma_{0J}^2}{1-\sigma^2{}_{0J}}}\right]$$

The effect of this cancellation pressure at any point P(x,y) is then:

$$\Delta C_{P_{JP}}(x,y) = \Delta C_{P_{JK}}(x,b/2)\frac{2}{\pi}\tan^{-1}\sqrt{\frac{\eta+\sigma_{JP}}{-\sigma_{JP}(1+\eta)}} \qquad (48)$$

Now the interval JK is any interval upstream of the Mach line from P passing through the wing tip. If m is the total number of intervals upstream of P, then the total lifting pressure coefficient at point P(x,y) within region 5 is:

$$\Delta C_P = \Delta C_{P_2} + \Delta C_{P_4} + \sum_{i=n}^{i=m} \Delta C_{P_{iP}}$$

where $\Delta C_{P_{iP}}$ is given at each interval by Equation (48).

The force and moment coefficients can now be found by substituting the expressions for ΔC_p in each region into the Equations (37) through (44) and performing the indicated operations. The integrations could be carried out in closed form for regions 1 through 4, but the formulas are very lengthy for even the simpliest cases.[23] A more straightforward approach is to simply numerically integrate the integrals over the entire surface, particularly since the pressures in region 5 have to be numerically integrated.

b. Subsonic Leading Edge

For subsonic leading edges, the velocity and lifting pressures approach infinite values near the leading edge. The solution for ΔC_p is complicated somewhat by this singularity, but due to the conical nature of the flow from the vertex points 0 and D (Figure 12), a closed form solution can be obtained. For region 1 of Figure 12 this is:[21]

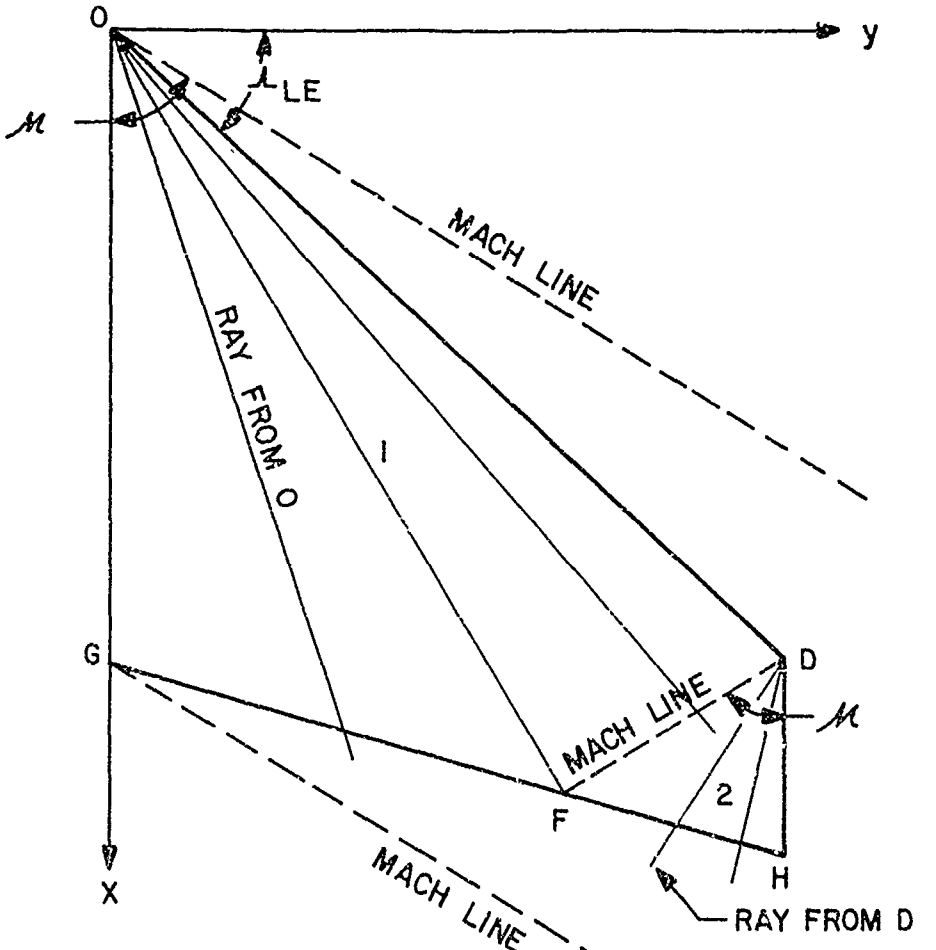

REGION	AREA
1	ODFG
2	DFH

FIGURE 12. FLAT PLATE WING PLANFORM WITH SUBSONIC LEADING EDGE AND SUPERSONIC TRAILING EDGE.

$$\Delta C_p = \Delta C_{p_2} = \frac{4\alpha}{E \tan \Lambda_1 \sqrt{1 - \sigma_0^2}} \tag{49}$$

where E is a constant dependent only on the leading edge sweep angle and Mach number.

That is,

$$E(k) = \int_0^{\pi/2} \sqrt{1 - k^2 \sin^2 \theta} d\theta \tag{50}$$

and $k = \sqrt{1 - \beta^2/\tan^2 \Lambda_{LE}}$. The value of the complete elliptic integral E(k) has been tabulated and appears in standard mathematical handbooks.

The lift to be cancelled at the tip is variable as was the case for supersonic leading edges when the Mach line intersected the tip. However, in this case the integration can be carried out in closed form. Thus, the cancellation lifting pressure is:[23]

$$\Delta C_{p_2} = \frac{4\alpha}{\pi \beta \eta^{3/2} E\left(\frac{\eta^2 - 1}{\eta}\right)} \left[K(k) \sqrt{\frac{2\beta(b/2 - y)}{x + \beta y}} - 2x \sqrt{\frac{\eta}{x^2 - \beta^2 y^2 \eta^2}} \left\{ \frac{F(k', \psi)}{K(k')} \left[\frac{\pi}{2} - K(k) E(k') \right] + K(k) F(k', \psi) \right\} \right] \tag{51}$$

where

$$k = \sqrt{\frac{(1 - a_0 \eta)(\eta - 1)}{2\eta(a_0 + 1)}}, \quad k' = \sqrt{1 - k^2}$$

$$\psi = \sin^{-1} \sqrt{\frac{a_0(x + \beta y \eta)}{\beta b/2 (1 + \eta a_0)}}, \quad a_0 = \frac{\beta b/2}{x + \beta(y - b/2)}$$

Here $F(\theta_1,\theta_2)$ and $E(\theta_1,\theta_2)$ are elliptic integrals of the first and second kind, respectively, which again can be found in any standard mathematical handbook. The complete elliptic integral K is related to $F(\theta_1,\theta_2)$ by $K = F(\theta_1,\pi/2)$ and the complete elliptic integral E of Equation (50) is related to $E(\theta_1,\theta_2)$ by $E = E(\theta_1,\pi/2)$.

The total lifting pressure coefficient at any point within region 2 is then

$$\Delta C_p = \Delta C_{p_1} + \Delta C_{p_2}$$

The integrations for spanwise lift and pitching moment can be obtained by integrating Equations (37) and (39) numerically. However, caution must be taken in these integrations because for subsonic leading edges, the lifting pressure goes like $1/\sqrt{x}$ near the leading edge. In this vicinity, more mesh points must be added to the flow field to get an accurate integration.

The total wing normal force and pitching moment can be easily obtained by numerical integration of Equations (38) and (40). The chordwise center of pressure is then found from Equation (43) and the spanwise center of pressure from Equation (44).

3. Transonic Flow

As mentioned earlier, airfoil thickness has a second order effect on lift in subsonic and supersonic flow. However, this is not true in transonic flow so the assumption of a flat plate with zero thickness is no longer valid except for very thin wings. Furthermore, as M_∞ approaches unity, Equation (1) cannot be applied because the term $(1 - M_\infty^2)\phi_{xx}$ becomes of the same order as nonlinear terms which have been neglected in deriving this equation from small perturbation theory.

Recent progress in the field of transonic aerodynamics has greatly advanced the state-of-the-art. However, at present, practical methods for flow field computation are still severely limited. For example, solutions for three-dimensional swept and tapered wings with thickness do not exist, even in approximate form. In light of these considerations, an empirical approach to wing lift in transonic flow will be used. The method adopted is that presented in DATCOM.[24] This procedure accounts, in an empirical manner, for sweep, Mach number, aspect ratio, and thickness ratio but not for airfoil section.

To apply the above empirical procedure, the force break Mach number is found from Figure 13A for a wing of zero sweep and corrected for sweep by Figure 13B. The lift curve slope at the force break Mach number is then computed by a simple expression derived from lifting line theory:[25]

$$(C_{N_\alpha})_{fb} = \frac{2\pi AR}{2 + [AR^2(\beta^2 + \tan^2 \Lambda_{1/2}) + 4]^{1/2}} \tag{59}$$

This value is corrected to agree with experiment according to Figure 14A. The abrupt decrease in lift curve slope associated with thick wings is approximated by the relation:

$$(C_{N_\alpha})_a = (1 - a/c)(C_{N_\alpha})_{fb} \tag{60}$$

where a/c is given in Figure 14B. The Mach number at point a is:

$$M_a = M_{fb} + 0.07 \tag{60A}$$

The subsequent rise in C_{N_α} to a value at point b is

$$(C_{N_\alpha})_b = (1 - b/c)(C_{N_\alpha})_{fb} \tag{61}$$

where b/c is given in Figure 14C. The Mach number at point b is

$$M_b = M_{fb} + 0.14 \tag{61A}$$

The normal force curve slope at $M \geq 1.2$ is calculated by supersonic thin wing theory and for $M < M_{fb}$ by lifting surface theory. From this empirical correlation one obtains $(C_{N_\alpha})_{fb}$, $(C_{N_\alpha})_a$, $(C_{N_\alpha})_b$ at the Mach numbers M_{fb}, $M_{fb} + .07$, and $M_{fb} + .14$. For values of C_{N_α} in transonic flow in between these Mach numbers, interpolation is used.

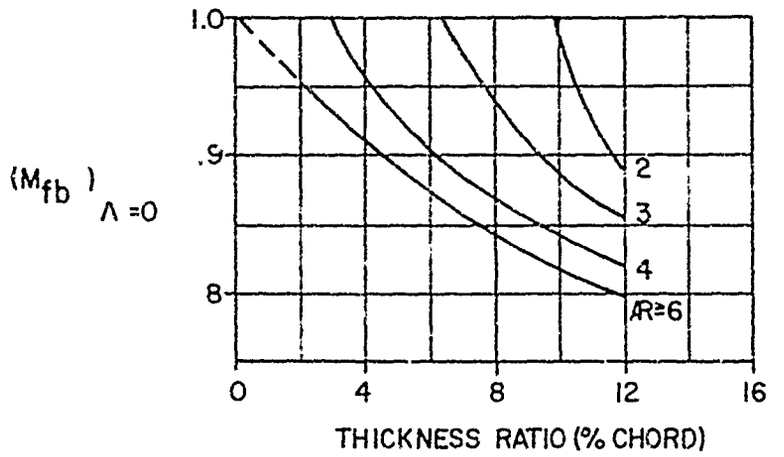

FIGURE 13A. FORCE-BREAK MACH NUMBER FOR ZERO SWEEP

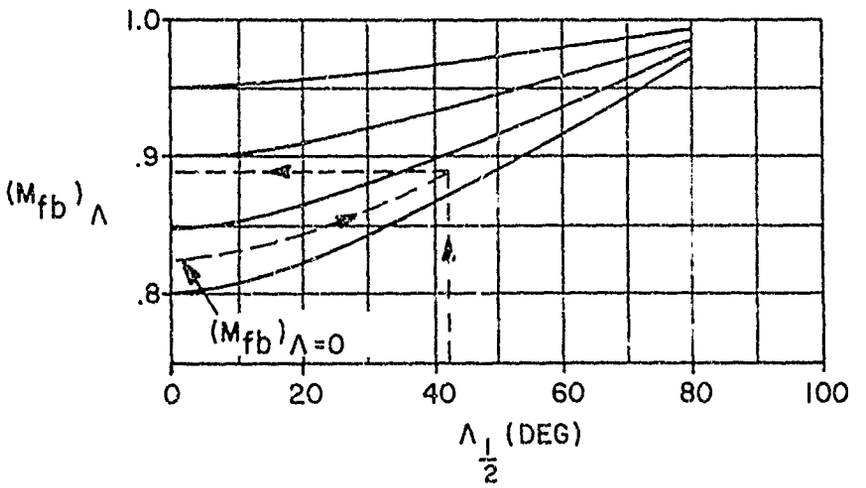

FIGURE 13B. SWEEP CORRECTION FOR FORCE-BREAK MACH NUMBER

FIGURE 13. TRANSONIC FORCE-BREAK MACH NUMBER

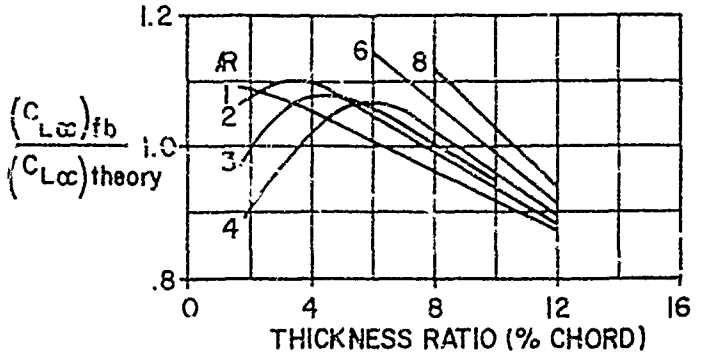

FIGURE 14A. CORRECTION TO LIFT-CURVE SLOPE AT FORCE-BREAK MACH NUMBER

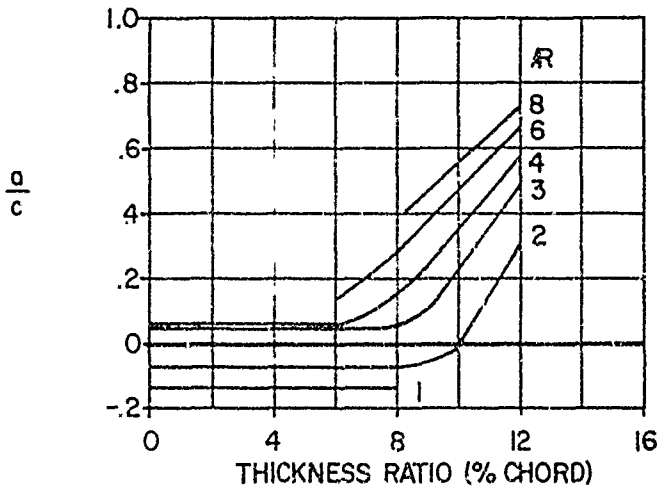

FIGURE 14B. CHART FOR DETERMINING LIFT-CURVE SLOPE AT M_a

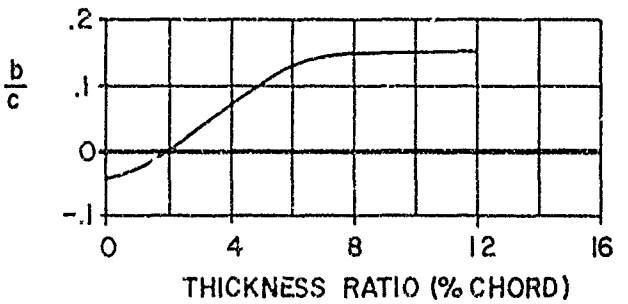

FIGURE 14C. CHART FOR DETERMINING LIFT-CURVE SLOPE AT M_b

FIGURE 14. CHART FOR DETERMINING TRANSONIC LIFT-CURVE SLOPE AT M_a AND M_b

The center of pressure of wing alone lift is usually around the quarter chord for subsonic flow and half chord for supersonic flow. Transition from subsonic to supersonic flow is assumed to occur in a linear fashion between values calculated at M_∞ slightly less than M_{fb} and $M_\infty > 1.2$. The pitching moment coefficient derivative of the wing alone is then:

$$C_{M_{\alpha_w}} = -x_{CP} C_{N_\alpha} \tag{62}$$

D. Interference Lift

Interference lift is broken down into three parts: lift of canard or tail due to presence of body, lift of body due to presence of wing or canard, and vortex lift on tail due to wing shed or body shed vortices. The methods used to calculate the interference lift components are essentially those presented in Reference 26. The necessary equations for the various calculations will be repeated herein, but for the details of the derivations, the reader is referred to the above reference.

The method used by Morikawa[27] for presenting lift interference is adopted. He defines the wing alone as the exposed half wings joined together. The lift of the combination is related to the lift of the wing alone by the factor K_C so that

$$L_C = K_C L_w \tag{63}$$

K_C is actually composed of three components,

$$K_C = K_{B(w)} + K_{w(B)} + K_B \tag{64}$$

which are the ratios of the body lift in presence of the wing, wing lift in presence of body, and body lift to the lift of the wing alone. That is:

$$K_{B(w)} = \frac{L_{B(w)}}{L_w} \tag{65A}$$

$$K_{w(B)} = \frac{L_{w(B)}}{L_w} \tag{65B}$$

$$K_B = \frac{L_B}{L_w} \tag{65C}$$

We will not be concerned with K_B as it was found in Reference i as discussed earlier. The factors $K_{B(w)}$ and $K_{w(B)}$ are found from a straightforward application of slender body theory and are:

$$K_{B(w)} = \frac{(1 - r^2/s^2) - 2/\pi \left\{(1 + r^4/s^4)[\tfrac{1}{2} \tan^{-1} \tfrac{1}{2}(s/r - r/s) + \pi/4]\right.}{(1 - r/s)^2}$$

$$\left. - \frac{r^2/s^2[(s/r - r/s) + 2 \tan^{-1} (r/s)]\right\}}{(1 - r/s)^2} \tag{66}$$

$$K_{w(B)} = \frac{2/\pi \left\{(1 + r^4/s^4)[\tfrac{1}{2} \tan^{-1} \tfrac{1}{2}(s/r - r/s) + \pi/4]\right.}{(1 - r/s)^2}$$

$$\left. - \frac{r^2/s^2[(s/r - r/s) + 2 \tan^{-1} (r/s)]\right\}}{(1 - r/s)^2} \tag{67}$$

$K_{w(B)}$ and $K_{B(w)}$ of Equations (66) and (67) are related to each other by:

$$K_{w(B)} + K_{B(w)} = (1 + r/s)^2 \tag{68}$$

Values of these parameters are plotted in Figure 15. Equation (66) is used to calculate $K_{B(w)}$ for all subsonic Mach numbers and for supersonic Mach numbers if $\beta AR(1+\lambda)[1/(m\beta)+1] \leq 4$. If $\beta AR(1+\lambda)[1/(m\beta)+1] > 4$, Nielsen[28] has shown that for no afterbody (see Figure 16), a more appropriate value of $K_{B(w)}$ can be found from:

$$K_{B(w)}[\beta(C_{N_\alpha})_w](\lambda+1)(s/r-1) = \frac{8}{\pi\sqrt{\beta^2m^2-1}}\left(\frac{\beta d}{c_r}\right)\left[\left(1+\frac{mc_r}{d}\right)^2\right.$$

$$\cos^{-1}\left[\frac{m\beta + c_r/(\beta d)}{1+mc_r/d}\right] - m^2\beta^2\left(\frac{c_r}{\beta d}\right)^2\cos^{-1}\left(\frac{1}{m\beta}\right)$$

$$\left. + m\beta\left(\frac{c_r}{\beta d}\right)^2\sqrt{m^2\beta^2-1}\sin^{-1}\left(\frac{\beta d}{c_r}\right) - \sqrt{m^2\beta^2-1}\cosh^{-1}\left(\frac{c_r}{\beta d}\right)\right] \qquad (69A)$$

when $\beta m > 1$ and $c_r/\beta > d$. If $\beta m < 1$ and $c_r/\beta > d$, $K_{B(w)}$ is found from:

$$K_{B(w)}[\beta(C_{N_\alpha})_w](\lambda+1)(s/r-1) = \frac{16\sqrt{m\beta}}{\pi(m\beta+1)}\left(\frac{\beta d}{c_r}\right)\left\{\left(1+\frac{mc_r}{d}\right)\sqrt{\left(\frac{c_r}{\beta d}-1\right)\left(\frac{mc_r}{d}+1\right)}\right. \qquad (69B)$$

$$-\left(\frac{c_r}{\beta d}\right)^2(m\beta)^{3/2} + m\beta\left(\frac{c_r}{\beta d}\right)^2(\beta m+1)\left[\tan^{-1}\sqrt{\frac{1}{\beta m}} - \tan^{-1}\sqrt{\left(\frac{c_r}{\beta d}-1\right)\Big/\left(\frac{mc_r}{d}+1\right)}\right]$$

$$\left. - \frac{m\beta+1}{\sqrt{m\beta}}\tanh^{-1}\sqrt{m\beta\left(\frac{c_r}{\beta d}-1\right)\Big/\left(\frac{mc_r}{d}+1\right)}\right\}$$

If $c_r/\beta \leq d$ in Equations (69A) or (69B), c_r/β is set equal to d. For an infinite afterbody behind the wing or canard (see Figure 16), Equations (69A) and (69B) are replaced by:

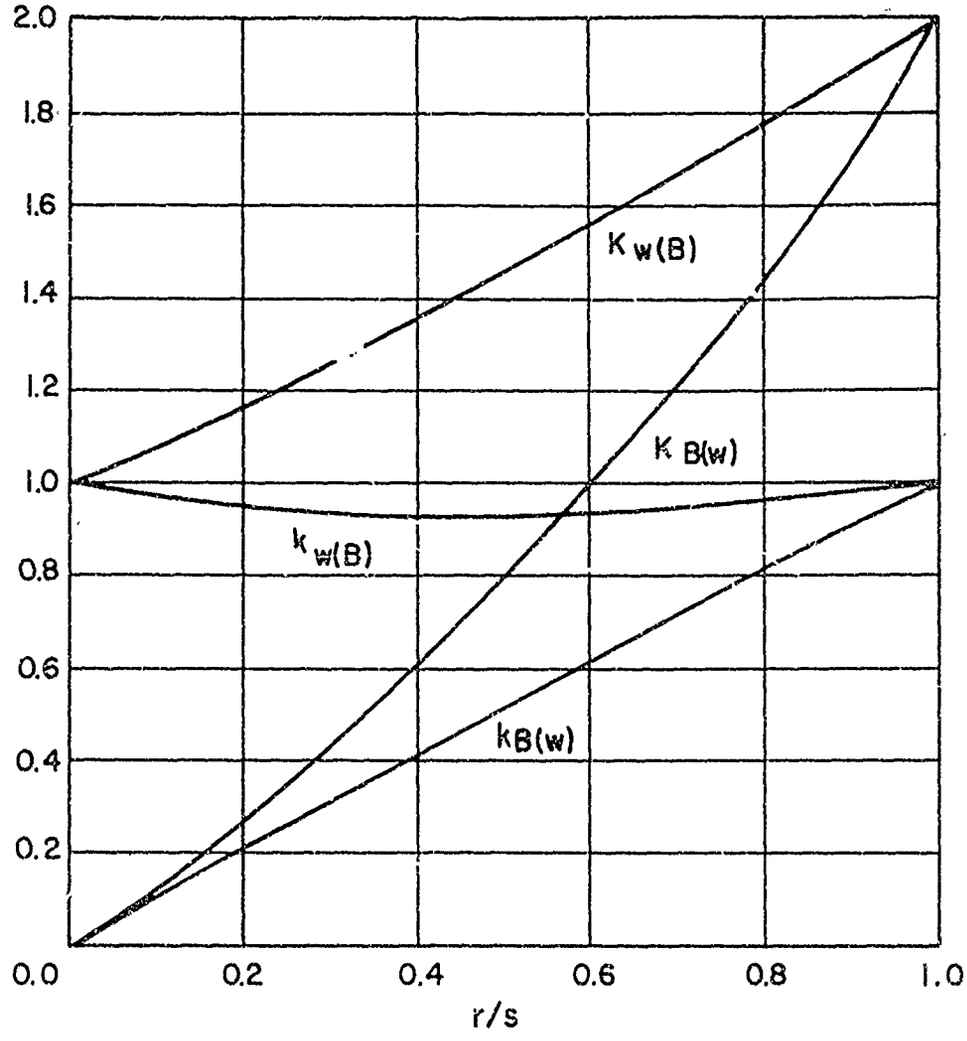

FIGURE 15. SLENDER BODY INTERFERENCE LIFT FACTORS

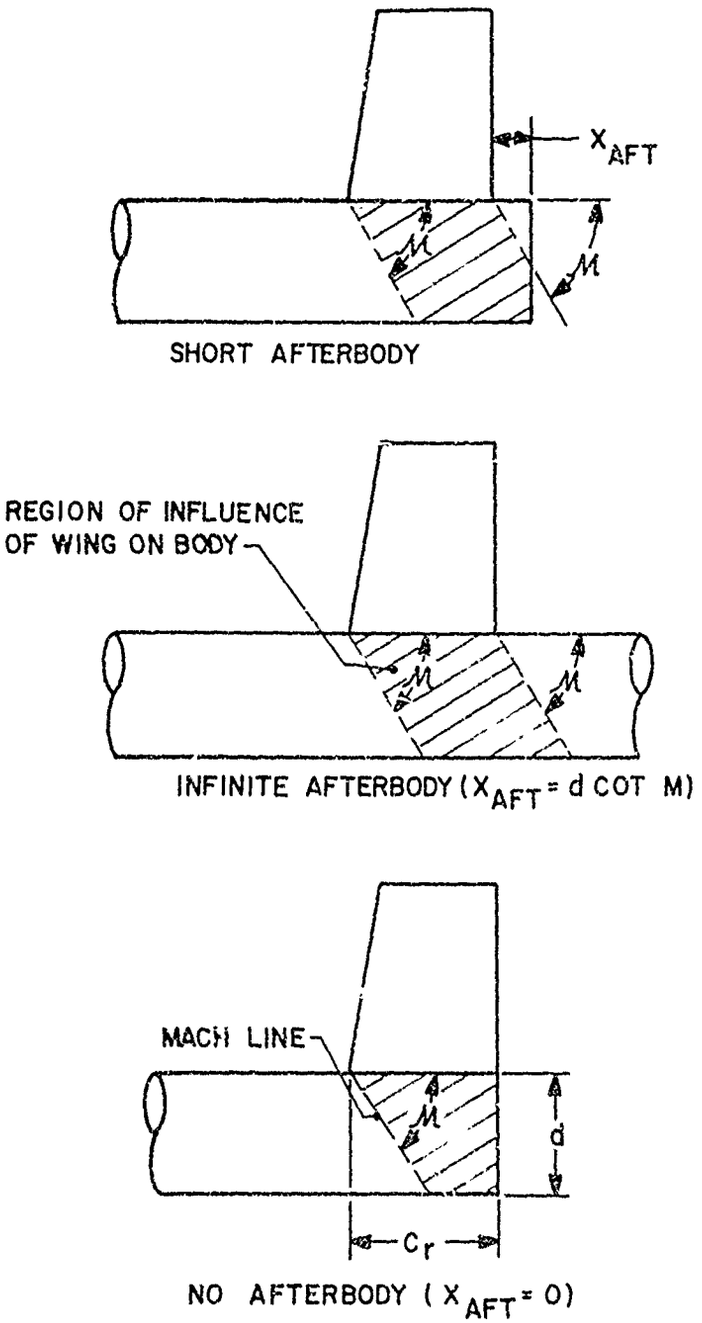

FIGURE 16. DETERMINATION OF $K_{B(W)}$ FOR HIGH-ASPECT-RATIO RANGE AT SUPERSONIC SPEEDS.

$$K_{B(w)}\left[\beta(C_{N_\alpha})_w\right](s/r-1)(1+\lambda) = \frac{8\beta m}{\pi\sqrt{\beta^2 m^2-1}}\left(\frac{c_r}{\beta d}\right)\left\{\left(\frac{\beta m}{1+\beta m}\right)\left[1+\right.\right.$$

$$\left.(1+1/(\beta m))\beta d/c_r\right]^2 \cos^{-1}\left[\frac{1+(1+\beta m)\beta d/c_r}{\beta m+(1+\beta m)\beta d/c_r}\right]$$

$$+\frac{\sqrt{\beta^2 m^2-1}}{(\beta m+1)}\left[\sqrt{1+2\beta d/c_r}-1\right]-\frac{\sqrt{\beta^2 m^2-1}}{\beta m}\left(\frac{\beta d}{c_r}\right)^2\cosh^{-1}\left(1+\frac{c_r}{\beta d}\right)$$

$$\left.-\frac{\beta m}{1+\beta m}\cos^{-1}\left(\frac{1}{\beta m}\right)\right\} \qquad (70A)$$

for $m\beta > 1$ and by

$$K_{B(w)}\left[\beta(C_{N_\alpha})_w\right](s/r-1)(1+\lambda) = \frac{16}{\pi}\left(\frac{c_r}{\beta d}\right)\left(\frac{\beta m}{1+m\beta}\right)^2\left\{\left[1+(1+1/(m\beta))\frac{\beta d}{c_r}\right]^{3/2}-\right.$$

$$\left.\left[1+(1+1/(m\beta))\frac{\beta d}{c_r}\right]^{1/2}-2-\left[(1+1/(m\beta))\frac{\beta d}{c_r}\right]^2\tanh^{-1}\sqrt{\frac{1}{1+(1+1/(m\beta))\beta d/c_r}}\right\} \qquad (70B)$$

for $m\beta < 1$. For cases in between no afterbody and an infinite aferbody, $K_{B(w)}$ may be found approximately by linearly interpolating between the values given by Equations (69) and (70). That is, referring to Figure 16,

$$\left[K_{B(w)}\right]_{SA} = \left(\frac{[K_{B(w)}]_{IA}-[K_{B(w)}]_{NA}}{d\cot\mu}\right)x_{AFT}+\left[K_{B(w)}\right]_{NA} \qquad (71)$$

Here the subscripts SA, IA, and NA refer to short, infinite, and no afterbody, respectively.

In addition to the normal force due to angle of attack, there is a normal force created due to wing deflection δ. The lift of a wing due to a deflection δ is given by:

$$C_{N_{w(B)}} = k_{w(B)} (C_{N_\alpha})_w \delta \tag{72}$$

where

$$k_{w(B)} = \frac{1}{\pi^2} \left\{ \frac{\pi^2 (s/r+1)^2}{4 (s/r)^2} + \frac{\pi [(s/r)^2+1]^2}{(s/r)^2 (s/r-1)^2} \sin^{-1} \left[\frac{(s/r)^2-1}{(s/r)^2+1} \right] \right.$$

$$\frac{2\pi (s/r+1)}{s/r(s/r-1)} + \frac{[(s/r)^2+1]^2}{(s/r)^2 (s/r-1)^2} \left(\sin^{-1} \left[\frac{(s/r)^2-1}{(s/r)^2+1} \right] \right)^2$$

$$\left. \frac{4(s/r+1)}{s/r(s/r+1)} \sin^{-1} \left[\frac{(s/r)^2-1}{(s/r)^2+1} \right] + \frac{8}{(s/r-1)^2} \log \left[\frac{(s/r)^2+1}{2 s/r} \right] \right\} \tag{73}$$

The lift on the body due to the control deflection is

$$C_{N_{B(w)}} = k_{B(w)} (C_{N_\alpha})_w \delta \tag{74}$$

where

$$k_{B(w)} = k_{w(B)} - k_{w(B)} \tag{75}$$

$k_{w(B)}$ and $k_{B(w)}$ are given in Figure 15 as a function of r/s.

Strictly speaking, Equations (66), (67), and (73) apply to slender wing-body configurations which have low aspect ratio wings. Furthermore, the trailing edges of these wings must be perpendicualr to the body axis or swept forward but cannot be swept back. Neilsen[26] has shown that good results can be obtained for the interference lift components for high aspect ratio wings even though the slender body approximation is made. However, if the wing trailing edge is swept back the previous slender body formulas are not applicable without further study. For wings which have swept back trailing edges, and where slender body theory is used to calculate interference lift, it seems reasonable to assume the increased lift on the wing due to the presence of the body is distributed evenly along the wing chord and is concentrated near the root. With this assumption, the interference lift components of a swept back wing may be approximated by:

$$\left[K_{B(w)}\right]_{II} = \left[K_{B(w)}\right]_{I} G$$

$$\left[K_{w(b)}\right]_{II} = 1 + \left(\left[K_{w(B)}\right]_{I} - 1\right) G$$

$$\left[k_{w(B)}\right]_{II} = 1 + \left(\left[k_{w(B)}\right]_{I} - 1\right) G$$

$$\left[k_{B(w)}\right]_{II} = \left(\left[K_{w(B)}\right]_{I} - \left[k_{w(B)}\right]_{I}\right) G$$

where $G = (c_r)_{II}/(c_r)_I$ and the subscript II refers to the actual wing being considered and subscript I refers to the wing for which the slender body Equations (66), (67), and (73) assumes. Figure 17 indicates how the above procedure is carried out.

The negative lift caused by downwash of the canard shed vortex on the tail is given by:

$$C_{N_1} = \frac{(C_{N_\alpha})_w (C_{N_\alpha})_1 \left[K_{w(B)} \sin\alpha + k_{w(B)} \sin\delta\right]_{II} (s - r)_w S_w}{2\pi A R_w (f_w - r_w) S_{ref}} \tag{76}$$

This equation is determined from line-vortex theory assuming only one trailing vortex per forward wing panel. The lateral location of the vortex, f_w, measured from the body center line is:

$$f_w = r + \frac{(C_n)_w S_w}{2\left[(C_n c)_r\right]_w} \tag{77}$$

The span loading at the root $(C_n c)_r$ and normal force coefficient are known for the particular wing geometry as discussed previously. The interference factor, i, of Equation (76) is.

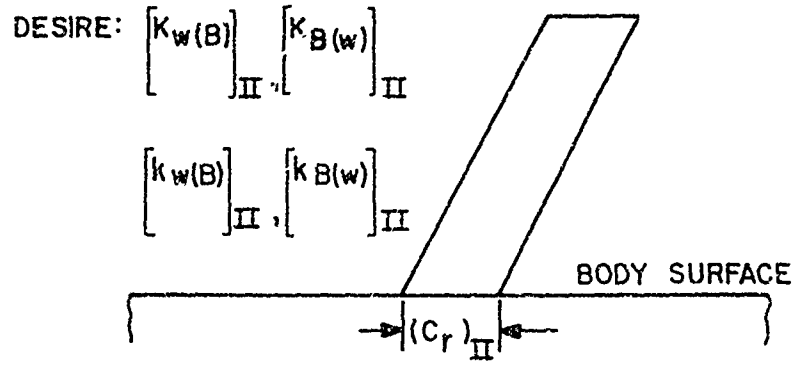

FIGURE 17A. WING FOR WHICH INTERFERENCE LIFT IS DESIRED

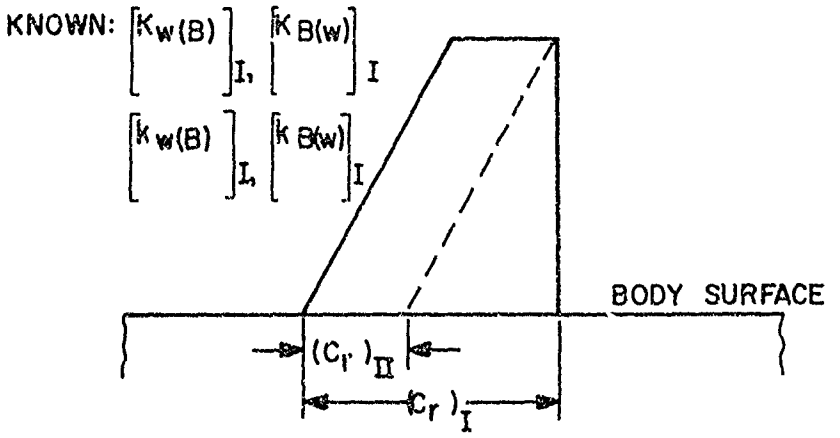

FIGURE 17B. ASSUMED SLENDER BODY REPRESENTATION

FIGURE 17. PROCEDURE USED TO CALCULATE INTERFERENCE LIFT FOR WINGS WITH SWEPT BACK TRAILING EDGES WHEN SLENDER BODY THEORY IS USED.

$$i = \left(\frac{2}{1+\lambda}\right)\left[L\left(\lambda, \frac{r}{b}, \frac{f}{b}, \frac{h}{b}\right) - L\left(\lambda, \frac{r}{b}, \frac{f}{b}, \frac{h}{b}\right)\right.$$

$$\left. - L\left(\lambda, \frac{r}{b}, \frac{f_1}{b}, \frac{h_1}{b}\right) + L\left(\lambda, \frac{r}{b}, -\frac{f_1}{b}, \frac{h_1}{b}\right)\right] \tag{78}$$

where

$$L\left(\lambda, \frac{r}{b}, \frac{f}{b}, \frac{h}{b}\right) = \left\{\frac{s - r\lambda - (1-\lambda)}{2(s-r)} \ell n\left(\frac{h^2 + (f-s)^2}{h^2 + (f-r)^2}\right)\right.$$

$$\left. - \frac{1-\lambda}{s-r}\left[(s-r) + h \tan^{-1}\left(\frac{f-s}{h}\right) - h \tan^{-1}\left(\frac{f-r}{h}\right)\right]\right\},$$

$$f_i = \frac{f_r^2}{f^2 + h^2}, \quad h_i = \frac{h_r^2}{f^2 + h^2}$$

and

$$h = -3(c_r)_w/4 \sin\delta + [\ell_T - \ell_w - 3(c_r)_w/4]\sin\alpha$$

Here it is assumed that the hinge line of the wing is at the quarter chord.

The only remaining lift is the negative lift on the tail due to the body shed vortex. This is

$$C_{N_{B(V)}} = \frac{-4\Gamma}{S_w V_\infty}\left[\frac{f_w^2 - r_w^2}{f_w} - f_T + \frac{r_T^2}{\sqrt{f_T^2 + h_T^2}}\right] \tag{79}$$

where

$$\frac{\Gamma}{V_\infty} = \frac{K_{w(B)}\alpha + k_{w(B)}\delta}{4(r_w - r_w)}(C_{N_\alpha})_w \; S_w$$

The center of pressure of the wing lift in presence of the body, canard shed vortex lift, and body shed vortex lift are all assumed to act at the center of pressure of the wing alone. The center of pressure of the body lift caused by the wing is Mach number dependent. Complicated expressions could be derived for center of pressure of this lift component in supersonic speeds analogous to Equations (69) and (70). However, a good engineering approximation is to assume that the center of pressure is at the centroid of the cross-hatched area in Figure 16. This eliminates the need for considering separately the afterbody, no afterbody, and short afterbody cases. Thus, for supersonic flow, the center of pressure of the body lift caused by the wings is (measured from the wing leading edge):

$$x_{cp} = \frac{c_r^2 d/2 - \beta^2 d^3/6 + x_{AFT}(2d - x_{AFT}/\beta)\bar{x}_3/2}{dc_r - \beta d^2/2 + x_{AFT}(2d - x_{AFT}/\beta)/2} \qquad (80A)$$

where

$$\bar{x}_3 = c_r + x_{AFT}\left[\frac{d/2 - x_{AFT}/(3\beta)}{d - x_{AFT}/(2\beta)}\right]$$

for

$$\beta d - x_{AFT} \geq 0 \text{ and } (\beta d - c_r - x_{AFT}) < 0.$$

If $\beta d - x_{AFT} \geq 0$ and $(\beta d - c_r - x_{AFT}) > 0$, then:

$$x_{cp} = \frac{3/2(c_r + x_{AFT})^3 - (c_r + 2/3x_{AFT})x^2_{AFT}}{(c_r + x_{AFT})^2 - x^2_{AFT}} \qquad (80B)$$

Finally, if $\beta d - x_{ALT} < 0$, then

$$x_{CP} = \frac{c_r + \beta d}{2} \tag{80C}$$

Equation (80A) represents the case where the Mach line from the trailing edge intersect the base whereas that from the leading edge intersects the opposite side. Equation (80B) is used when both leading and trailing edge Mach lines from the wing root chord intersect the base whereas Equation (80C) is used when both Mach lines intersect the opposite side.

For subsonic and transonic flow, there is much less tendency for the lift to be carried aft. For subsonic flow it is reasonable to assume the body carry-over lift acts at the center of pressure of the wing alone lift. In transonic flow, the center of pressure is assumed to vary linearly between its value at the force break Mach number and that computed for M = 1.2 by Equation (80).

E. Summary Configuration

The total normal force of the entire configuration is:

$$C_N = C_{N_B} + \left[\left(K_{w(B)} + K_{B(w)}\right)\alpha + \left(k_{w(B)} + k_{B(w)}\right)\delta\right] \quad (C_{N_\alpha})_w$$

$$+ \left[\left(K_{T(B)} + K_{B(T)}\right)\alpha\right](C_{N_\alpha})_T + C_{N_{T(V)}} + C_{N_{B(V)}} \tag{81}$$

Defining

$$C_{N_{w(B)}} = \left[K_{w(B)}\alpha + k_{w(B)}\delta\right](C_{N_\alpha})_w$$

$$C_{N_{B(w)}} = \left[K_{B(w)}\alpha + k_{B(w)}\delta\right](C_{N_\alpha})_w$$

$$\ell_{w(B)} = \ell_w + (\bar{x}_{cp})_w$$

$$\ell_{B(w)} = \ell_w + (\bar{x}_{cp})_{B(w)}$$

$$\ell_{T(B)} = \ell_T + (\bar{x}_{cp})_T$$

$$\ell_{B(T)} = \ell_w + (\bar{x}_{cp})_{B(T)}$$

the center of pressure referenced to the nose tip may be written as:

$$\ell = \left[\ell_B C_{N_B} + C_{N_{w(B)}} \ell_{w(B)} + C_{N_{B(w)}} \ell_{B(w)} + C_{N_{T(B)}} \ell_{T(B)} + C_{N_{B(T)}} \ell_{B(T)} + \left(C_{N_{T(V)}} + C_{N_{B(V)}} \right) \ell_T \right] \Big/ C_N \tag{82}$$

The pitching moment about the nose is then:

$$C_M = C_N \ell \tag{83}$$

A summary of the various theoretical and empirical procedures used to calculate the static aero[illegible] of the wing or tail alone and interference effects is given in Figure [illegible]. As already indicated, a summary of the body alone procedures was given [illegible] Figure 2.

COMPONENT \ MACH NUMBER REGION	SUBSONIC	TRANSONIC	SUPERSONIC
INVISCID LIFT AND PITCHING MOMENT	LIFTING SURFACE THEORY	EMPIRICAL	LINEAR THEORY
WING-BODY INTERFERENCE	SLENDER BODY THEORY AND EMPIRICAL		LINEAR THEORY, SLENDER BODY THEORY & EMPIRICAL
WING-TAIL INTERFERENCE	LINE VORTEX THEORY		
WAVE DRAG	——	EMPIRICAL	LINEAR THEORY + MODIFIED NEWTONIAN
SKIN FRICTION DRAG	VAN DRIEST		
TRAILING EDGE SEPARATION DRAG	EMPIRICAL		
BODY BASE PRESSURE DRAG CAUSED BY TAIL FINS	EMPIRICAL		

FIGURE 18. METHODS USED TO COMPUTE WING ALONE AND INTERFERENCE AERODYNAMICS

III. RESULTS AND DISCUSSION

A. Comparison With Exact Linear Theory

1. Wing Wave Drag

For wings which have simple planforms, exact linear theory solutions exist by which the present numerical solutions may be compared. Simple planforms are defined as wings with double wedge or biconvex airfoil sections with the same airfoil section and thickness ratio all along the span. Simple planforms also have sharp leading and trailing edges.

Figure 19 compares the pressure coefficient of the present method with that of exact linear theory for a biconvex airfoil design.[13] The pressure coefficient has been divided by t/c, the thickness to chord ratio, since it is constant all along the span. As seen from the figure, the numerical solution gives essentially exact results when compared with the solution of Reference 13.

Section wave drag along the span of a wing with a double wedge airfoil section is given in Figures 20 and 21. Figure 20 is for a wing tapered to a point (no tip effects) and Figure 21 is for a wing with fifty percent taper. The exact analytical solution is taken from Reference 31. Section wave drag at seventeen spanwise stations were computed but, as will be discussed later, only nine are necessary for reasonably accurate total wing drag. Again confidence in the numerical solution is gained by the near perfect agreement with analytical solutions.

The final two figures comparing numerical drag calculations of simple planforms with exact solutions give total wing wave drag for biconvex and double wedge airfoil sections. The analytical solutions come directly from the charts of Reference 30 Figure 22 is for the double wedge airfoil wing and Figure 23 for the biconvex airfoil section wing. Both wings have zero taper. Slight discrepancies of up to three to five percent between the numerical and analytical solutions exist at some Mach numbers as seen from the figures. This is due to the numerical integration which smoothes out kinks in the pressure curves and due to truncation errors. However, in light of the accuracy of the exact linear theory compared with experiment, this discrepancy is quite acceptable for design.

All of the preceding cases were for sharp leading and trailing edge wings with simple planforms. For more complicated configurations, closed form linear theory solutions for drag have not been obtained. However, the present method, which determines the source strength locally can still be applied. For

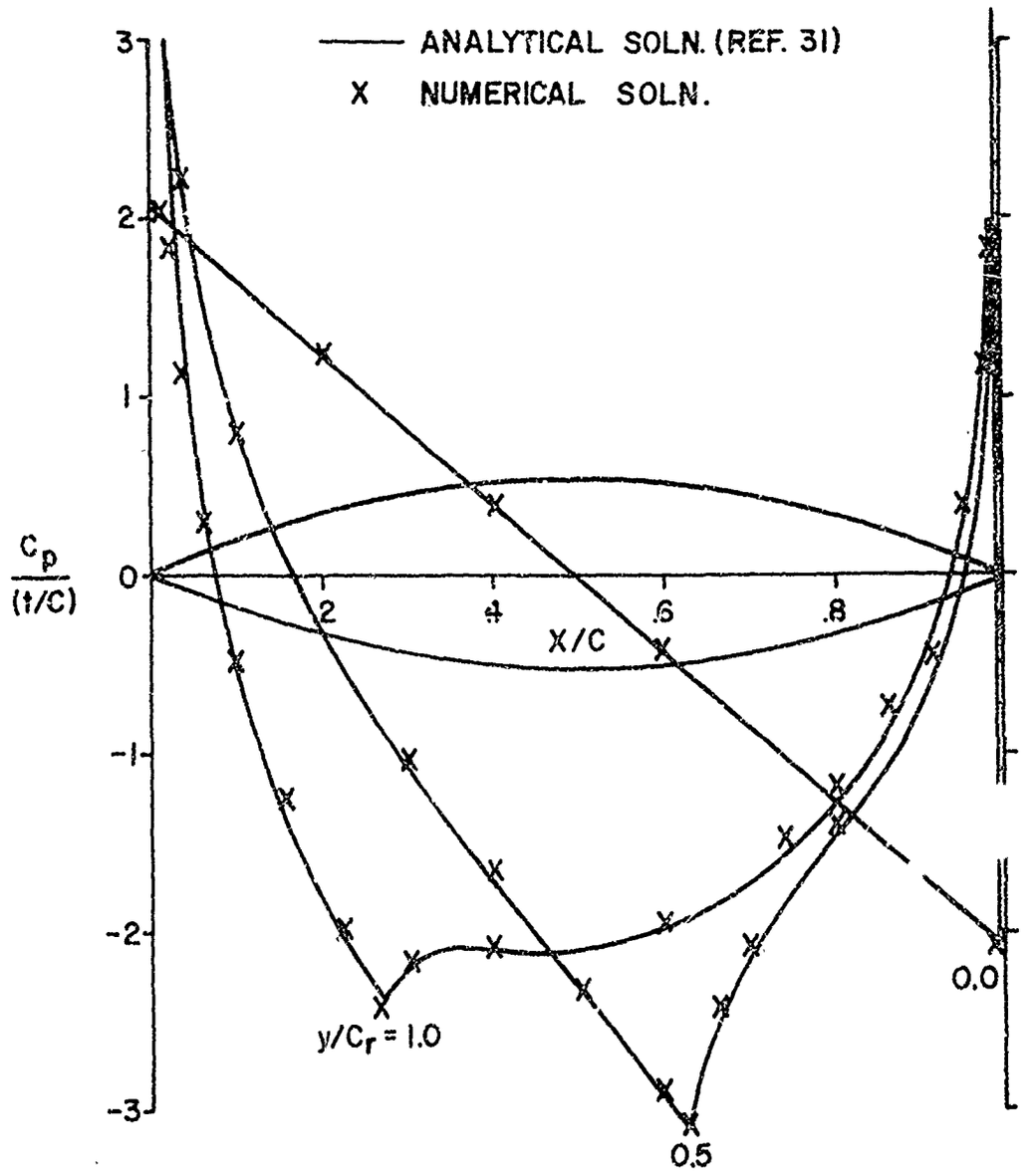

FIGURE 19. PRESSURE DISTRIBUTION ALONG THE SPAN OF A SWEPTBACK WING WITH A SYMMETRICAL CIRCULAR ARC AIRFOIL; $\Lambda_L = 60°$, $M_\infty = 1.4$, $C_t / C_r = 1$.

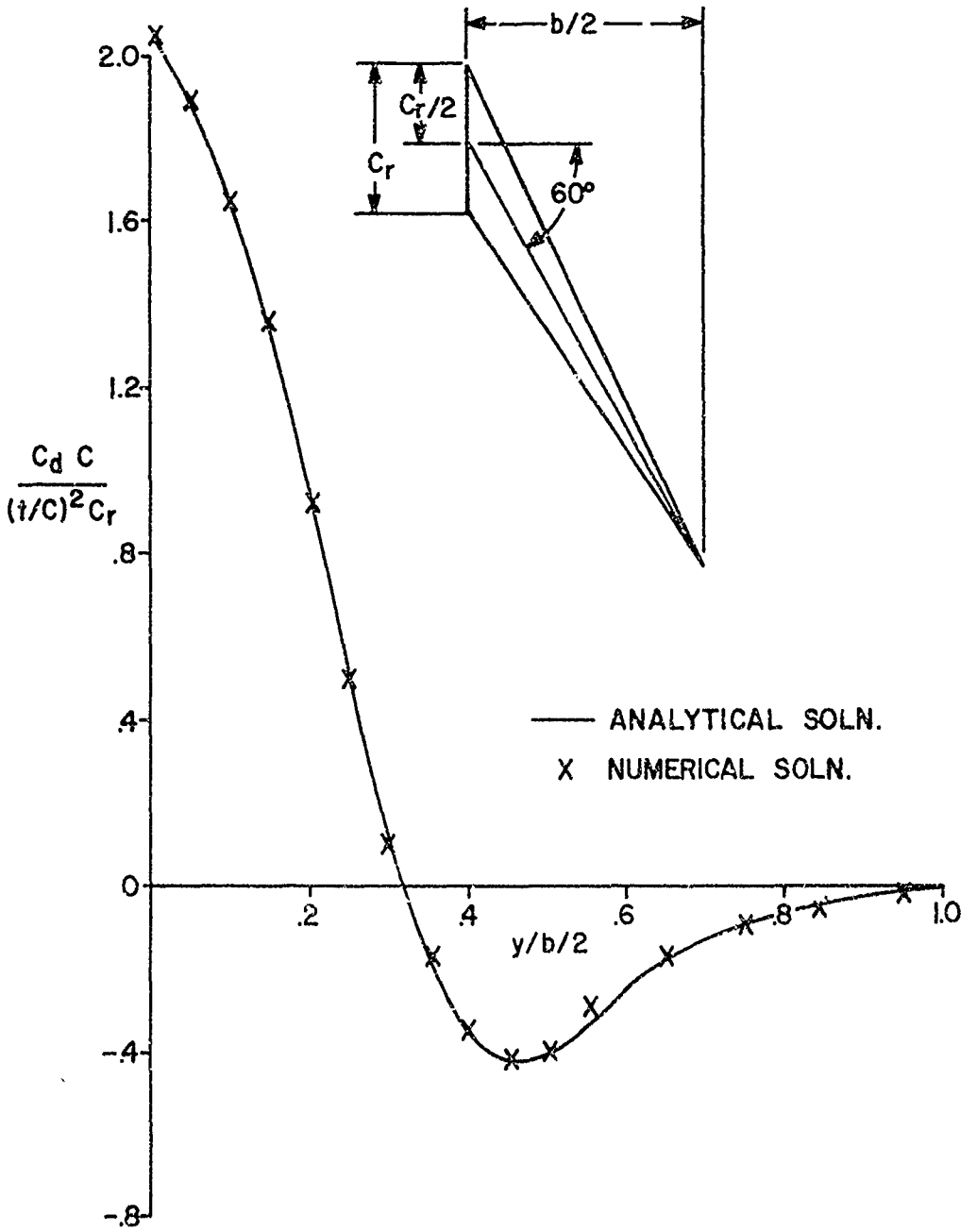

FIGURE 20. SPANWISE WAVE DRAG DISTRIBUTION ON WING WITH DOUBLE WEDGE AIRFOIL SECTION; $AR = 6.92$, $M_\infty = 1.414$, $C_t / C_r = 0$

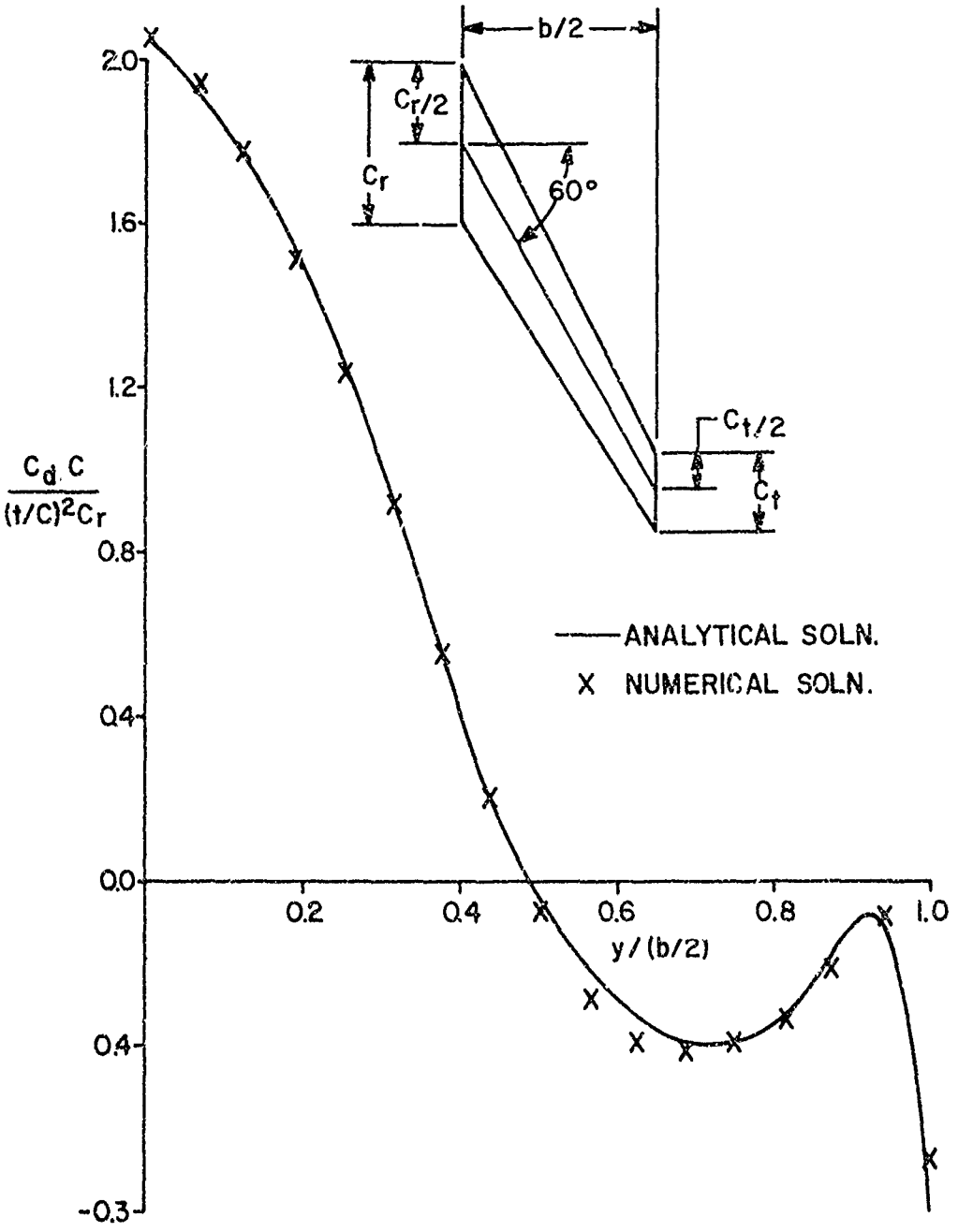

FIGURE 21. SPANWISE WAVE DRAG DISTRIBUTION ON WING WITH WEDGE AIRFOIL SECTION; $AR = 3.26$, $M_\infty = 1.414$, $C_t / C_r = 0.5$

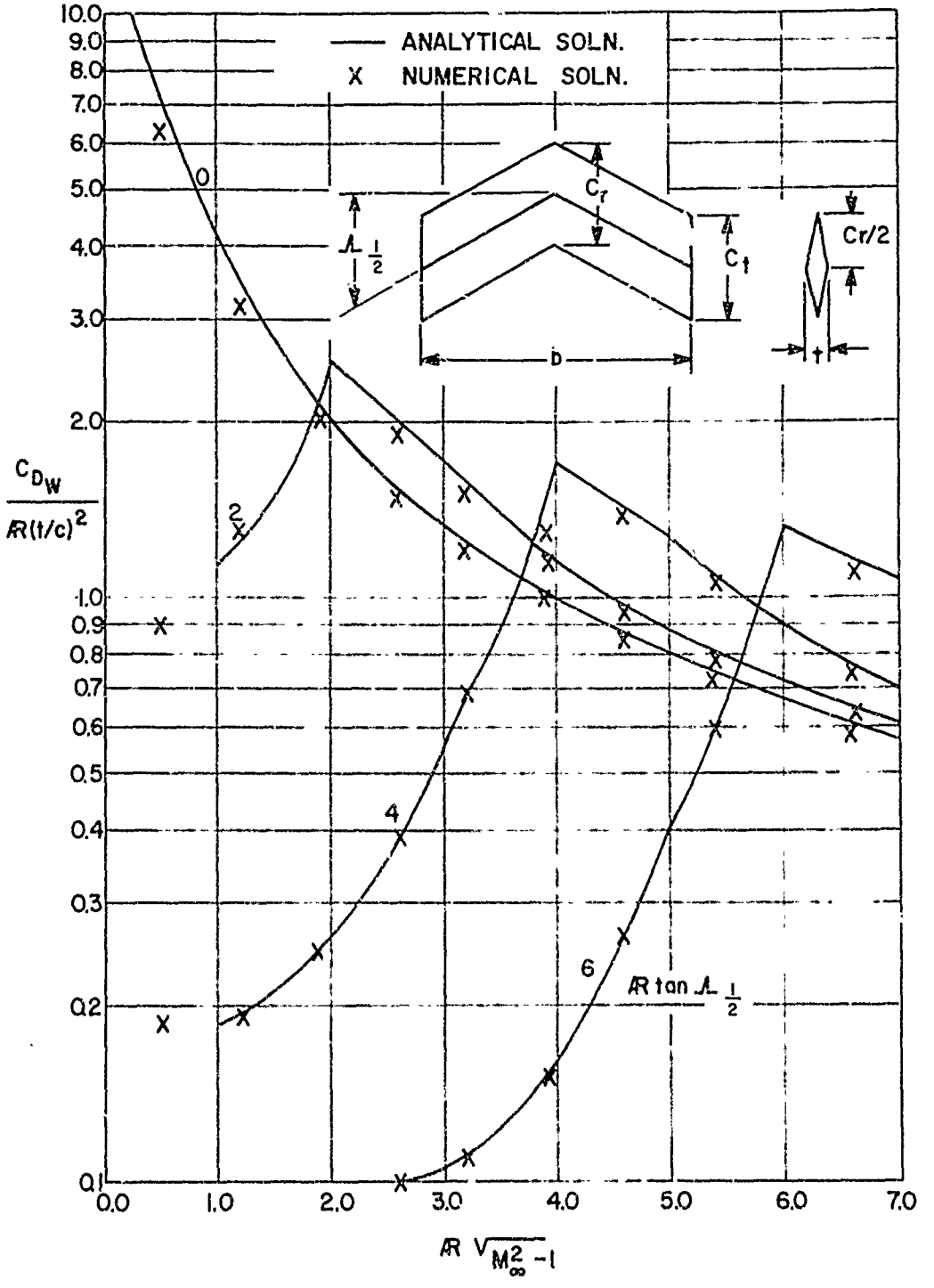

FIGURE 22. WAVE DRAG OF WING WITH DOUBLE WEDGE AIRFOIL SECTION; $C_t / C_r = 1.0$

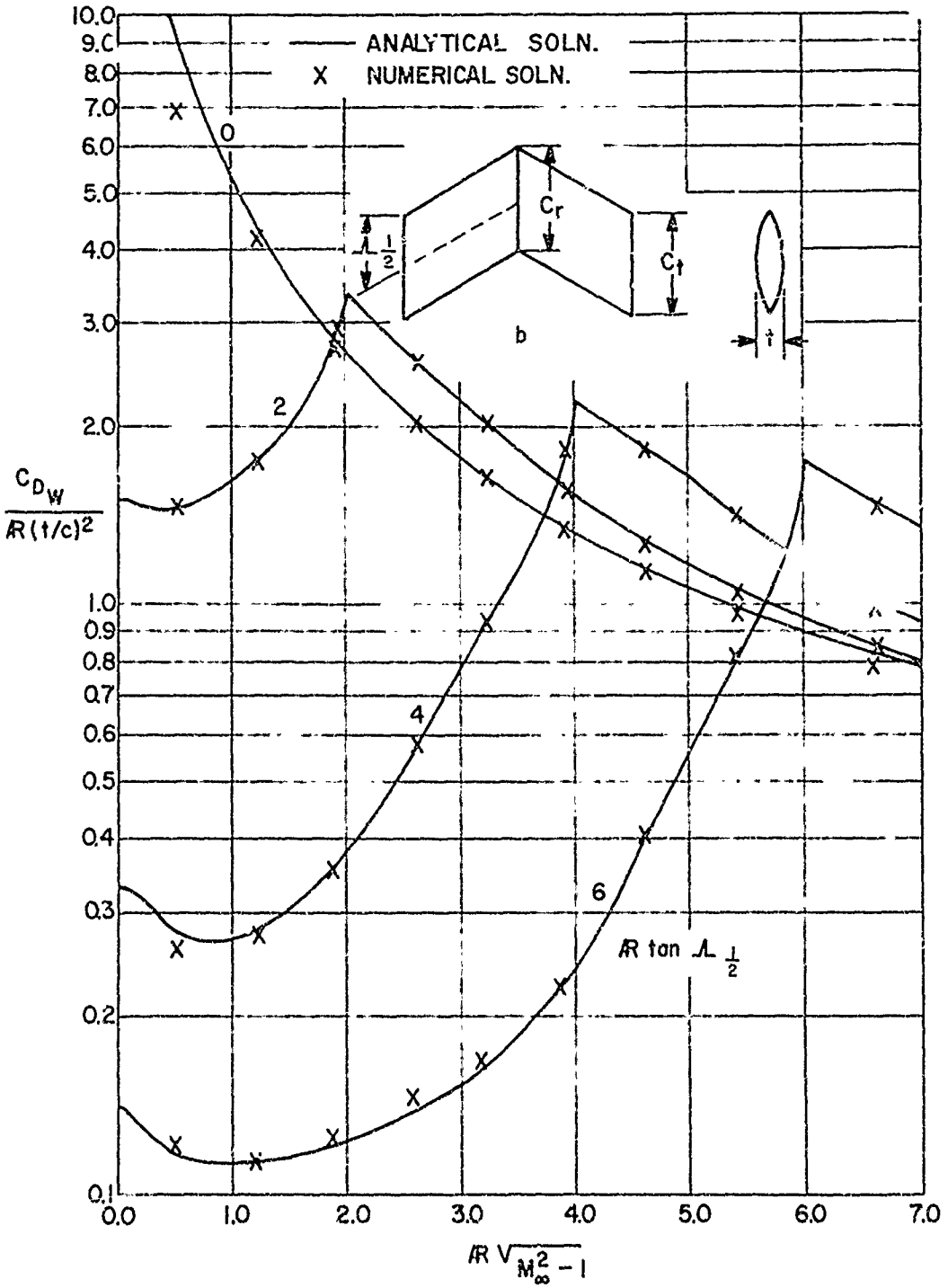

FIGURE 23. WAVE DRAG OF WING WITH BICONVEX AIRFOIL SECTION

example, consider the wing shown in Figure 24. This wing has a variable airfoil section and variable thickness all along the span. Its design is dictated by structural, rather than aerodynamic, considerations. Also shown on the figure is a plot of pressure coefficient along the chord for two spanwise locations.

A second example of wings not covered by exact linear theory is the wing with blunt leading and trailing edges. Figure 25 gives the total drag coefficient (wave plus friction plus trailing edge separation) for a biconvex airfoil with blunt leading and trailing edges and for three Mach numbers. Although no experimental data exist to compare the theory with, the trends are generally what one would expect. That is bluntness has a large effect on drag at high supersonic Mach numbers but at low supersonic Mach numbers, the effect is not so large. However, at these low supersonic Mach numbers the linear theory results for very small bluntness ratios are questionable. This is because in the neighborhood of the leading edge where the slope is near the maximum of fifteen degrees (linear theory starts at slopes of fifteen degrees where Newtonian theory ends), the pressure coefficients predicted by linear theory are quite large. The discontinuity between the pressure coefficient of Newtonian theory and that of perturbation theory is thus much larger. However, as the bluntness ratio is increased the area over which linear theory is applied decreases and hence one expects the results to be somewhat better.

2. Wing Lift

Three cases are considered as test cases to compare the numerical solutions with closed form analytical solutions such as presented in References 32 and 33. These include a wing with subsonic leading and supersonic trailing edges, a wing with supersonic leading and trailing edges with the Mach line intersecting the tip, and a wing with supersonic leading and trailing edges with the Mach line intersecting the trailing edge. Each of these cases is sufficiently different so as to check all methodology developed in the numerical calculation of lift on wings in supersonic flow. The theory used in subsonic flow has been previously verified by Chadwick.[22] Test data must suffice to determine the correctness and accuracy of the transonic methodology.

Figure 26 compares the wing loading along the span of a wing with subsonic leading and supersonic trailing edges corresponding to the first test case above. The Mach lines and regions where linear superposition of solutions occur are indicated on the figure. As is apparent, the numerical solution is the same as the analytical solution to the accuracy of plotting the data.

Figures 27 and 28 compare the analytical and numerical span loading calculations for a supersonic leading and trailing edge wing. In Figure 27, the Mach line just barely intersects the trailing edge whereas in Figure 28 the Mach line

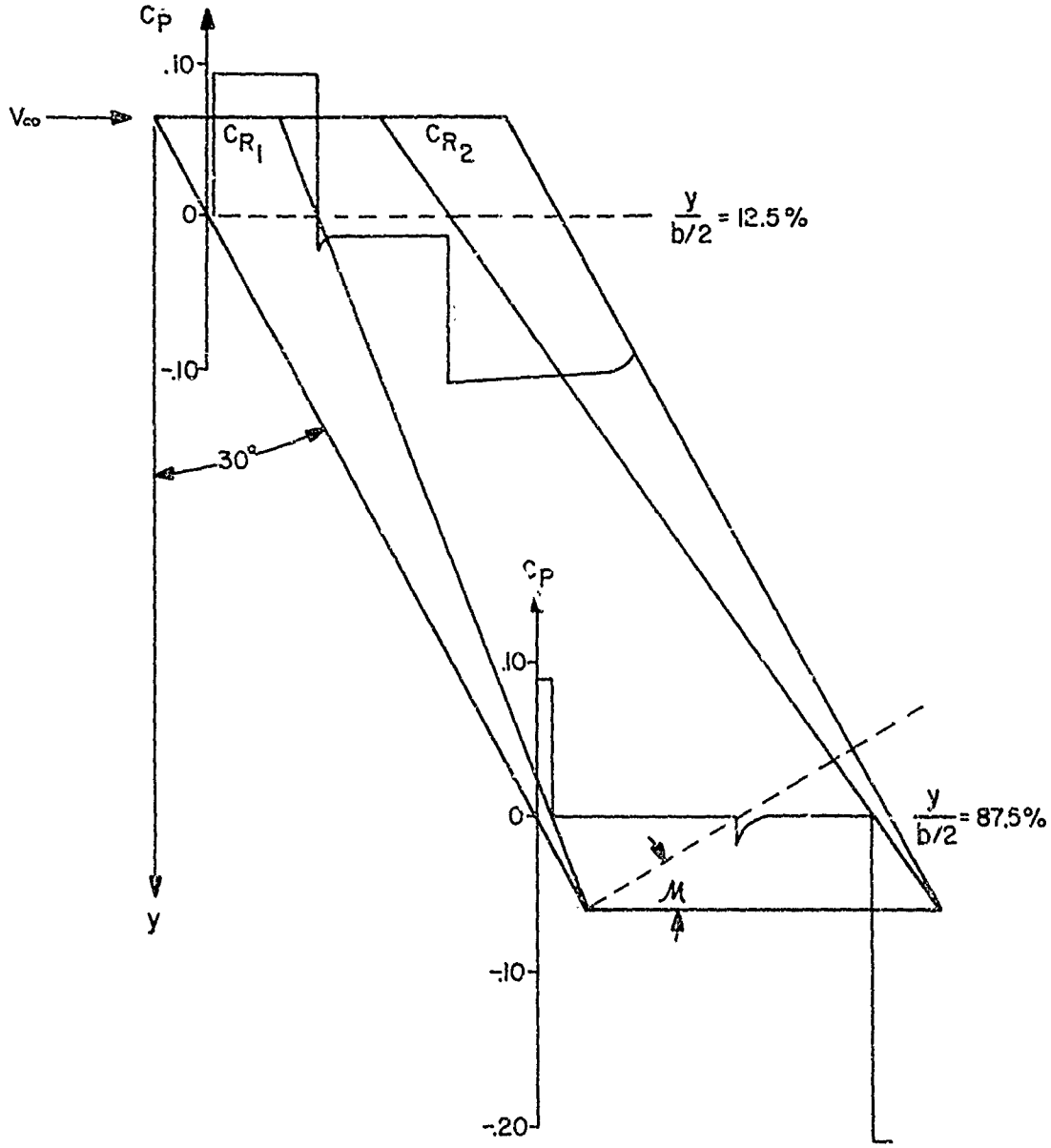

FIGURE 24. PRESSURE COEFFICIENT ON WING WITH MODIFIED DOUBLE WEDGE AIRFOIL SECTION. $M_\infty = 2.0$, $b = 1.02'$, $C_R = .24'$, $C_{R_1} = .086'$, $C_{R_2} = .086'$, $t_R = .0167'$, $t_t = .0042'$.

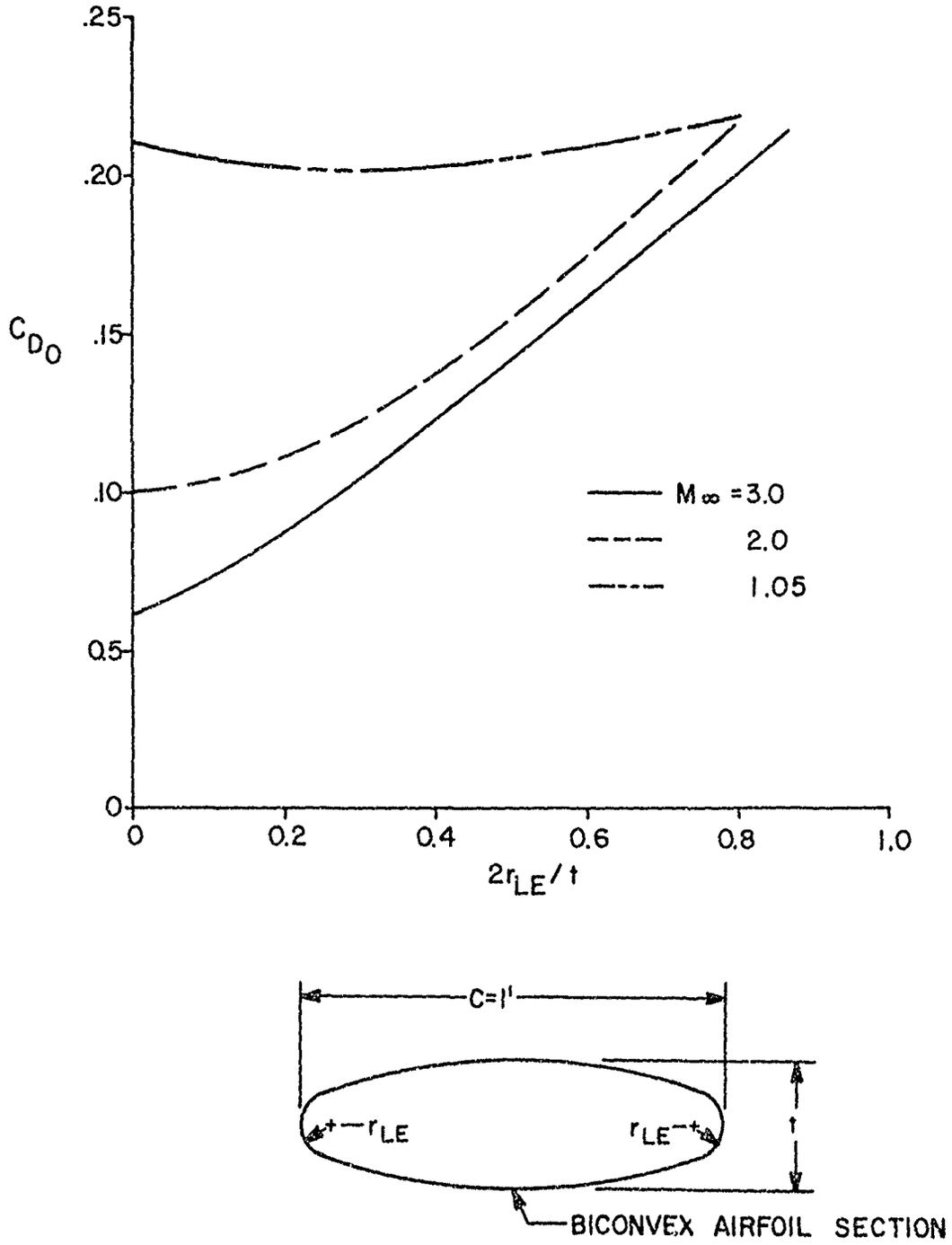

FIGURE 25. ZERO LIFT DRAG OF WINGS AS A FUNCTION OF LEADING EDGE BLUNTNESS; $\mathcal{A}$=2, $\Lambda_1 = \Lambda_4 = 30°$, t/c = 0.12.

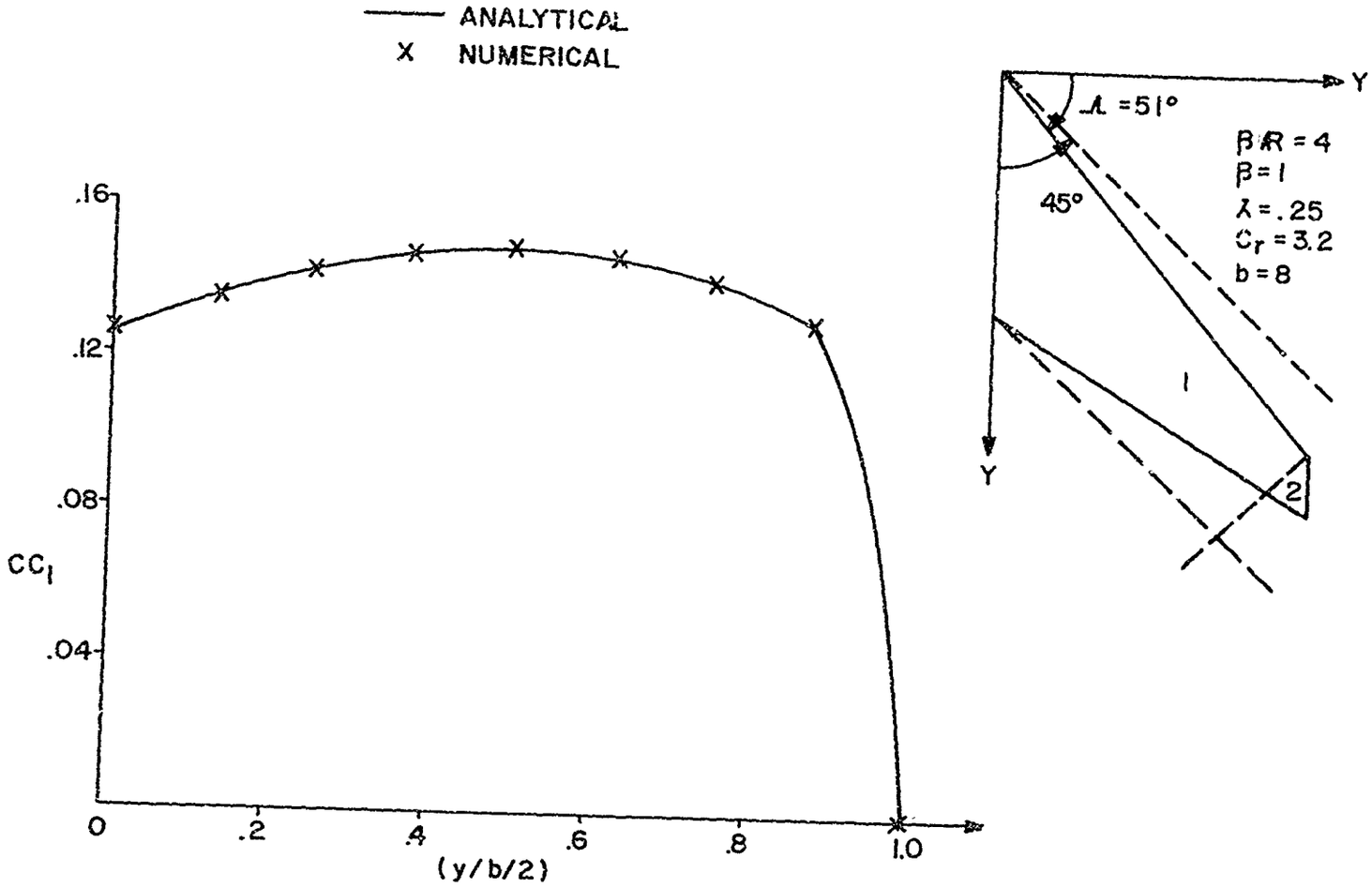

FIGURE 26. WING WITH SUBSONIC LEADING AND SUPERSONIC TRAILING EDGE

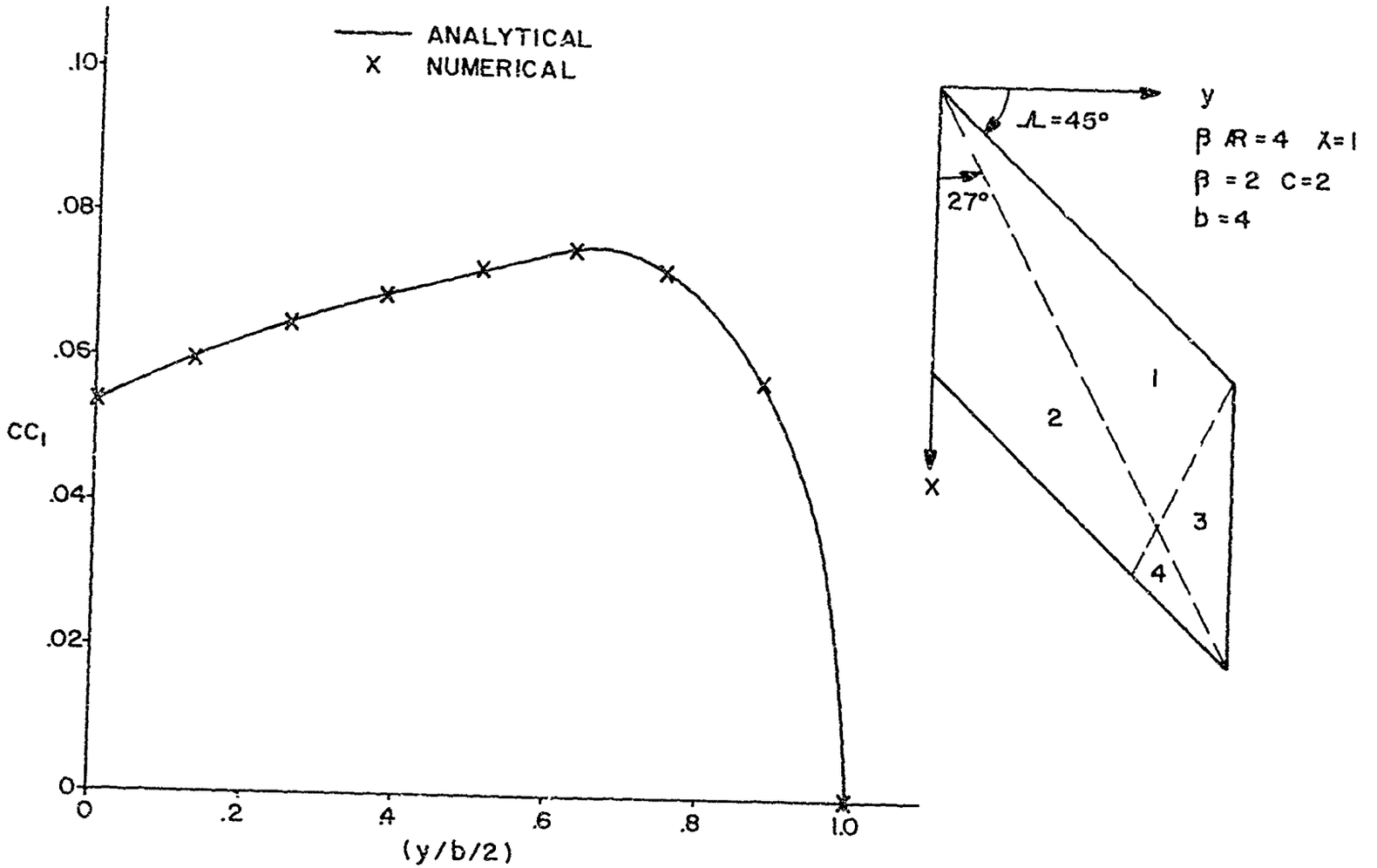

FIGURE 27. WING WITH SUPERSONIC LEADING AND TRAILING EDGES; MACH LINE INTERSECTS TRAILING EDGE.

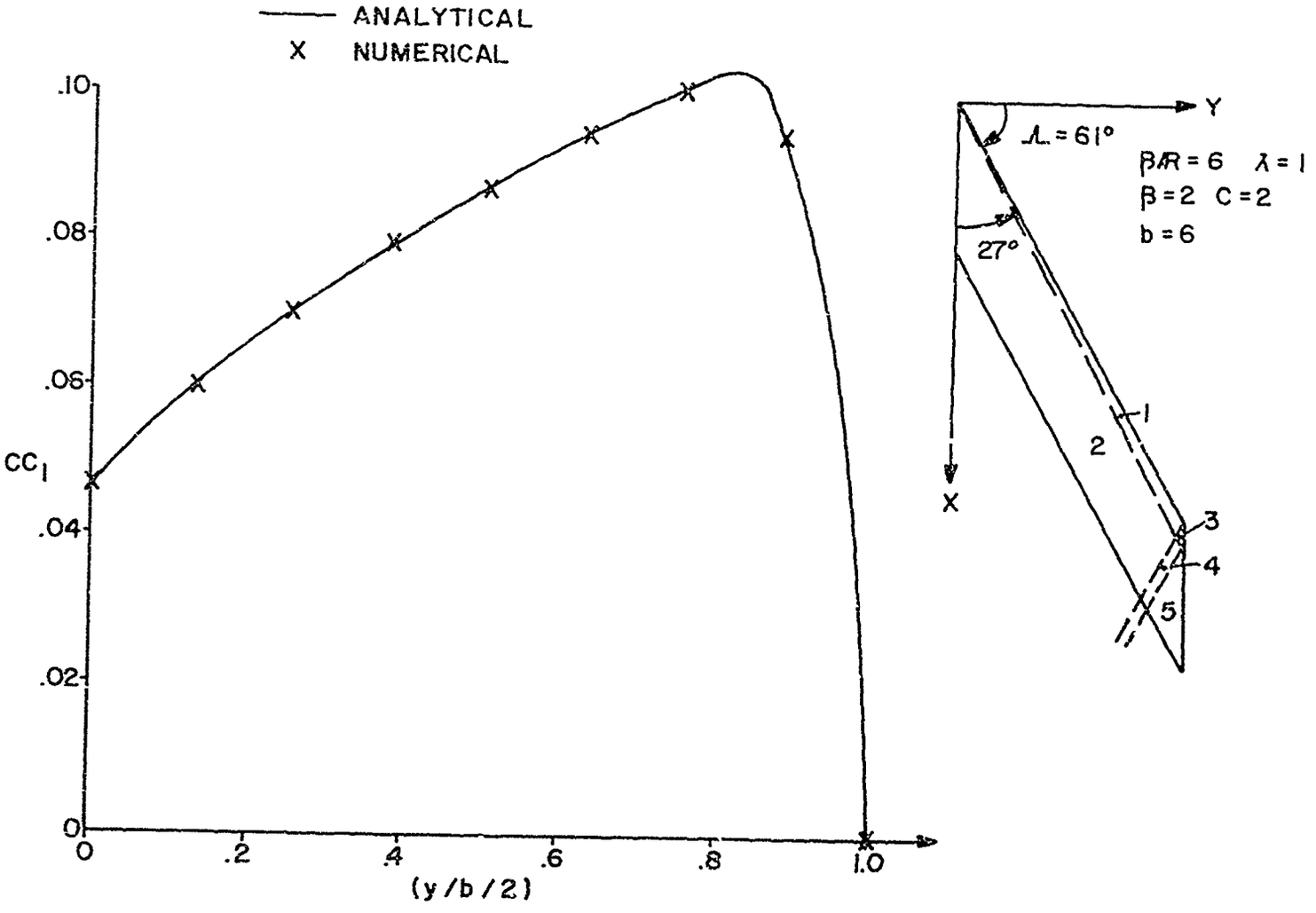

FIGURE 28. WING WITH SUPERSONIC LEADING AND TRAILING EDGES; MACH LINE INTERCEPTS TIP

intersects the tip. In both cases, the analytical solution is reproduced by the numerical procedure.

B. Comparison With Experiment

Several example cases are chosen to compare with experimental data so as to place some degree of accuracy on the theory. The first of these is a ten caliber missile with clipped delta tail fins. The experimental data are taken from Reference 34, which gives the static aerodynamics for $0.8 \leqslant M_\infty \leqslant 1.3$. Figure 29 compares theoretical drag coefficient, normal force coefficient derivative, and center of pressure with the experiment as a function of Mach number and for $\alpha = 1°$. Recall that for $M_\infty \geqslant 1.2$, the lift and drag (except for base drag) was calculated numerically whereas for $0.8 < M_\infty < 1.2$, the theory consists of mostly empirical procedures. For $M_\infty \leqslant 0.8$, the wing lift is calculated analytically but most other force components are computed empirically. With the exception of the normal force coefficient slope at $M_\infty = 0.8$ and 0.85, the theory is well within ten percent of experiment. The maximum error in center of pressure for this configuration is five percent of the length or half a caliber.

The next case considered is again taken from Reference 34 where the same body geometry was tested with several different fins present. The case considered is for aspect ratio two rectangular fins flush with the base. The body is the same as that shown in Figure 29. Figure 30A presents the small angle-of-attack results for C_D, C_{N_α}, and x_{cp} as a function of Mach number and Figure 30B gives C_D, C_N, and x_{cp} as a function of α for Mach number 1.3. In both Figures 30A and 30B, the results are acceptable from an accuracy standpoint, although the drag coefficients at $M_\infty = 1.20$ and 1.3 are off more than for most configurations considered. The reason most likely lies with the empirical estimation of base pressure increase due to presence of fins. At $M_\infty = 1.3$, this component accounts for about 0.05 of the drag coefficient, which, for this wing-body configuration, appears high.

The final example chosen is a complex canard-body-tail configuration. The body nose is sixty percent blunt with two ogive segments and a 0.7 caliber boattail. The canard has an aspect ratio of two with a sweepback angle of 15°. Its shape consists of a sharp wedge leading edge with a constant thickness section following. The trailing edge is truncated parallel to the leading edge. The tail has an aspect ratio of four with cylindrical leading and trailing edges and where $\Lambda_1 = 30°$, $\Lambda_2 = 22.5°$, $\Lambda_3 = 37°$, and $\Lambda_4 = 30°$. The tail thickness to chord ratio also varies along the span. The detailed canard and wing geometry listed above is not needed in calculating lift, but it must be known for drag computations. The results of the calculations for this configuration are shown in Figure 31. Figure 31A gives the

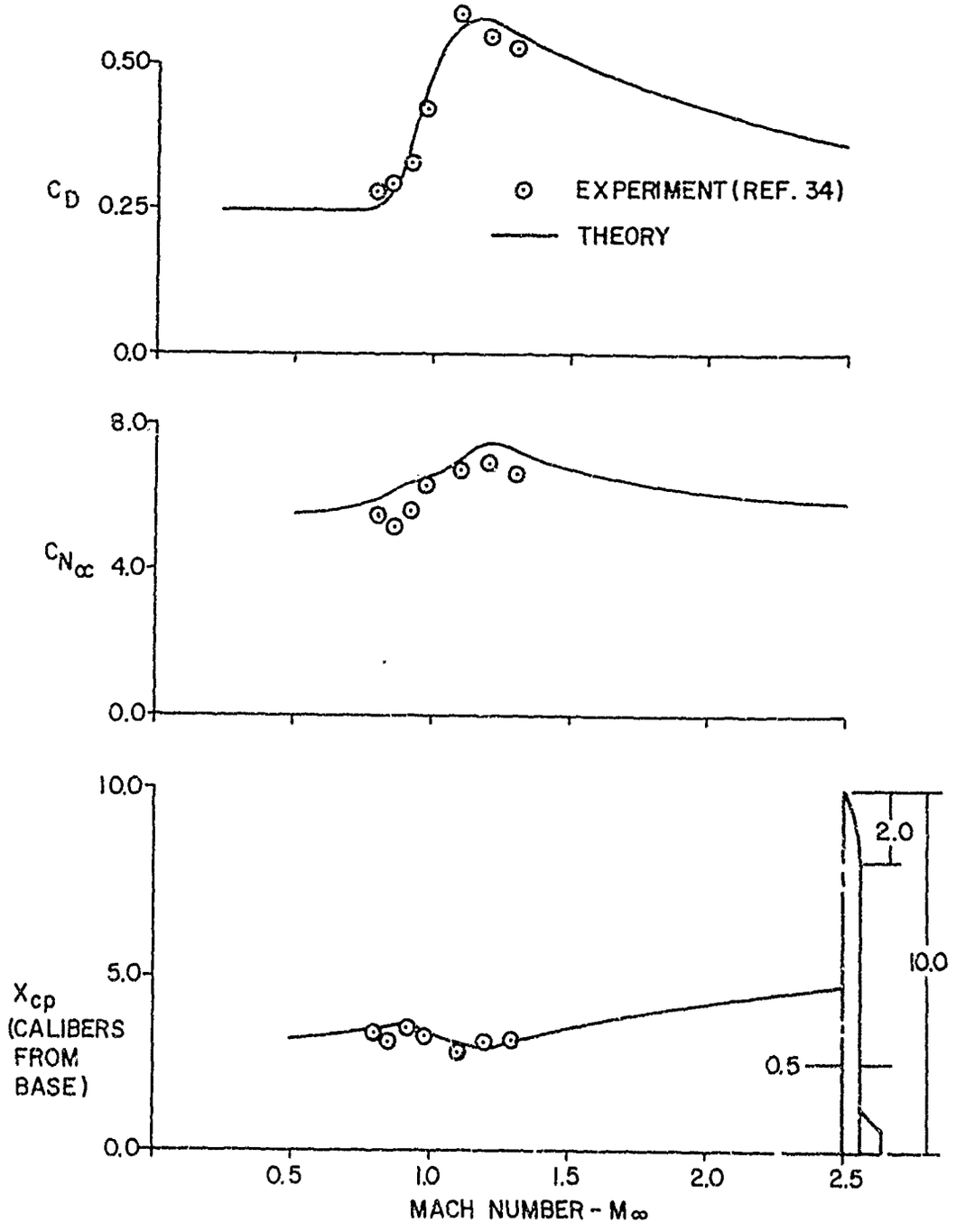

FIGURE 29. STATIC AERODYNAMICS OF A MISSILE CONFIGURATION; $AR = 1.0, \Lambda_{L_1} = 53.1°, \lambda = 0.5, \alpha = 1°$

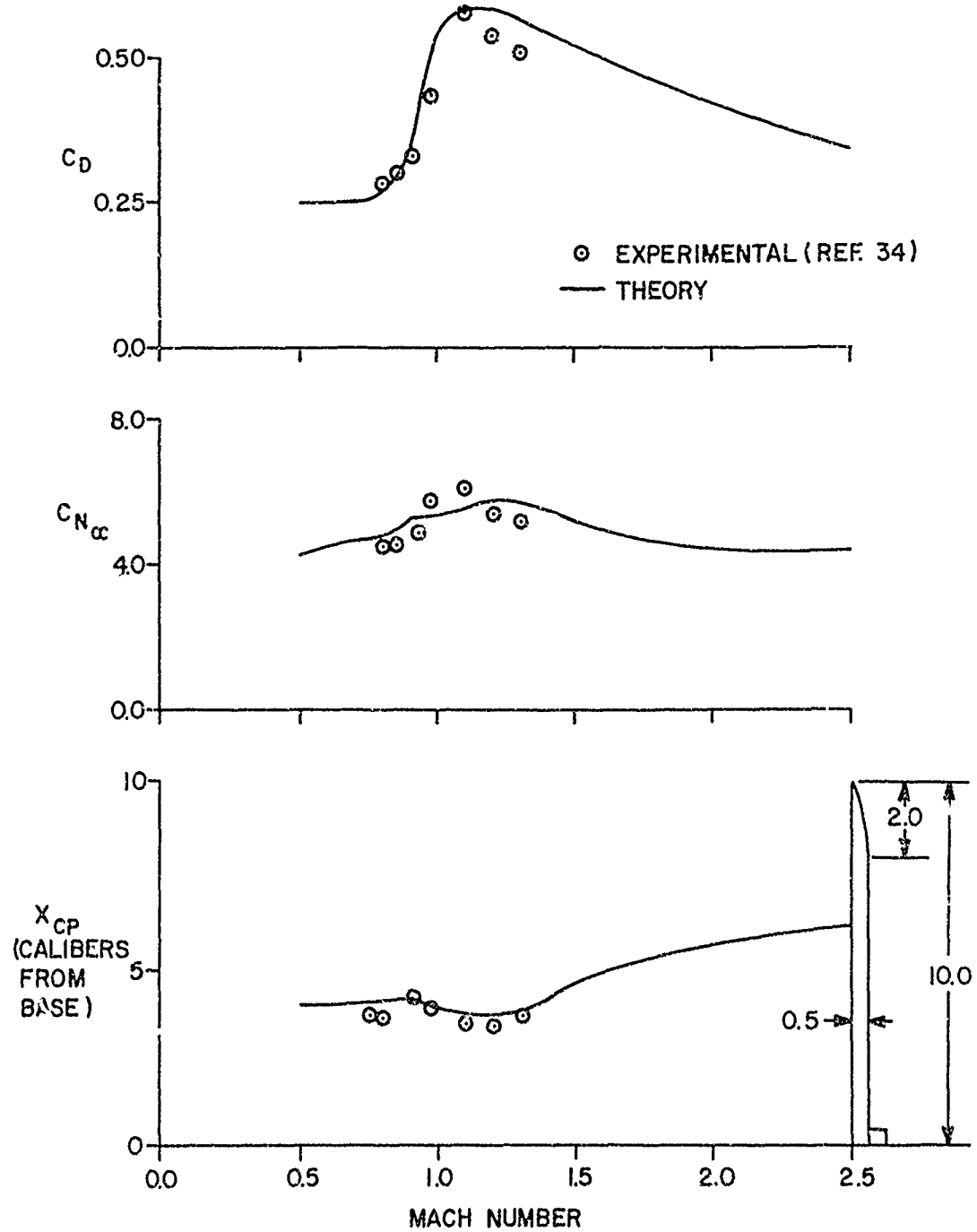

FIGURE 30A. STATIC AERODYNAMICS OF A MISSILE CONFIGURATION; AR=2.0, Λ_{LE} =0°, λ = 1.0 α = 1°

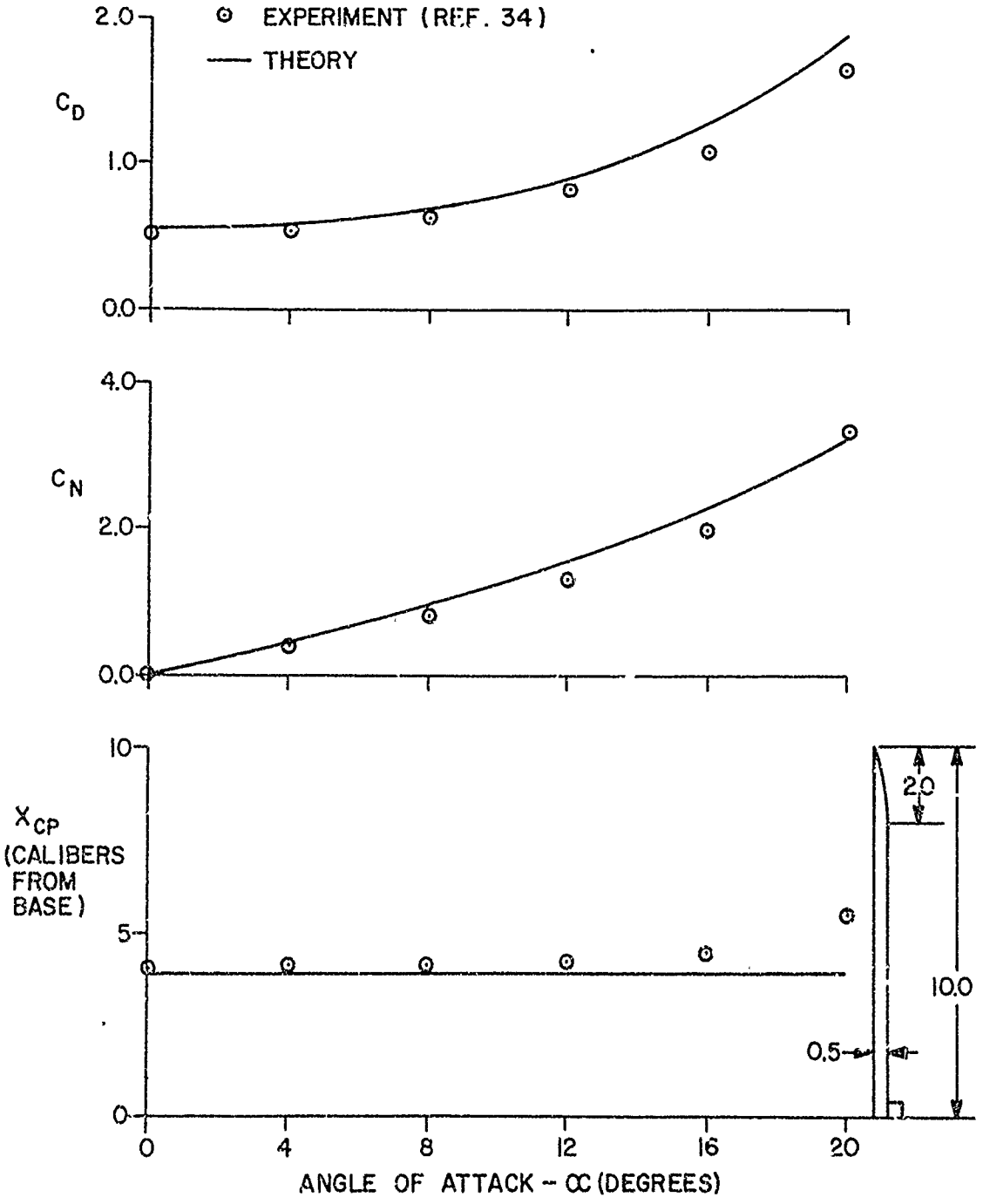

FIGURE 30B. STATIC AERODYNAMICS OF A MISSILE CONFIGURATION ; $AR = 2.0$, $\Lambda_{LE} = 0°$, $\lambda = 1.0$, $M_\infty = 1.3$

normal force and center of pressure for M_∞ = 1.6 and at various angles of attack. Four curves are shown in the figure, canard-body-tail with canards deflected up by ten degrees, canard-body-tail with no canard deflection, body-tail, and finally body alone. Several points are worthy of note in this figure. First of all the body alone solution agrees very well with the unpublished experimental data up to α = 16. Above α = 16°, the theory is low which is probably due to not taking into account Reynold's number effect in the body crossflow drag coefficient. The next point is that for this configuration, the tail lift is about ten percent too high and the canard lift about 15% too low so that the total lift agrees almost perfectly with the experimental data up to the point where stall begins to occur ($\alpha \geq 14°$). This in turn causes the center of pressure to be more rearward than the experimental data suggest by about half a caliber. It is suspected that the theory being high for the high aspect ratio tail and low for the moderate aspect ratio canard is due to the flowfield interaction effects from the complex configuration and will not in general be true for other cases. However, it does indicate that the theory can be used quite effectively in design, even for quite complex wing-body-tail geometries. The final point to be emphasized from Figure 31A is the fact that no attempt has been made to predict stall characteristics. As seen in the figure, for this configuration, stall occurs around α = 15° at M_∞ = 1.6. However, if the wing thickness or freestream Mach number is changed the stalling angle of attack will also change.

The drag characteristics for this same missile are shown in Figure 31B. The drag is shown as a function of Mach number and again the total force is broken down into its components: body alone, body tail, and canard-body-tail The body alone drag is acceptable in supersonic and subsonic flow but is unacceptable in transonic flow where the empirical nature of the theory does not account for nose bluntness correctly. The wing alone drag shown at the bottom figure, includes the increase in base drag due to tails. This causes the tail drag to be high because the theory predicts this base drag increase to be significantly higher than the experimental data suggest. However, the body-tail drag is still within the ±10% catagory. Finally, the canard drag shown at the bottom figure, is added to the body-tail drag and the overprediction of tail drag is compensated somewhat by the under prediction of canard drag.

As was mentioned earlier, the tail has a cylindrical leading edge for which the combined Newtonian perturbation theory must be used to calculate the pressure coefficient Figure 31C presents this pressure coefficient in the vicinity of the leading edge for Mach number two and at a spanwise station of y/(b/2) = 12.5%. The discontinuity in pressure coefficient caused by the difference in Newtonian and perturbation theory estimates occurs at a mach point of x/c = 0.009.

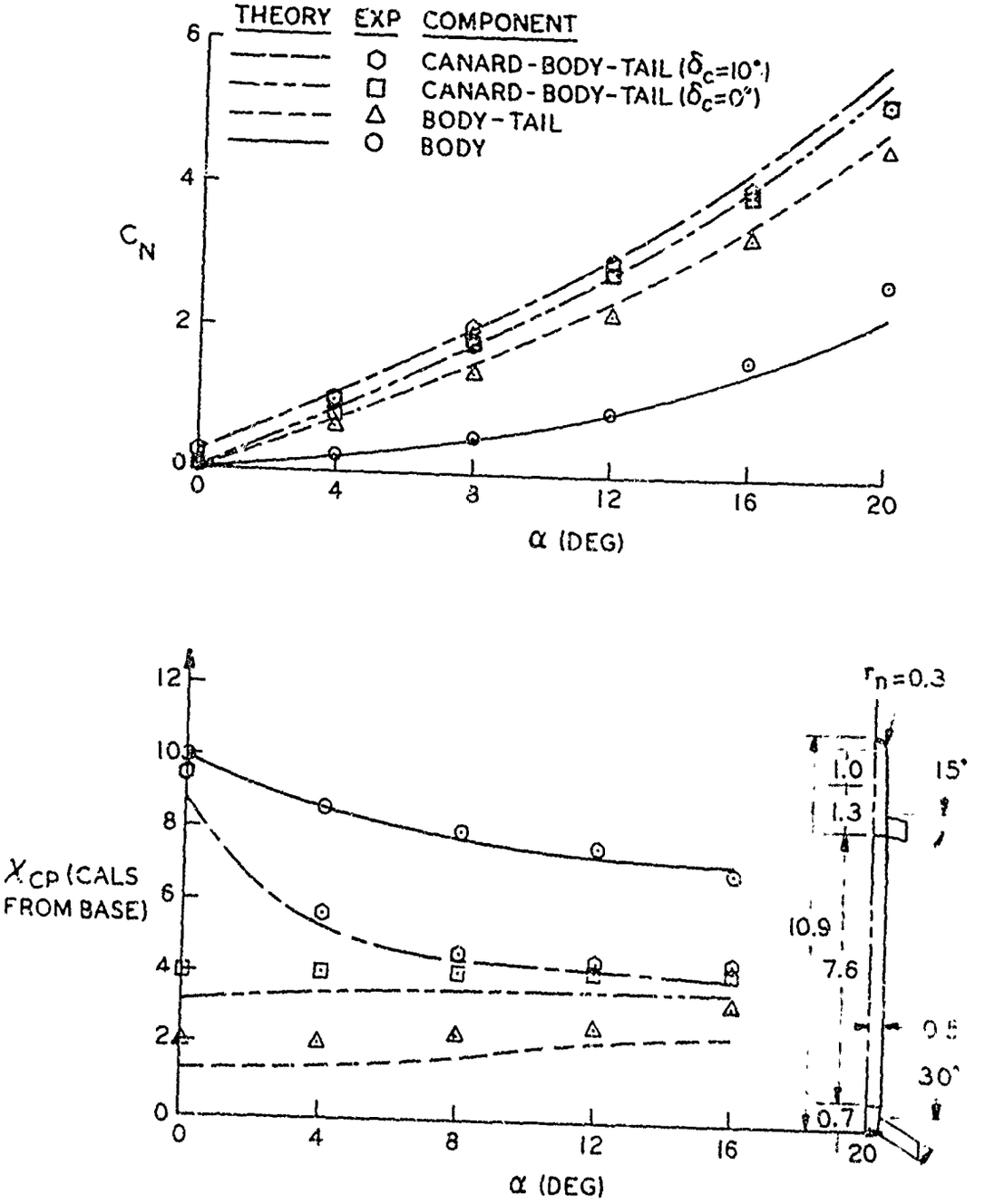

FIGURE 31A. NORMAL FORCES AND CENTER OF PRESSURE OF A MISSILE CONFIGURATION; AR_t=4, AR_c=2, M_∞=1.6

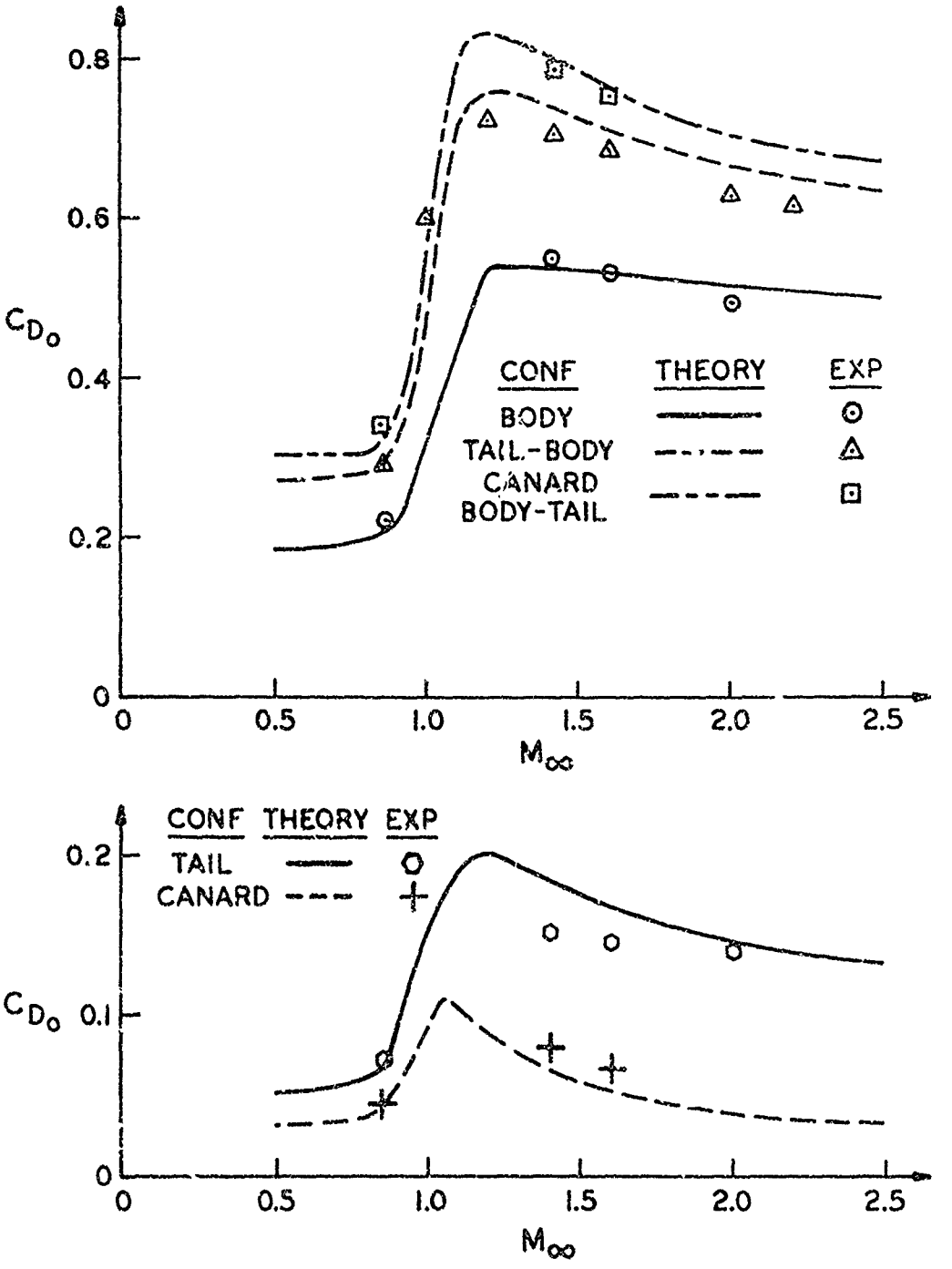

FIGURE 31B. DRAG OF A MISSILE CONFIGURATION AND ITS COMPONENTS

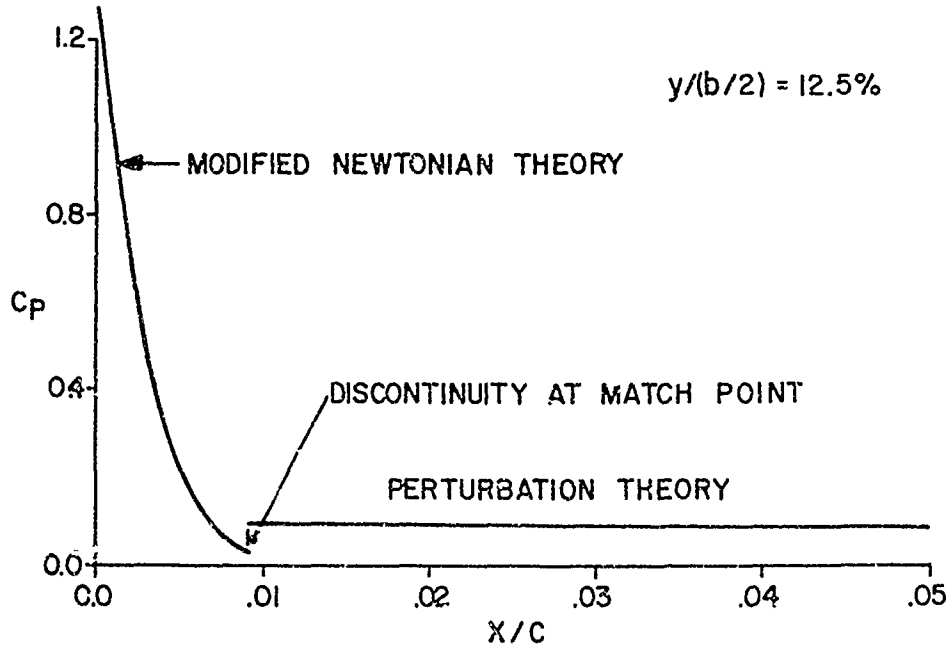

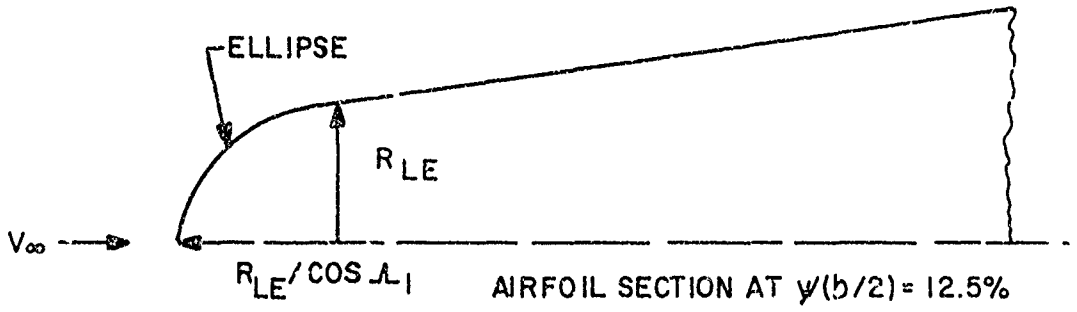

FIGURE 31C. PRESSURE COEFFICIENT ON LEADING EDGE OF A BLUNT LEADING EDGE WING; $\Lambda_1 = 30°$, $M_\infty = 2$, $b = 0.92'$, $C_R = .23'$, $R_{LE} = .0021'$, $t_R = .0167'$, $t_t = .0042'$

C. Computational Time and Cost

Although the method presented herein for computing aerodynamics of guided or unguided projectiles actually consists of several rather complicated theoretical and empirical procedures, the cost to obtain force and moment predictions is relatively small. For example, the most complicated configuration considered to date was the canard-body-tail shape in Figure 31. To compute the aerodynamics at ten Mach numbers for a small angle-of-attack takes about five minutes on the CDC 6700 computer or costs about $75. Aerodynamics at supersonic Mach numbers costs about twice as much per Mach number than at subsonic or transonic Mach numbers. If the body has a pointed nose, or if there are no canards, or if the tails are absent, the above time and cost can be reduced considerably. For example, consider the pointed body-tail configurations of Figures 29 and 30. These take less than two minutes of execution time for ten Mach numbers and cost about $25. It is thus believed that the present method is very cost effective compared to experimental method. in that reasonably accurate results for forces and moments can be obtained at a relatively small cost.

IV. CONCLUSIONS AND RECOMMENDATIONS

1. A general method has been developed consisting of several theoretical and empirical procedures to calculate lift, drag, and center of pressure on wing-body-tail configurations from Mach number zero to about three and for angles of attack to about fifteen degrees.

2. Comparison of this method with experiment for several configurations indicates that accuracies of ±10% can be obtained for force coefficients of most configurations. This is at a cost of $75 or less for ten Mach numbers in the range $0 \leqslant M_\infty \leqslant 3$.

3. First-order theory can be used in conjunction with modified Newtonian theory, to calculate wave drag on wings with blunt leading edges. However, at low supersonic Mach numbers ($M_\infty < 1.5$) relatively large discontinuities in pressure coefficient exist at the match point.

4. Wave drag of wings with variable airfoil section and thickness to chord ratio along the span can still be calculated by conical flow theory if the local source strength is computed at each point on the wing based on the local slope at the point.

5. Changes in body base pressure due to the presence of tail surfaces is not known sufficiently for all airfoil shapes. It is recommended that a systematic wind tunnel study be conducted for Mach number, $0 \leqslant M_\infty \leqslant 3$, angle of attack, $0 \leqslant \alpha \leqslant 20°$, and various airfoil geometries to empirically estimate this change.

6. Although much progress has been made in transonic flow theory, no simple method exists for calculating wing lift or wave drag on complicated wing configurations. It is thus recommended that much work continue in this area until practical tools are developed.

REFERENCES

1. Moore, F. G., *"Body Alone Aerodynamics of Guided and Unguided Projectiles at Subsonic, Transonic, and Supersonic Mach Numbers"*, NWL TR-2796, 1972.

2. Saffell, B. F., Jr.; Howard, M. L.; Brooks, F. N., Jr.; *"A Method for Predicting the Static Aerodynamic Characteristics of Typical Missile Configurations for Angles-of-Attack to 180 Degrees"*, NSRDC Report 3645, 1971.

3. Whyte, R. H., *"'Spinner' – A Computer Program for Predicting the Aerodynamic Coefficients of Spin Stabilized Projectiles"*, General Electric Class 2 Reports, 1969.

4. Woodward, F. A., *"Analysis and Design of Wing-Body Combinations at Subsonic and Supersonic Speeds"*, Journal of Aircraft, Vol. 5, No. 6, 1968, pp. 528-534.

5. Van Dyke, M. D., *"First and Second-Order Theory of Supersonic Flow Past Bodies of Revolution"*, JAS, Vol. 18, No. 3, March 1951, pp. 161-179.

6. Tsien, H. S.; *"Supersonic Flow Over an Inclined Body of Revolution"*, JAS Vol. 5, No. 12, October 1938, pp. 480-483.

7. Wu, J. M.; Aoyoma, K.; *"Transonic Flow-Field Calculation Around Ogive Cylinders by Nonlinear-Linear Stretching Method"*, U. S. Army Missile Command Technical Report No. RD-TR-70-12, April 1970. Also AIAA 8th Aerospace Sciences Meeting, AIAA Paper 70-189, January 1970.

8. Wu, J. M., Aoyoma, K.; *"Pressure Distribution for Axisymmetric Bodies with Discontinuous Curvature in Transonic Flow"*, U. S. Army Missile Command Technical Report No. RD-TR-70-25, November 1970.

9. Van Driest, E. R.; *"Turbulent Boundary Layer in Compressible Fluids"*, JAS, Vol. 18, No. 3, 1951 pp. 145-160, 216.

10. Allen, J. H.; Perkins, E. W.; *"Characteristics of Flow Over Inclined Bodies of Revolution"*, NACA RM A 50L07, 1965.

11. Jackson, C. M., Jr.; Sawyer, W. C.; Smith, R. S.; *"A Method for Determining Surface Pressures on Blunt Bodies of Revolution at Small Angles-of-Attack in Supersonic Flow"*, NASA TN D-4865, 1968.

12. Powers, S. A., Niemann, A. F.; Der, J.; *"A Numerical Procedure for Determining the Combined Viscid-Inviscid Flow-Fields Over Generalized Three-Dimensional Bodies"*, Volume I: Discussion of Methods and Results and Instructions for Use of Computer Program, AFFDL-TR-67-124, Vol. I, 1967.

13. Ferri, Antonio, Elements of Aerodynamics of Supersonic Flows, The MacMillan Company, New York, 1949, pp. 292-343.

14. Puckett, A. E., *"Supersonic Wave Drag of Thin Airfoils"*, JAS, September 1946, pp. 475-484.

15. Chapman, D. R., Wimbrow, W. R.; Kester, R. H.; *"Experimental Investigation of Base Pressure on Blunt-Trailing-Edge Wings at Supersonic Velocities"*, NACA Rep 1109, 1952 (supersedes NACA TN-2611).

16. Heyser, A., Maurer, F.; and Oberdorffer, E.; *"Experimental Investigation on the Effect of Tail Surfaces and Angle-of-Attack on Base Pressure in Supersonic Flow"*, Conference Proceedings: The Fluid Dynamic Aspects of Ballistics, AGARD-CP-10, 1966, pp. 263-290.

17. Spahr, J. R. and Dickey, R. R.; *"Effect of Tail Surfaces on the Base Drag of a Body of Revolution at Mach Numbers of 1.5 and 2.0"*, NACA TN-2360, 1951.

18. Love, E. S.; *"Base Pressure at Supersonic Speeds on Two-Dimensional Airfoils and on Bodies of Revolution With and Without Turbulent Boundary Layers"*, NACA TN-3819, 1957.

19. Krens, F. J., *"Full-Scale Transonic Wind Tunnel Test of the 8-Inch Guided Projectile"*, NWL TR-2535, 1971.

20. Shapiro, A. H., *The Dynamics and Thermodynamics of Compressible Fluid Flow*, Vol I, The Ronald Press Company, New York.

21. Ashley, H., Landahl, M.; Aerodynamics of Wings and Bodies, Addison-Wesley Publishing Company, Reading, Massachusetts.

22. Chadwick, W. R., *"The Application of Non-Planar Lifting Surface Theory to the Calculation of External Store Loads"*, Complete 1972.

23. Jones, R. T. Cohen Doris; High Speed Wing Theory, Princeton Aeronautical Paperbacks, Number 6 [illegible]

24. Douglas Aircraft Co., Inc.: **USAF Stability and Control DATCOM,** Revisions by Wright Patterson Air Force Base, July 1963, 2 Vols.

25. Lowry, J. G.; Polhamus, E. C.; *"A Method for Predicting Lift Increments Due to Flap Deflection at Low Angles-of-Attack in Incompressible Flow"*, NACA TN-3911, 1957.

26. Pitts, W. C.; Nielsen, J. N.; Kaattari, G. E.; *"Lift and Center of Pressure of Wing-Body-Tail Combinations at Subsonic, Transonic, and Supersonic Speeds"*, NACA TR 1307, 1957.

27. Morikawa, George; *"Supersonic Wing-Body-Lift"*, JAS, Vol. 18, April 1951, pp. 217-228.

28. Neilsen, J. N.; Pitts, W. C.; *Wing-Body Interference at Supersonic Speeds With an Application to Combinations With Rectangular Wings"*, NACA TN 2677, 1952.

29. Eaton, P. T.; *"A Method for Predicting the Static Aerodynamic Characteristics of Low-Aspect Ratio Configurations"*, NSRDC Rpt. 2216, AD 647234, 1966.

30. Bishop, R. A. and Cane, E. G.; *"Charts of the Theoretical Wave Drag of Wings at zero Lift"*, R.A.E. Tech. Note AERO 2421, 1956.

31. Margolis, Kenneth; *"Supersonic Wave Drag of Sweptback Tapered Wings at Zero Lift"*, NACA TN 1448, 1947.

32. Hannah, M. E. and Margolis, K.; *"Span Load Distribution Resulting From Constant Angle-of-Attack, Steady Rolling Velocity, Steady Pitching Velocity, and Constant Vertical Acceleration for Tapered Sweptback Wings With Streamwise Tips"*, NACA TN 2831, 1952.

33. Martin, J. C. and Jeffreys, I.; *"Span Load Distribution Resulting From Angle-of-Attack, Rolling, and Pitching for Tapered Sweptback Wings With Streamwise Tips"*, NACA TN 2643, 1952.

34. Craft, J. C. and Skorupski, J.; *"Static Aerodynamic Stability Characteristics of Munitions Designs at Transonic Mach Numbers"*, U. S. Army Missile Command, Redstone Arsenal, Alabama, 1973.

APPENDIX A

GEOMETRY FOR BLUNT LEADING EDGE WING

Assuming the wing has a cylindrical leading edge when viewed in a plane normal to the wing, it will have an elliptical cross-section when viewed in a plane parallel to the freestream. The equation of an ellipse is:

$$\frac{x^2}{a_1^2} + \frac{z^2}{a_2^2} = 1 \tag{A-1}$$

where a_1 and a_2 are the semi-major and semi-minor axis, respectively. If the radius of the cylindrical leading edge is denoted by r_{LE} then:

$$a_1 = r_{LE}/\cos \Lambda_1 \tag{A-2}$$

$$a_2 = r_{LE}$$

Differentiating Equation (1), the local slope at any point along the elliptical airfoil leading edge is:

$$\left(\frac{dz}{dx}\right) = \frac{\cos \Lambda_1}{z} \left[r_{LE} - x \cos \Lambda_1\right] \tag{A-3}$$

Defining δ as the angle which the tangent to the surface at the point x,y,z makes with the x axis, then

$$\delta(x,y,z) = \tan^{-1} \left(\frac{dz}{dx}\right) = \tan^{-1} \left\{\frac{\cos \Lambda_1}{z} \left[r_{LE}(y) - x \cos \Lambda_1\right]\right\} \tag{A-4}$$

Here the leading edge radius, r_{LE}, is allowed to vary in the spanwise direction.

Now if it is desired to determine the coordinates of a given point on the ellipse given a value of δ, then Equations (A-1) and (A-2) can be solved simultaneously to obtain:

$$x = \frac{r_{LE}(y)}{\cos \Lambda_1} \left[1 - \sqrt{1 - F} \right] \qquad \text{(A-5)}$$

$$z = \frac{r_{LE}(y) \cos \Lambda_1}{\tan \delta} \left[1 - \frac{x \cos \Lambda_1}{r_{LE}(y)} \right] \qquad \text{(A-6)}$$

where

$$F = \frac{\left(\frac{\cos \Lambda_1}{\tan \delta} \right)^2}{1 + \left(\frac{\cos \Lambda_1}{\tan \delta} \right)^2}$$

APPENDIX B

NEWTONIAN WAVE DRAG COEFFICIENT OF BLUNT LEADING EDGE WING

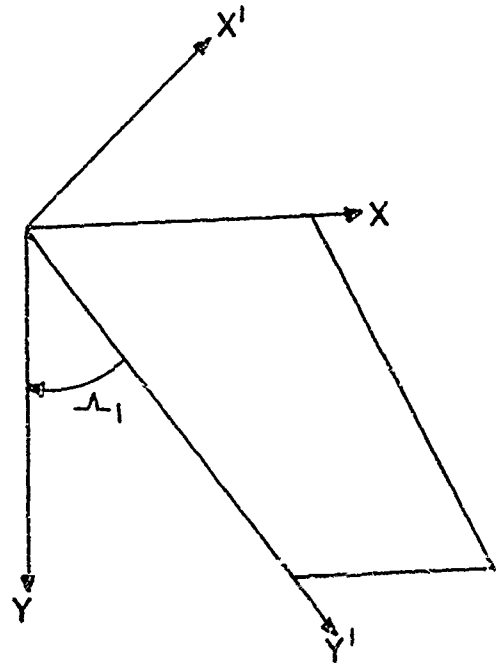

The wing planform and coordinate systems are shown in the above sketch. Consider a cross-section perpendicular to the leading edge or along the x′ axis. The leading edge will be cylindrical in shape as seen below.

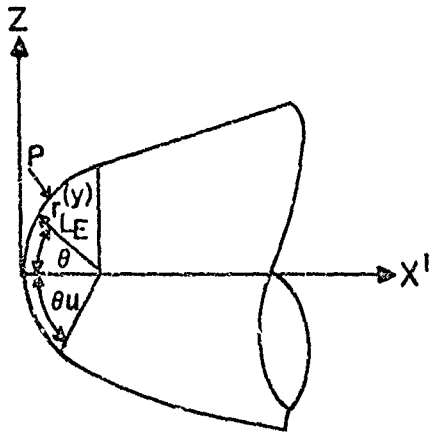

The elemental force acting on the surface area of the wing leading edge is:

$$dC_{x'} = \frac{P \cos \theta}{\frac{1}{2} \rho_\infty V_\infty^2 S_{ref}} \, dA \tag{B-1}$$

where

$$dA = r_{LE}(y')d\theta dy'$$

Hence, for one fin we have

$$C_{x'} = \frac{1}{S_{ref}} \int_{-\theta_u}^{\theta_u} \int_0^{b/(2 \cos \Lambda_1)} \frac{P - P_\infty}{\frac{1}{2} \rho_\infty V_\infty^2} \cos \theta r_{LE}(y')d\theta dy'$$

$$+ \frac{P_\infty}{S_{ref} \frac{1}{2} \rho_\infty V_\infty^2} \int_{-\theta_u}^{\theta_u} \int_0^{b/(2 \cos \Lambda_1)} \cos \theta r_{LE}(y')d\theta dy' \tag{B-2}$$

But the last integral of Equation (B-2) is zero when considered over the entire airfoil surface so Equation (B-2) may be written:

$$C_{x'} = \frac{2}{S_{ref}} \int_0^{\theta_u} \int_0^{b/(2 \cos \Lambda_1)} C_p \cos \theta r_{LE}(y')d\theta dy' \tag{B-3}$$

For modified Newtonian theory,

$$C_p = C_{p_0} \cos^2 \theta \tag{B-4}$$

where θ is the angle between a normal to the surface and the freestream velocity vector.

To find θ define $\hat{\eta}$ as the unit vector normal to the surface so:

$$\hat{\eta} = \eta_{x'}\hat{e}_{x'} + \eta_{y'}\hat{e}_{y'} + \eta_{z'}\hat{e}_{z'} \tag{B-5}$$

Here $\eta_{x'}$, $\eta_{y'}$, $\eta_{z'}$ are the direction cosines in the $\hat{e}_{x'}$, $\hat{e}_{y'}$, $\hat{e}_{z'}$ directions, respectively and are $\eta_{x'} = \cos\theta$, $\eta_{y'} = 0, \eta_{z'} = \sin\theta$. Now according to the dot product of two vectors, $A \cdot B = |A||B|\cos\theta$, one may write:

$$\cos\theta = \frac{\overline{V}_\infty \cdot \hat{\eta}}{|V_\infty| \, |\eta|} \tag{B-6}$$

But,

$$\overline{V}_\infty = u'_\infty \hat{e}_{x'} + v'_\infty \hat{e}_{y'} + w'_\infty \hat{e}_{z'} \tag{B-7}$$

where

$u'_\infty = V_\infty \cos \Lambda_1$, $v'_\infty = V_\infty \sin \Lambda_1$, and $w'_\infty = 0$.

Substituting (B-5) and (B-7) into (B-6) and performing the dot product there is obtained:

$$\cos\theta = \cos\Lambda_1 \cos\theta \tag{B-8}$$

Thus,

$$C_P = C_{P_0} \cos^2 \Lambda_1 \cos^2 \theta$$

and (B-3) becomes:

$$C_{x'} = \frac{2\cos^2 \Lambda_1}{S_{ref}} \int_0^{b/(2\cos\Lambda_1)} \left[r_{LE}(y') \int_0^{\theta_u} \cos^3 \theta d\theta \right] dy' \qquad \text{(B-9)}$$

Integrating the inside integral,

$$C_{x'} = 2\frac{C_{P_0}\cos^2 \Lambda_1}{S_{ref}} \left(\sin\theta_u - \frac{\sin^3 \theta_u}{3} \right) \int_0^{b/(2\cos\Lambda_1)} r_{LE}(y')dy'$$

If it is assumed that the leading edge radius varies linearly from its maximum at the root chord to its minimum at the tip chord then:

$$r_{LE}(y') = (R_T - R_R)\frac{y'}{b}(2\cos\Lambda_1) + R_R \qquad \text{(B-10)}$$

Substituting this relation into the above integral and performing the integration there is obtained:

$$C_{x'} = \frac{bC_{P_0}\cos\Lambda_1}{S_{ref}} R_{AVG} \left(\sin\theta_u - \frac{\sin^3 \theta_u}{3} \right) \qquad \text{(B-11)}$$

where $R_{AVG} = (R_R + R_T)/2$. Equation (B-11) is for one fin. If there are four fins present then the axial force coefficient in the x direction for the blunt portion of the fin is:

$$C_{A_{LE}} = 4C_{x'}\cos\Lambda_1 \quad \frac{4bC_{P_0}\cos^2\Lambda_1 R_{AVG}}{S_{ref}} \left(\sin\theta_u - \frac{\sin^3 \theta_u}{3} \right) \qquad \text{(B-12)}$$

APPENDIX C

TRAILING EDGE SEPARATION DRAG

The incremental force on the elemental area of the wing trailing edge shown in the sketch below is:

$$dC_{A_B} = C_p \frac{dA}{S_{ref}} = C_p \frac{t\,dy}{S_{ref}} \qquad (C\text{-}1)$$

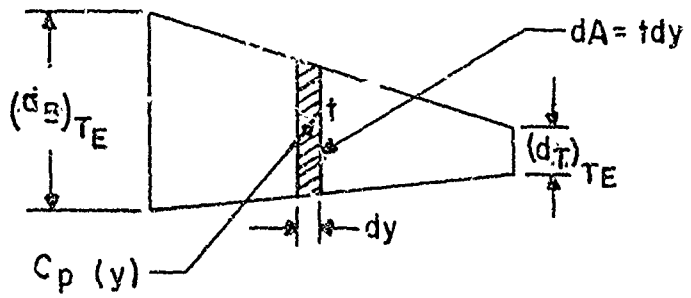

In analogy to the work of Reference 1, an empirical expression which takes into account the slope of the wing trailing edge is

$$C_p(y) = C_{p_B} \frac{d(y)}{t(y)} \qquad (C\text{-}2)$$

Again, assuming a linear variation of the trailing edge diameter from $(d_R)_{TI}$ at the root to $(d_T)_{TI}$ at the tip, the diameter at any y location is:

$$d_{TI}(y) = (d_R)_{TI} + \left[(d_T)_{TI} - (d_R)_{TI}\right] \bar{y} \qquad (C\text{-}3)$$

where

$$\bar{y} = 2y/b.$$

Then Equation (C-1) becomes:

$$C_{A_B} = \frac{C_{P_B}}{2S_{ref}} b \int_0^1 \frac{d_{TE}(\bar{y})}{t(y)} t(y)\, d\bar{y} = \frac{bC_{P_B}}{2S_{ref}} \int_0^1 d_{TE}(\bar{y}) d\bar{y} \qquad (C\text{-}4)$$

Substituting (C-3) into (C-4) and integrating yields

$$C_{A_B} = \frac{bC_{P_B}}{2S_{ref}} \left[(R_R)_{TE} + (R_T)_{TE} \right] \qquad (C\text{-}5)$$

or for four fins:

$$C_{A_B} = \frac{bC_{P_B}}{S_{ref}} \left[(d_R)_{TE} + (d_T)_{TE} \right] = \frac{2bC_{P_B}}{S_{ref}} \left[(R_R)_{TE} + (R_T)_{TE} \right] \qquad (C\text{-}6)$$

APPENDIX D

GLOSSARY

GLOSSARY

AR	Aspect ratio
b	Wing span (does not include body radius)
c	Chord length at any point along span
C_A	Axial force coefficient = C_{D_0}
C_{A_f}	Axial skin-friction drag coefficient
C_{A_B}	Trailing edge separation drag coefficient
C_{D_0}	Zero lift drag coefficient
C_{D_w}	Wave drag coefficient of wing
C_{d_c}	Cross-flow drag coefficient of wing
C_{d_w}	Spanwise wave drag coefficient
C_{f_ℓ}	Laminar skin-friction coefficient
C_{f_T}	Turbulent skin-friction coefficient
C_M	Pitching moment coefficient measured about nose tip (positive nose up).
C_M	Spanwise pitching moment of wing
C_{M_α}	Pitching moment coefficient derivative (dC_M/d_α)
C_N	Normal force coefficient
$C_{N_{B(V)}}$	Normal force coefficient on tail of body shed vortex.
C_{N_i}	Normal force coefficient on tail due to canard shed vortex.
C_{N_α}	Normal force coefficient derivative (dC_N/d_α)

GLOSSARY (Continued)

C_n	Spanwise normal force of wing
C_P	Pressure coefficient
C_{P_B}	Base pressure coefficient
C_{P_0}	Stagnation pressure coefficient
c_{r_1}	Chord length at root of the leading edge portion of a modified double wedge airfoil section
c_{r_2}	Chord length at root of the trailing edge portion of a modified double wedge airfoil section
ΔC_P	Lifting pressure on wing
d	Body diameter
E,F,K	Elliptic integrals
f_c	Canard vortex semispan at canard trailing edge
h	Height of canard shed vortex above body axis at tail center of pressure
i	Tail interference factor
K_B	Ratio of lift of body to that of wing
$K_{B(w)}$	Ratio of lift of body in presence of wing to that of the wing alone
K_C	Ratio of lift of canard-body-tail combination to that of wing alone
$K_{w(B)}$	Ratio of lift of wing in presence of body to that of wing alone
$k_{B(w)}$	Ratio of lift on body in presence of wing, due to a wing deflection δ, to that of wing alone
k_i	$k_i = \tan\Lambda_i$

GLOSSARY (Continued)

$k_{w(b)}$	Ratio of lift of wing in presence of body, due to a wing deflection δ, to that of wing alone
L_C	Lift of canard-body-tail combination
M	Mach number
m	$m = \beta \cot \Lambda_1$
R_N	Reynold's number
r	Radius of body (variable)
r_{LE}	Radius of wing leading edge in a plane normal to leading edge
r_{TE}	Radius of wing trailing edge in a plane normal to trailing edge
S_{ref}	Reference area (maximum body cross-sectional area unless wing alone is considered in which case the wing planform area is used)
S_w	Wing planform area
s	Wing semispan plus body radius at wing root chord
T_w	Wall temperature
t	Wing thickness (variable)
u,v,w	Perturbation velocities in the x,y,z directions, respectively
V	Total velocity, $V^2 = (U_\infty + u)^2 + v^2 + w^2$
x,y,z	Rectangular coordinate system with x at nose tip, y out right wing, and z positive up. If no body is present, x begins at wing root chord.
α	Angle of attack
β	$\sqrt{M_\infty^2 - 1}$

GLOSSARY (Continued)

Γ	Circulation at wing-body juncture of combination
γ	Ratio of specific heats (γ = 1.4 for air)
δ	Wing deflection angle
η	$\eta = k_i/\beta = 1/m$
θ	Angle between a tangent to the local wing surface and freestream direction
θ_1	Angle on blunt leading edge where Newtonian theory stops and perturbation theory begins (match point)
Λ_i	Sweepback angle of a wing generator (i = 1,2,3,4) with i = 1 the wing leading edge and i = 4 the wing trailing edge
λ	Ratio of tip chord to root chord (c_t/c_r)
μ	Mach angle, $\mu = \sin^{-1}(1/M_\infty)$
ν	Coefficient of kinematic viscosity
σ	$\sigma = k_i y/x$
ϕ	Velocity potential
χ	Wedge half angle (measured parallel to freestream) of wing airfoil section.

Subscripts

a	Conditions at transonic Mach number $M_a = M_{fb} + 0.07$
b	Conditions at transonic Mach number $M_b = M_{fb} + 0.14$
cp	Center of pressure
fb	Force break Mach number
IA	Infinite afterbody

Subscripts

ℓ	Laminar
NA	No afterbody
r	Root chord
SA	Short afterbody
T	Turbulent
t	Tip chord
VIS	Viscous component
I	Wing for which slender body values of interference lift are known.
II	Wing with sweep for which representative values of interference lift are desired
∞	Freestream conditions

APPENDIX E

DISTRIBUTION